An iterative algorithm for frequency-domain optimization of fixed-structure controllers

A multi-model approach

Georgios Skaltsis

Master of Science Thesis

TU Delft Delft University of Technology

Delft Center for Systems and Control

An iterative algorithm for frequency-domain optimization of fixed-structure controllers

A multi-model approach

Master of Science Thesis

For the degree of Master of Science in Systems and Control at Delft University of Technology

Georgios Skaltsis

March 17, 2020

Faculty of Mechanical, Maritime and Materials Engineering (3mE) · Delft University of Technology

Delft University of Technology
Department of
Delft Center for Systems and Control (dcsc)

The undersigned hereby certify that they have read and recommend to the Faculty of Mechanical, Maritime and Materials Engineering (3mE) for acceptance a thesis entitled

An iterative algorithm for frequency-domain optimization of fixed-structure controllers

by

Georgios Skaltsis

in partial fulfillment of the requirements for the degree of

Master of Science Systems and Control

Dated: March 17, 2020

Supervisor(s):

prof.dr.ir. J.W. van Wingerden

dr.ir. Folkert Ritsma

Reader(s):

prof.dr.ir. J.W. van Wingerden

prof.dr.ir. M. Mendel

dr.ir. J. Frederik

Abstract

Data-driven control approaches have been proved highly effective in applications where the dynamics of the system are unknown. The reason is that the use of data in control overcomes the challenge of parametric modeling which requires effort and often leads to an insufficient description of the system's behavior. By contrast, the behavior of the system can be captured more accurately when input-output data is used.

In this project a frequency-domain approach is proposed for robust controller design for controllers of pre-specified structure. Specifically, an existing technique is extended so that it guarantees not only nominal, but also robust performance. This is achieved by ensuring performance for multiple frequency-domain models acquired from data. The related computational efficiency in the overall approach is also a fundamental criterion and thus we propose a series of techniques by which it can be improved. Additionally, a major contribution of this work is an iterative algorithm that minimizes a linear approximation of the H_∞ norm of the closed-loop system. Last but not least, a method to optimize the linear constraints of the optimization scheme is proposed.

Table of Contents

List of Figures

List of Tables

Acknowledgements

This document is the result of my research during my graduation project. Having a sincere interest in data-driven control techniques I decided to perform my research under the guidance of prof.dr.ir. J.W. van Wingerden. He suggested we worked over robust techniques in data-driven control. I was both challenged and fascinated to work on a topic which is relatively new and thus less explored. I initially explored the potential of robustifying the output feedback Linear Quadratic (LQ) problem, by imposing simultaneous stabilization of multiple models. However, such an approach leads to computationally complex algorithms, and for that we decided to examine frequency-domain techniques. After some research on the field, I found a gap promising for contributions, and that is how my topic came to be "An iterative algorithm for frequency-domain optimization of fixed-structure controllers: a multi model approach". During the period that I worked in this project the feedback from my supervisor prof.dr.ir. J.W. van Wingerden and Folkert Ritsma kept me motivated to keep up with my research and I am very thankful for that. Moreover, I would like to thank my family and my friends Kostas, Noor, Alex, Nicolas and Georgios for the valuable support.

Delft, University of Technology
March 17, 2020

Georgios Skaltsis

"To measure is to know."
— *Lord Kelvin*

To my brother, Giannis.

Chapter 1

Introduction

A mathematical representation of the physical world, not matter how reliable, can only be an approximation of a complex underlying behavior. Similarly, a system can be modeled precisely with a parametric model, yet it will always deviate from the real-world physical system due to manufacturing defects or unmodeled dynamics. Therefore, a controller that is designed based on a parametric model is likely to result in suboptimal control performance compared to controllers based on data and system identification.

Data-driven control refers to a wide range of approaches that make use of input-output data with the purpose of controller design. The several approaches can initially be separated in two classes: model-free methods and model-based methods. Model-free methods make direct use of data, bypassing the representation of the system by any model. Such methods usually develop a control strategy relying on an iterative learning procedure. On the other hand, in model-based methods the key idea is the identification of the system. That is, a persistently exciting input and the corresponding output can be used to build a representation, that is a model, of the system that best fits to the data acquired. The controller synthesis then follows by using traditional controller design tools.

The techniques that are proposed in this project, lie on the field of model-free data-driven control, since the system that is to be controlled is not described by an analytical identified model. Instead, its behavior is represented by frequency-domain data, which can be used to facilitate robust controller synthesis. Frequency-domain data can be acquired from time-domain data by using Fourier analysis or spectral analysis. Specifically, we are going to make use of data in the form of Frequency Response Function (FRF) measurements [9], acquired in a closed-loop system configuration. Then, the frequency response of the plant, denoted as $G(j\omega)$, can be extracted from the closed-loop FRF measurements. Finally, the response of the plant can be exploited to build controllers that satisfy stability and performance conditions.

A simple schematic criterion which can be employed in combination with frequency-domain data, in order to satisfy stability and nominal performance specifications is the generalized Nyquist criterion. That is, one can impose a number of linear constraints to the Nyquist diagram of a certain function, so as to ensure a specific number of encirclements of the origin,

which will result to a well performing controller. A commonly used method to extend simply nominal to robust performance is to guarantee that a controller satisfies performance for a set of system's representations.

The work at hand is based on a technique for frequency-domain, convex optimization of fixed-structure controllers presented in [12]. This initial approach employs the generalized Nyquist criterion and makes use of user-defined linear constraints to facilitate data-driven controller design that satisfies H_∞ nominal performance for a stable plant. Given this default technique, we propose multi-model controller design, which leads to the satisfaction of robust performance. Additionally, we propose an updated optimization scheme and an algorithm that automatically constructs optimal, in the sense of minimum conservatism, linear constraints. As a result the designer is relieved from the burden of constructing user-defined constraints, which can often be a cumbersome procedure. Moreover, we explore different methods of reducing the size of the problem by reducing the number of the resulting linear inequalities. Finally, we extend the entire technique so that unstable plants with right-half plane (RHP) poles can also be considered, retaining the convexity of the proposed optimization algorithm.

Namely, in chapter 2 we develop the existing technique presented in [12], that provides an algorithm for optimization of fixed-structure controllers that satisfy H_∞ nominal performance based on frequency-domain data, for a stable plant. Next, in chapter 3 the extension of the algorithm so that it satisfies H_∞ robust performance is proposed and additionally, a series of techniques by which the resulting computational complexity can be reduced are suggested. Moreover, in chapter 3 we propose an iterative, computational algorithm that seeks to minimize a certain convex approximation of the infinity norm of the actual plant, with the minimum amount of information. By minimum information it is meant that a single stabilizing controller parameters' combination suffices so as to perform the proposed iterative, convex optimization. Next to that, an iterative algorithm for optimization of the linear constraints that are imposed is proposed. In chapter 4, we employ a stable plant to evaluate the suggested algorithms and we present some extended comparisons between the different approaches. In chapter 5, we extend the proposed techniques for unstable systems, where the Nyquist criterion requires a more complex condition for stability and performance, and then we employ the dynamics of a magnetically levitated train in order to evaluate the performance of our algorithms. Finally, in chapter 6, we comment on the conclusions of this project, presenting its advantages and drawbacks, while we also consider the potential for future research and applications of the proposed technique.

Chapter 2

Frequency-Domain Optimization of Fixed-Structure Controllers

In this chapter we develop a frequency-domain technique for optimization of controllers with pre-specified structure, as presented in [12]. It is noted that a significant part of the notation and the theoretical description remains the same. Specifically, the goal of the method is to tune the parameters of a linearly parametrized controller in order to satisfy H_∞ performance, using a measured Frequency Response Function (FRF) obtained from the plant. We note that the corresponding unstructured robust control problem is convex, yet it typically results to controllers with high order [14], which is not convenient in practice.

The key idea behind this algorithm lies on exploiting the generalized Nyquist criterion. Specifically, a set of linear constraints are employed to impose stability and performance specifications. The initial approach in [12] considers Multiple-Input Multiple-Output (MIMO) stable systems, which result to a multi-linear problem. Next, it is proved that for Single-Input Single-Output (SISO) and Single-Input Multiple-Output (SIMO) systems the configuration of the system can suitably be modified so that the resulting algorithm is convex. In the following sections we develop the main principles and the structure of the algorithm.

2-1 Problem formulation

In this section the H_∞ control synthesis problem is defined, the class of admissible controllers is described and finally the stability and performance conditions are specified.

2-1-1 Problem statement

Consider the generalized plant expressed as:

$$\begin{bmatrix} z \\ y \end{bmatrix} = \begin{bmatrix} P_{11}(s) & P_{12}(s) \\ P_{21}(s) & P_{22}(s) \end{bmatrix} \begin{bmatrix} w \\ u \end{bmatrix}, \tag{2-1}$$

where $z \in \mathbb{R}^{n_z}$ denotes the error signal, $w \in \mathbb{R}^{n_w}$ denotes the external inputs, whereas $u \in \mathbb{R}^{n_m}$ and $y \in \mathbb{R}^{n_m}$ denote the input and output of the generalized plant. The transfer functions $P_{11}(s)$, $P_{12}(s)$, $P_{21}(s)$ and $P_{22}(s)$ have corresponding dimensions and are all assumed to be stable. Part of the controller is considered to be absorbed in the transfer functions of the generalized plant. On the other hand, the tunable parameters of the controller are extracted and finally the control law takes a form of static output feedback for which it holds:

$$u = \underbrace{\begin{bmatrix} \phi_1 & & 0 \\ & \ddots & \\ 0 & & \phi_m \end{bmatrix}}_{\mathrm{K}} y, \tag{2-2}$$

where $\phi_1, \cdots, \phi_m$ denote the tunable parameters of the controller K. The closed-loop transfer function of the generalized plant, from w to z, is expressed as

$$T_{wz} = F_l(P, K) = P_{11}(s) + P_{12}(s)K(I - P_{22}(s)K)^{-1}P_{21}(s), \tag{2-3}$$

where F_l denotes the lower linear fractional transformation (LFT). The objective is to find values for the parameters ϕ_i, for $i = 1, \cdots, m$, such that $||T_{wz}(s)||_\infty < 1$.

2-1-2 Linearly parametrized controllers

The class of controllers that are available for feedback is a set of linearly parametrized controllers. Such controllers take the form

$$C(s, \phi) = \phi^T l(s), \text{where } \phi^T = [\phi_1, \phi_2, \cdots, \phi_n], l^T(s) = [l_0(s), l_1(s), \cdots, l_{n-1}(s)],$$

n is the number of controller parameters and $l_i(s)$ are stable transfer functions. In the general case, any stable rational finite order transfer function $F(s)$ can be approximated by some orthonormal basis functions. An example is Laguerre basis functions [7], where:

$$l_0(s) = 1, \quad l_i(s) = \frac{\sqrt{2\xi}(s-\xi)^{i-1}}{(s+\xi)^i} \quad \text{for } i \geq 1, \quad \xi > 0 \tag{2-4}$$

Then, it holds that for arbitrarily small $\epsilon > 0$ there exists a sufficiently large n for which

$$||F(s) - \phi^T l(s)||_p < \epsilon \quad \text{for } 0 < p < \infty \tag{2-5}$$

Thus, with Laguerre basis functions parametrization any finite order stable transfer function can be approximated with higher accuracy as the number of controller parameters n increases. A practical guideline about how to select the tuning parameter ξ and the number of controller parameters n is given in [4]. In the context of this approach, the Laguerre basis functions are absorbed into the generalized plant and the tunable parameters are extracted in a diagonal form as shown in equation 2-2.

Naturally, the most commonly used linearly parametrized controller is the PID type. Consider the PID controller

$$K_{PID}(s) = k_p + \frac{k_i}{s} + \frac{k_d s}{T_f s + 1}, \tag{2-6}$$

with k_p, k_i and k_d denoting the proportional, integral and derivative gain, respectively. Then, it can be easily integrated with the generalized plant with the tunable parameters in a diagonal form and this is shown in figure 2-1

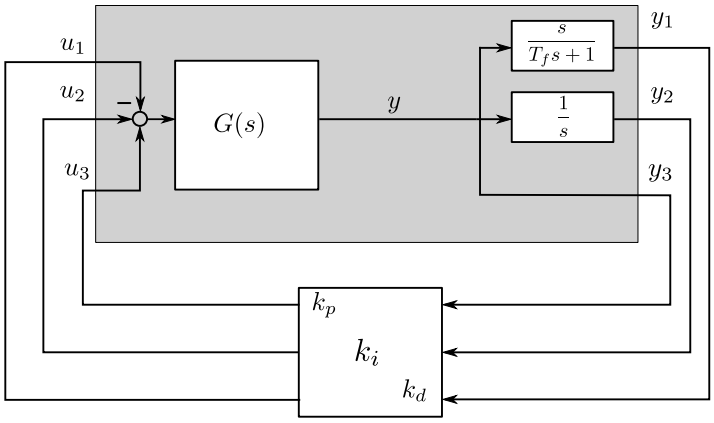

Figure 2-1: Configuration of the generalized plant for a PID controller

2-1-3 Condition for stability and performance

As mentioned before, the objective of this algorithm is to find the values of the tunable parameters of a pre-specified structure controller that satisfy $||T_{wz}(s)||_\infty < 1$. Consider the stable generalized plant $P(s)$ and its frequency response that is denoted as $P(j\omega)$ and can be obtained using FRF data of the plant. The generalized Nyquist criterion for stability [6] is employed to formulate the condition for stability and performance.

Definition for stability The closed-loop system T_{wz} illustrated in figure 2-2, is asymptotically stable if for a stable generalized plant $P(s)$, the Nyquist plot of

$$\det\left(I - \begin{bmatrix}\phi_1 & & 0\\ & \ddots & \\ 0 & & \phi_m\end{bmatrix} P_{22}(j\omega)\right), \quad \forall\omega, \tag{2-7}$$

does not encircle the origin. This is the generalized Nyquist theorem for a positive feedback system with stable loop transfer function $KP_{22}(j\omega)$.

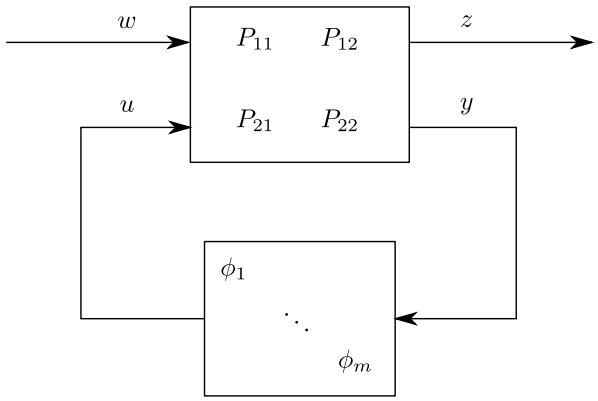

Figure 2-2: Generalized plant with linearly parametrized controller

Definition for performance The closed-loop system T_{wz} satisfies the performance specification $||T_{wz}||_\infty < 1$ if for a stable generalized plant $P(s)$, the Nyquist plot of

$$\det\left(I - \left[\begin{array}{c|ccc} \Delta_p(j\omega) & & 0 & \\ \hline & \phi_1 & & 0 \\ 0 & & \ddots & \\ & 0 & & \phi_m \end{array}\right] P(j\omega)\right), \quad \forall\omega, \forall\Delta_p(j\omega) \tag{2-8}$$

does not encircle the origin for any stable rational transfer function $\Delta_P \in \mathcal{RH}_\infty^{n_w \times n_z}$ and $||\Delta_P(s)||_\infty \leq 1$.

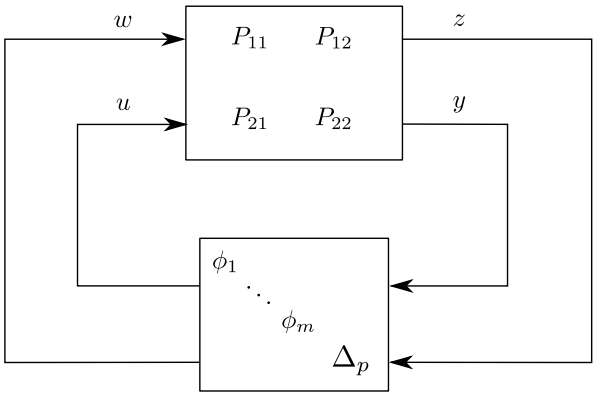

Figure 2-3: Closed-loop system including $\Delta_P(s)$

It can be noticed that figure 2-3 can be obtained by figure 2-2 by including a full complex perturbation block $\Delta_P(j\omega)$ in feedback from the exogenous input w to the exogenous output z. This perturbation is only used to examine the performance specification and is not a physical perturbation. The proof of 2-8 is derived from [11]. In the context of this project, we use the definitions for stability and performance as expressed in 2-7 and 2-8.

2-2 Controller design

In this section we describe the procedure that is used for controller synthesis such that the closed-loop system is stable and $||T_{wz}||_\infty < 1$. First we examine the relation between the controller parameters and the determinant expression that is involved in the conditions for stability and performance. Then, we introduce the linear constraints that are employed in order to prevent the Nyquist curve from encircling the origin. Additionally we examine the realization of the perturbation and the way that it can be utilized in the linear constraints that refer to performance. Last, we consider the resulting feasibility problem and propose a modification that leads to a convex optimization problem for certain controllers.

2-2-1 Determinant expression and controller parameters

In this paragraph, the expression of the determinant for equations 2-7 and 2-8 is examined. Specifically, consider the simple case of a controller with two parameters ϕ_1 and ϕ_2 and a

scalar perturbation. Then, the generalized plant is of the form

$$P(j\omega) = \begin{bmatrix} P_{11}(j\omega) & P_{12}^{(11)}(j\omega) & P_{12}^{(12)}(j\omega) \\ P_{21}^{11}(j\omega) & P_{22}^{(11)}(j\omega) & P_{22}^{(12)}(j\omega) \\ P_{21}^{21}(j\omega) & P_{22}^{(21)}(j\omega) & P_{22}^{(22)}(j\omega) \end{bmatrix} \tag{2-9}$$

Let the determinant, that is related to the stability condition, be denoted as $Q(\phi, j\omega)$. Then, for this case with two controller parameters it becomes

$$Q(\phi, j\omega) = 1 - P_{22}^{(11)}\phi_1 - P_{22}^{(22)}\phi_2 + \left(P_{22}^{(11)}P_{22}^{(22)} - P_{22}^{(12)}P_{21}^{(11)}\right)\phi_1\phi_2 \tag{2-10}$$

Respectively, let the determinant related to the performance condition be denoted as $Q_\Delta(\phi, j\omega)$. Then, for a scalar perturbation, that is for single exogenous input w and exogenous output z, it becomes

$$\begin{aligned} Q_\Delta(\phi, j\omega) =& 1 - P_{11}\Delta_P + \left(P_{11}P_{22}^{(11)}\Delta_P - P_{12}^{(11)}P_{21}^{(11)}\Delta_P - P_{22}^{(11)}\right)\phi_1 \\ &+ \left(P_{11}P_{22}^{(22)}\Delta_P - P_{12}^{(12)}P_{21}^{(21)}\Delta_P - P_{22}^{(22)}\right)\phi_2 \\ &+ \Big(P_{22}^{(11)}P_{22}^{(22)} - P_{22}^{(12)}P_{22}^{(21)} - P_{11}P_{22}^{(11)}P_{22}^{(22)}\Delta_P \\ &+ P_{11}P_{22}^{(12)}P_{22}^{(21)}\Delta_P + P_{12}^{(11)}P_{21}^{(11)}P_{22}^{(22)}\Delta_P \\ &+ P_{12}^{(11)}P_{22}^{(12)}P_{21}^{(21)}\Delta_P - P_{12}^{(12)}P_{21}^{(11)}P_{22}^{(21)}\Delta_P + P_{12}^{(12)}P_{22}^{(11)}P_{21}^{(21)}\Delta_P\Big)\phi_1\phi_2 \end{aligned} \tag{2-11}$$

It can be seen in equations 2-10 and 2-11 that both $Q(\phi, j\omega)$ and $Q_\Delta(\phi, j\omega)$ are bilinear with respect to the controller parameters ϕ_1 and ϕ_2. Respectively, for controllers with multiple parameters the relation will be multi-linear. In the following paragraph, the determinant expressions $Q(\phi, j\omega)$ and $Q_\Delta(\phi, j\omega)$ are constrained by some linear inequalities such that the Nyquist criterion is satisfied.

2-2-2 Constraints in the Nyquist diagram

The main idea behind this algorithm is to constrain the Nyquist curves of $Q(\phi, j\omega)$ and $Q_\Delta(\phi, j\omega)$ from encircling the origin. An example of such a constraint is illustrated in figure 2-4, where the Nyquist curve of $Q(\phi, j\omega)$ for a certain stable generalized plant $P(j\omega)$ is depicted with the solid line. The discs with centers at the solid line correspond to the Nyquist curve of $Q_\Delta(\phi, j\omega)$. The closed-loop system T_{wz} is stable if and only if the Nyquist diagram of $Q(\phi, j\omega)$ does not encircle the origin. Additionally, performance is satisfied if and only if the Nyquist diagram of $Q_\Delta(\phi, j\omega)$ does not encircle the origin. These two restrictions are imposed by some linear constraints which in figure 2-4 are noted as $l_1(j\omega)$ and $l_2(j\omega)$. It is noted that the linear constraints are imposed per frequecy point and additionally naturally a different constraint is active for different ranges of frequency. This is illustrated in 2-4 by the use of different colors which are indicating which linear constraint is active for a specific range of frequencies for $Q(\phi, j\omega)$ and $Q_\Delta(\phi, j\omega)$. That is, the area of $Q(\phi, j\omega)$ which is in black color is contrained by $l_1(j\omega)$, whereas the area in grey color is constrained by $l_2(j\omega)$.

Linear constraints such as $l_1(j\omega)$ and $l_2(j\omega)$ are defined by the designer and require some insight into the plant that is to be controlled. Generally, they have the following form, i.e.

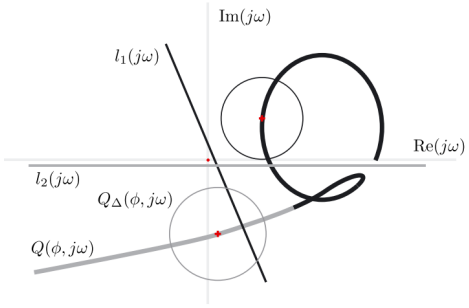

Figure 2-4: Nyuquist diagram [12].

for stability,

$$l_1(\phi, j\omega) = \text{Im}(Q(\phi, j\omega)) + a_1\text{Re}(Q(\phi, j\omega)) + c_1 < 0, \quad \omega \in [\omega_1, \omega_2] \tag{2-12}$$

where $\text{Re}(\cdot)$ and $\text{Im}(\cdot)$ denote the real and imaginary part of a complex number, and a_1 and c_1 are the slope and the offset of the constrain l_1. The frequencies ω_1 and ω_2 denote the range of frequencies for which this constraint is active. Similarly, the Nyquist curve of $Q(\phi, j\omega)$ can be constrained as

$$l_2(\phi, j\omega) = \text{Im}(Q(\phi, j\omega)) + a_2\text{Re}(Q(\phi, j\omega)) + c_2 < 0, \quad \omega \in [\omega_2, \omega_3], \tag{2-13}$$

where a_2 and c_2 denote the slope and the offset of the constraint, while ω_3 denotes the upper limit of the active frequency range for l_2.

Similar constraints, denoted as $l_{\Delta 1}$ and $l_{\Delta 2}$, are defined for performance if the value of $Q_\Delta(\phi, j\omega)$ is replaced instead of $Q(\phi, j\omega)$ in the linear inequalities 2-12 and 2-13. Hence, when linear constraints for $Q(\phi, j\omega)$ are imposed, the resulting controller will satisfy stability requirements. Similarly, when constraints for $Q_\Delta(\phi, j\omega)$ are considered, the resulting controller will satisfy performance.

Since the developed method is a computational algorithm that is based on linear constraints that are applied per frequency point, it is essential to find a way to realize the performance perturbation Δ_P, and this is discussed in the following subsection.

2-2-3 Realization of perturbation Δ_P

In the following paragraphs the realization of the performance perturbation Δ_P is discussed. It holds that $||\Delta_P(s)||_\infty \leq 1$ and $\Delta_P \in \mathcal{RH}_\infty^{n_w \times n_z}$. Hence, realizing $l_\Delta(\phi, j\omega)$ would require to evaluate an infinite number of constraints. For example realizing the constraint for a particular frequency point it would be needed to realize all $\Delta_P(j\omega)$ for which $\max_\omega \bar{\sigma}(\Delta_P(j\omega)) \leq 1$. In order to circumvent this, the performance perturbation $\Delta_P(j\omega)$ is realized by n_d points randomly drawn from $\max_\omega \bar{\sigma}(\Delta_P(j\omega)) \leq 1$.

The relization of the perturbation $\Delta_P(j\omega)$ is denoted by $\bar{\Delta}_P(j\omega)$ and the corresponding determinant expression is denoted by $Q_{\bar{\Delta}}(\phi, j\omega)$. For satisfying performance specifications it should hold that the Nyquist diagram of $Q_{\bar{\Delta}}(\phi, j\omega)$ does not violate the constraints. For that, it suffices to check the worst case for the perturbation Δ_P which corresponds to realizing

$\Delta_P(j\omega)$ with maximum singular value, that is $\bar{\sigma}(\Delta_P(j\omega) = 1$. In other words, it suffices to check the boundary, since an LFT will map closed contours in closed contours [1]. Thus, finally we are interested in realizing the following set of perturbations

$$\bar{\Delta}_{\mathbf{P}} := \{\bar{\Delta}_P | \bar{\sigma}(\bar{\Delta}_P(j\omega)) = 1\}$$

It is noted that the resulting size of the feasibility problem is proportional to the number of realizations n_d of the perturbation. Naturally, by selecting a increased number of realizations n_d will reduce the probability of "missing" a critical uncertainty. On the other hand, an increased number of realizations implies an increased computational effort of the algorithm. This introduces a trade-off that the designer has to take under consideration when deciding on the number of realizations of Δ_P. After having resolved the issue of realizing Δ_P, the feasibility problem can be discussed.

2-2-4 Multilinear feasibility problem

In the following paragraphs we examine the feasibility problem, that is the details of setting up the proposed algorithm. We consider that frequency response data are available from an FRF of the plant which is denoted as $P(j\omega)$. Additionally, a set of linear constraints $l(\phi, j\omega)$ and $l_\Delta(\phi, j\omega)$ is constructed for stability and performance, respectively. Thus, the computational problem that addresses the satisfaction of stability requirements can be expressed as

$$\text{Find } \phi \text{ such that } l(\phi, j\omega) < 0 \quad \forall \omega \in \Omega, \tag{2-14}$$

where Ω is the finite discrete set containing the frequency grid of the FRF of the plant. Similarly, for performance the problem can be expressed as

$$\text{Find } \phi \text{ such that } l_\Delta(\phi, j\omega) < 0 \quad \forall \omega \in \Omega, \forall \bar{\Delta}_P(j\omega) \in \bar{\Delta}_{\mathbf{P}} \tag{2-15}$$

Solving the problems 2-14 and 2-15, controller parameters ϕ are obtained which satisfy closed-loop stability for the former case, and closed-loop stability and performance for the latter case. If the problem is not feasible the designer should consider either changing the structure of the fixed-order controller or refine the linear constraints imposed in the Nyquist diagram.

It is stressed that multiple constraints can be applied per frequency point if this is desired. Moreover, the size of the feasibility problem depends on the number of frequency points that are considered, on the number of constraints that are imposed in each point as well as on the number of realizations of the perturbation Δ_P. Thus, for a single constraint per frequency point the problem that addresses stability will lead to N linear constraints, where N denotes the number of frequency points in the FRF. On the other hand, when performance is considered, the problem will consist of $N \cdot n_d$ linear constraints. Finally, it is noted that the size of the problem does not depend on the number of the controller parameters.

2-2-5 Convex feasibility problem and optimization scheme

As discussed previously, extracting the controller parameters into a diagonal form results to having a feasibility problem that is multi-linear with respect to the parameters ϕ. In the following paragraphs we discuss the ways and conditions, under which the feasibility problem

can be convexified. For this, we need to modify the configuration of the generalized plant, and correspondingly of the controller as well, in a way that facilitates the transformation of the linear constraints. Specifically, the diagonal form of the controller with the perturbation Δ_P as presented previously

$$\left[\begin{array}{c|ccc} \Delta_p(j\omega) & & 0 & \\ \hline & \phi_1 & & 0 \\ 0 & & \ddots & \\ & 0 & & \phi_m \end{array}\right]$$

is modified to

$$K_I(\phi, j\omega) = \begin{bmatrix} \Delta_p(j\omega) & 0 \\ 0 & C_I(\phi, j\omega) \end{bmatrix}, \tag{2-16}$$

where $C_I(\phi, j\omega)$ denotes the full controller, including the tunable parameters. Naturally, the configuration of the generalized plant needs to change as well. This modification implies that instead of absorbing part of the controller into the generalized plant and extracting only the tunable parameters, the full controller is represented by $C_I(\phi, j\omega)$. In the case of a SISO controller this leads to a convex optimization problem. This can be shown by examining the determinant expression for the case of a scalar perturbation and a SISO controller. For performance, the Nyquist theorem requires that the Nyquist curve of

$$\det(I - K_I(\phi, j\omega)P(j\omega)) \tag{2-17}$$

does not encircle the origin. By substituting 2-16 in 2-8 results to

$$(1 - \Delta_P P_{11})\,(1 - C_I(\phi)P_{22}) - \Delta_P P_{12} C_I(\phi) P_{21} \tag{2-18}$$

which is affine with respect to the controller parameters ϕ. Thus, SISO controllers, such PID controllers, result in a convex feasibility problem. It is noted that the realization of the perturbation Δ_P can be multidimensional without affecting the convexity of the feasibility problem. Additionally, the feasibility problem remains convex for the case of a Multiple-Input Single-Output (MISO) controller, while for SIMO it is not anymore convex. This can be easily demonstrated by considering a simple case for each scenario.

Having described the configuration of the generalized plant that is required in order to have a convex feasibility problem, according to [12] the optimization algorithm can be expressed as

$$\begin{aligned} &\min \sum_{i=1}^{m} \phi_i^2 \\ \text{s.t. } & l^n(\phi, j\omega) < 0, \quad \forall \omega \in [\omega_i, \omega_{i+1}] \quad n = 1, \cdots, c-1 \\ & l_\Delta^n(\phi, j\omega) < 0, \quad \forall \omega \in [\omega_i, \omega_{i+1}] \quad n = 1, \cdots, c-1, \end{aligned} \tag{2-19}$$

where c denotes the total number linear constraints. It is stressed that the linear constraints that refer to stability, that is $l^n(\phi, j\omega) < 0$ for $n = 1, \cdots, c-1$, are more conservative than the ones that refer to performance, and thus they can be omitted in the optimization procedure.

Chapter 3

Robust Performance and Minimization of Conservatism

In the previous chapter the main mechanism and the principles of the algorithm were developed. Specifically, it was shown that by imposing some linear constraints in the Nyquist diagram one can satisfy closed-loop stability and performance specifications for a system, given that a frequency response of the plant is available. However, frequency responses in the form of Frequency Response Function (FRF) measurements often imply the existence of uncertainties due to measurement or process noise. This means that the generalized plant is not described accurately and hence the actual performance of the resulting controller might deviate from the desired behavior.

In order to deal with uncertainties we propose an extension of the algorithm so that it can guarantee stability and performance over a whole set of generalized plants, which are acquired from multiple FRF measurements. This way the nominal performance that was guaranteed in chapter 2 can be extended to robust performance. Such an extension naturally leads to the increase of linear constraints that need to be considered, as it will be shown in more detail in the following sections. As a solution to this problem we also develop a method of reducing the number of the linear constraints that are imposed. Additionally, we propose a refined optimization scheme which is based on an iterative algorithm that seeks to minimize a convex approximation of the H_∞ norm of the closed-loop. This refined optimization scheme arose as a solution to the conservatism of the default optimization scheme proposed in [12]. Finally, we propose an algorithm that constructs linear constraints, which are optimal in the sense that they induce the least amount of conservatism with respect to an initially stabilizing solution.

3-1 A multi-model approach

In this section the H_∞ controller design problem for a multi-model approach is addressed. Specifically, we directly approach controllers that lead to a convex feasibility problem as described in 2-2-5. Certainly, this extension to a multi-model approach can be applied in

the general case of controllers in a diagonal form as well. In the following subsections we propose a method that facilitates controller design in order to satisfy stability and performance requirements over a whole set of generalized plants.

3-1-1 Problem formulation

Consider a set of M generalized plants given as

$$\begin{bmatrix} z_i \\ y_i \end{bmatrix} = \begin{bmatrix} P_{11}^i(s) & P_{12}^i(s) \\ P_{21}^i(s) & P_{22}^i(s) \end{bmatrix} \begin{bmatrix} w_i \\ u_i \end{bmatrix} \quad i = 1, \cdots, M \tag{3-1}$$

where $z_i \in \mathbb{R}^{n_z}$ denotes the error signal, $w_i \in \mathbb{R}^{n_w}$ denotes the external inputs, whereas $u_i \in \mathbb{R}^{n_m}$ and $y_i \in \mathbb{R}^{n_m}$ denote the input and output of the generalized plant i, with $i = 1, \cdots, M$. The transfer functions $P_{11}^i(s)$, $P_{12}^i(s)$, $P_{21}^i(s)$ and $P_{22}^i(s)$ have corresponding dimensions and are all assumed to be stable.

As it was stressed previously, in this chapter we consider controllers that lead to a convex feasibility problem. That is, Single-Input Single-Output (SISO) and Multiple-Input Single-Output (MISO) controllers that can be represented as $C_I(\phi, s)$, where C_I is affine with respect to the controller parameters ϕ. In particular $C_I(\phi, s)$ can follow any linear parametrization that is described in 2-1-2. Thus, the control law for all M generalized plants can be described as

$$u_i = C_I(\phi, s) y_i, \quad i = 1, \cdots, M. \tag{3-2}$$

Given that, the closed-loop systems for $i = 1, \cdots, M$ are obtained by

$$T_{wz}^i(s) = F_l(P^i, C_I) = P_{11}^i + P_{12}^i C_I (I - P_{22}^i C_I)^{-1} P_{21}^i, \tag{3-3}$$

where F_l denotes the lower linear fractional transformation (LFT). The objective is to find controller parameters ϕ that satisfy $||T_{wz}^i(s)||_\infty < 1$, for $i = 1, \cdots, M$.

3-1-2 Condition for stability and performance

In this subsection the conditions for stability and performance for the closed-loop systems described in 5-2 are given. Consider that multiple frequency responses of the generalized plant $P(s)$ are given, which are denoted as $P^i(j\omega)$ for $i = 1, \ldots, M$. The two definitions are based on the generalized Nyquist criterion of [6].

Definition for stability The closed-loop systems T_{wz}^i, for $i = 1, \cdots, M$ in figure 3-1 are asymptotically stable if for the stable generalized plants $P^i(j\omega)$, the Nyquist plots of

$$Q^i(\phi, j\omega) = \det\Big(1 - C_I(\phi, j\omega) P_{22}^i(j\omega)\Big) \tag{3-4}$$

do not encircle the origin. This is the generalized Nyquist theorem considering positive feedback systems with stable loop transfer functions $C_I(\phi, j\omega) P_{22}^i(j\omega)$.

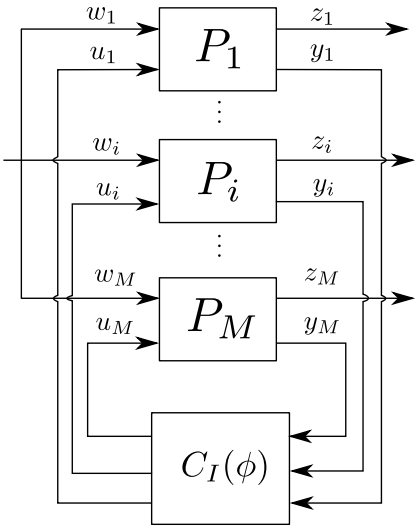

Figure 3-1: Generalized plant configuration considering multiple models

Definition for performance The closed-loop systems T^i_{wz} satisfy H_∞ performance with $||T^i_{wz}||_\infty < 1$, if for the stable generalized plants $P^i(j\omega)$, the Nyquist plots of

$$Q^i_\Delta(\phi, j\omega) = \det\left(I - \begin{bmatrix}\Delta_p(j\omega) & 0\\ 0 & C_I(\phi, j\omega)\end{bmatrix} P^i(j\omega)\right), \quad \forall\omega, \forall\Delta_P(j\omega), \tag{3-5}$$

do not encircle the origin for any stable rational transfer function $\Delta_P \in \mathcal{RH}_\infty^{n_w \times n_z}$ and $||\Delta_P(s)||_\infty \leq 1$.

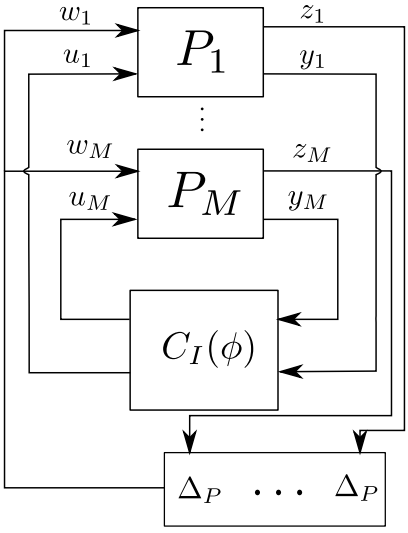

Figure 3-2: Generalized plant configuration considering multiple models and performance perturbation

3-1-3 Linear constraints

As it was described in the previous chapter, in subsection 2-2-2, the main idea of the algorithm is to constraint the Nyquist curves of $Q^i(\phi, j\omega)$ and $Q^i_\Delta(\phi, j\omega)$ from encircling the origin. Similarly to the single-model approach, some linear constraints are employed to guarantee that the stability and performance conditions in 5-3 and 5-4 are met.

The general form of such constraints is, i.e. for stability

$$l_1(\phi, j\omega) = \text{Im}(Q^i(\phi, j\omega)) + a_1\text{Re}(Q^i(\phi, j\omega)) + c_1 < 0, \quad \omega \in [\omega_1, \omega_2], \quad i = 1, \cdots, M, \quad \text{(3-6)}$$

where $\text{Re}(\cdot)$ and $\text{Im}(\cdot)$ denote the real and imaginary part of a complex number, while a_1 and c_1 are the slope and the offset of the linear constraint l_1. In order to satisfy the stability condition 5-3, multiple constraints are implemented for different ranges of frequency. For instance l_1 is active in the frequency interval $[\omega_1, \omega_2]$. The n^{th} linear constraint would have the form

$$l_n(\phi, j\omega) = \text{Im}(Q^i(\phi, j\omega)) + a_n\text{Re}(Q(^i\phi, j\omega)) + c_n < 0, \quad \omega \in [\omega_n, \omega_{n+1}], \quad i = 1, \cdots, M, \quad \text{(3-7)}$$

where a_n and c_n denote the slope and the offset of the constraint, while ω_n and ω_{n+1} denote the lower and the upper limit of the active frequency range for l_n, for $n = 1, \cdots, c$ with c being the number of total linear constraints. Given the stable generalized plants $P^i(j\omega)$ for $i = 1, \cdots, M$, if the linear constraints of the form of 3-6 and 3-7 are satisfied, then the closed-loop systems T^i_{wz} are asymptotically stable.

Similar linear constraints, denoted as $l^n_{\Delta i}$ for $i = 1, \cdots, M$, are defined for performance if the value of $Q^i_\Delta(\phi, j\omega)$ is replaced instead of $Q^i(\phi, j\omega)$ in the linear inequalities 3-6 and 3-7.

3-1-4 Performance perturbation

As it was described in subsection 2-2-3 for the performance perturbation Δ_P it holds that $||\Delta_P(s)||_\infty \leq 1$ and $\Delta_P \in \mathcal{RH}_\infty^{n_w \times n_z}$. In order to avoid an infinite number of realizations, and thus an infinite number of linear constraints, the perturbation $\Delta_P(j\omega)$ is realized by n_d points. In order to keep the number of sampled points low as possible the perturbation in not realized in the set for which $\bar{\sigma}(\Delta_P(j\omega)) \leq 1$. Instead, the worst case scenario is considered and thus we are interested in realizing the following set of perturbations

$$\bar{\Delta}_\mathbf{P} := \{\bar{\Delta}_P | \bar{\sigma}(\bar{\Delta}_P(j\omega)) = 1\}$$

As it was also described in 2-2-3, the size of the final problem is proportional to the number n_d of realizations of the perturbation Δ_P. Specifically, the number of linear inequalities that are implemented in the final algorithm is $N \cdot n_d \cdot M$. This introduces a dilemma for the designer. That is, an increased number of realizations n_d improves the description of Δ_P. On the other hand, this would imply that the complexity of the algorithm would significantly increase. In the following section we propose some methods that can drastically reduce the complexity of the algorithm, without reducing the efficiency of the technique.

3-1-5 Configuration of the optimization scheme

Having described the procedure that needs to be followed for the realization of the perturbation, and having defined the structure of the linear constraints, the optimization scheme for the multi-model approach can be constructed. As deployed in [12], the optimization algorithm can be expressed as

$$\begin{aligned} &\min \sum_{k=1}^{m} \phi_k^2 \\ \text{s.t. } & l_n^i(\phi, j\omega) < 0, \quad \forall \omega \in [\omega_n, \omega_{n+1}] \quad i = 1, \cdots, M, \quad n = 1, \cdots, c \\ & l_{\Delta n}^i(\phi, j\omega) < 0, \quad \forall \omega \in [\omega_n, \omega_{n+1}] \quad i = 1, \cdots, M, \quad n = 1, \cdots, c \end{aligned} \tag{3-8}$$

where c denotes the total number of linear constraints and M the total number of models that are considered. It is stressed that the linear constraints that refer to stability, that is $l_n^i(\phi, j\omega) < 0$ for $n = 1, \cdots, c$, are more conservative than the ones that refer to performance, and thus they can be omitted in the optimization procedure.

3-2 Reduction of computational complexity

The optimization algorithm proposed in section 3-1 for synthesis of fixed-structure controllers based on frequency-domain data is subject to $N \cdot n_d$ linear inequalities, where N is the number of the frequency points that are considered and n_d is the number of realizations of the perturbation Δ_P, per frequency point. Additionally, when a multi-model approach is considered, the total number of linear inequalities results to be $N \cdot n_d \cdot M$, where M is the number of the FRF models that are taken into consideration.

In practice, the number of linear inequalities can grow extremely. For instance, a regular number of frequency points could be $N = 400$, and the number of realizations of Δ_P can be $n_d = 100$, as it is used in [12]. That is, the optimization algorithm will be subject to 40.000 linear constraints. Additionally, if for example 10 FRF models are considered, then 400.000 linear inequalities need to be implemented. These numbers, which are conservative, indicate that the size of the problem can grow hugely as the number of frequency points, the number of realizations of Δ_P and the number of models increase. In the following subsections we propose some techniques that can scale down the size of the problem without jeopardizing the performance of the algorithm.

3-2-1 Reducing the realizations of Δ_P

As it was stressed in 3-1-3, the number of realizations of the perturbation Δ_P, denoted as n_d, should be sufficiently large in order to reduce the probability of "missing" a critical uncertainty, as depicted in [12]. In this subsection we make use of a simple geometrical rule that enables the realization of the perturbation Δ_P with just one sample per frequency point. That is, a single linear inequality is sufficient to guarantee the satisfaction of the remaining $n_d - 1$ inequalities.

Consider the case of a scalar perturbation $\Delta_P \in \mathcal{RH}^{1\times 1}$. Then the function $Q_\Delta(\phi, j\omega)$, with regard to a single model, that corresponds to the satisfaction of performance requirements becomes

$$\begin{aligned} Q_\Delta(\phi, j\omega) =& \det\left(I - \begin{bmatrix}\Delta_P(j\omega) & 0\\ 0 & C_I(\phi, j\omega)\end{bmatrix} P(j\omega)\right) \\ =& \det\left(\begin{bmatrix}1-\Delta_P P_{11} & -\Delta_P P_{12}\\ -C_I(\phi)P_{21} & 1-C_I(\phi)P_{22}\end{bmatrix}\right) \\ =&(1-\Delta_P P_{11})(1-C_I(\phi)P_{22}) - \Delta_P P_{12}C_I(\phi)P_{21} \\ =&(1-C_I(\phi)P_{22}) - \Delta_P[P_{11}(1-C_I(\phi)P_{22}) + P_{12}C_I(\phi)P_{21}] \end{aligned} \tag{3-9}$$

It can be noticed that the first term $(1 - C_I(\phi)P_{22})$ is actually the expression of $Q(\phi, j\omega)$ that is related to the satisfaction of stability. Additionally, the second term consists of a multiplication of the perturbation Δ_P and the quantity within the square brackets. If we denote this term as $R(\phi, j\omega) = P_{11}(1 - C_I(\phi)P_{22}) + P_{12}C_I(\phi)P_{21}$, then the expression of Q_Δ becomes

$$Q_\Delta(\phi, j\omega) = Q(\phi, j\omega) - \Delta_P R(\phi, j\omega). \tag{3-10}$$

This expression highlights the relation between the functions Q_Δ and Q. It is first reminded that Δ_P is realized in the set for which $\bar{\sigma}(\Delta_P(j\omega)) = 1$, or in other words Δ_P is realized with n_d points that lie on the unit circle. Thus, equation 3-10 reveals that for each frequency point, the Nyquist plot of Q_Δ is realized as a circle with radius $R(\phi, j\omega)$ and center equal to the value of $Q(\phi, j\omega)$ for that particular frequency. This observation allows a geometrical interpretation of the linear constraint that Q_Δ is subject to.

The satisfaction of performance specifications depends on whether the circle representing the function Q_Δ in the Nyquist plot is below a linear constraint. It can be proved that if a particular single point of the circle is below the linear constraint, that is under consideration, it is implied that the same holds for all the points of the circle. This point is naturally the point that has the least distance from the line and it can easily be found geometrically by drawing a vertical line from the center of the circle to the line under consideration. This is illustrated in figure 3-3, where it is denoted as Q^*.

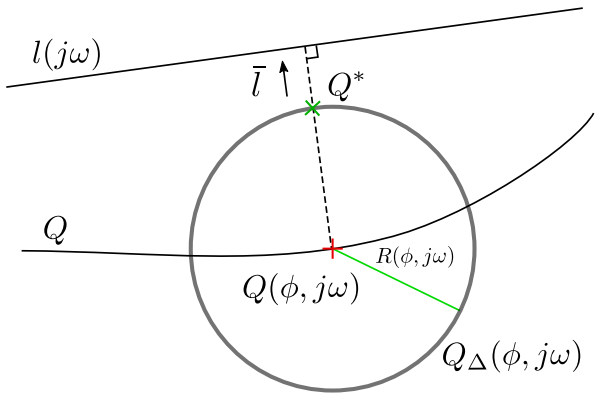

Figure 3-3: Least distance of circle from line

When considering equation 3-10, the corresponding Q^* point, that belongs to Q_Δ, can be found for each frequency point using the following expression

$$Q^*(j\omega) = Q(\phi, j\omega) + |R(\phi, j\omega)|\bar{l}, \tag{3-11}$$

where $\bar{l}$ denotes a unitary vector that is vertical to the linear constraint $l(j\omega)$, as illustrated in figure 3-3. Then, there is no need to produce n_d realizations for Δ_P, in order to calculate an accurate description of Q_Δ. Instead, it is only necessary to compute $Q^*(\phi, j\omega)$ and then performance specifications can be ensured if the following linear constraint is satisfied for all frequency points.

$$l_n(\phi, j\omega) = \mathrm{Im}(Q^*(\phi, j\omega)) + a_n \mathrm{Re}(Q^*(\phi, j\omega)) + c_n < 0, \quad \omega \in [\omega_n, \omega_{n+1}], \quad \forall\omega. \tag{3-12}$$

It is stressed that the calculation of the value of Q^* should always be performed with respect to the linear constraint that is active in a specific frequency point. Additionally, this method of reducing the linear inequalities obtained by performance requirements, can be straightforwardly extended to the case of dealing with multiple models.

However, although introducing the calculation of the Q^* point seems to be convenient for the reduction of the linear inequalities of the problem, it influences the complexity of the algorithm. Namely, the term $|R(\phi, j\omega)|$ in equation 3-11 implies that the expression of Q_Δ will be nonlinear with respect to the controller parameters ϕ. In order to circumvent this obstacle one could linearize $|R(\phi, j\omega)|$ around the values of the controller parameters that are considered in each iteration. Alternatively, instead of creating the Q^* point, selecting the point of Q_Δ that is closer to Q^* would be equally efficient. Unfortunately, in the former case there are no guarantees that the performance constraints will still be satisfied, whereas the latter solution requires initially considering all n_d realizations of Q_Δ and results to the exclusion of $n_d - 1$ of them only in the final stage of the algorithm. In any case, the implementation of this approach comes with great complexity.

3-2-2 Dealing with multiple models

As it was depicted previously, in the standard scenario the final number of linear inequalities that the optimization algorithm is subject to, results to be $N \cdot n_d \cdot M$. The parameters N, n_d and M denote the number of frequency points, the number of realizations of the perturbation Δ_P and the number of FRF models that are considered, respectively. In the previous subsection we explored an idea that could potentially reduce the number of realizations n_d. In this subsection we examine a way that will facilitate the reduction of the total number of linear constraints by utilizing a property of the FRF measurements.

Consider the FRF models acquired by input output data of a system that are illustrated in figure 3-5. As it can be seen the values of the models are similar in the lower frequencies and only at some point they start to differ. This implies that around such ranges of frequency there is low uncertainty. Nevertheless, from a practical point of view, the similarity of the models means that there will be multiple similar linear inequalities. For that, we propose a method that can reduce the number of linear inequalities that are considered. Specifically, let the i^{th} FRF model of the plant be denoted as $G_i(j\omega)$, for $i = 1, \cdots, M$. Then, the mean of those models is denoted as $\bar{G}(j\omega)$ and it is expressed as

$$\bar{G}(j\omega) = \frac{\sum_{i=1}^{M} G_i(j\omega)}{M}. \tag{3-13}$$

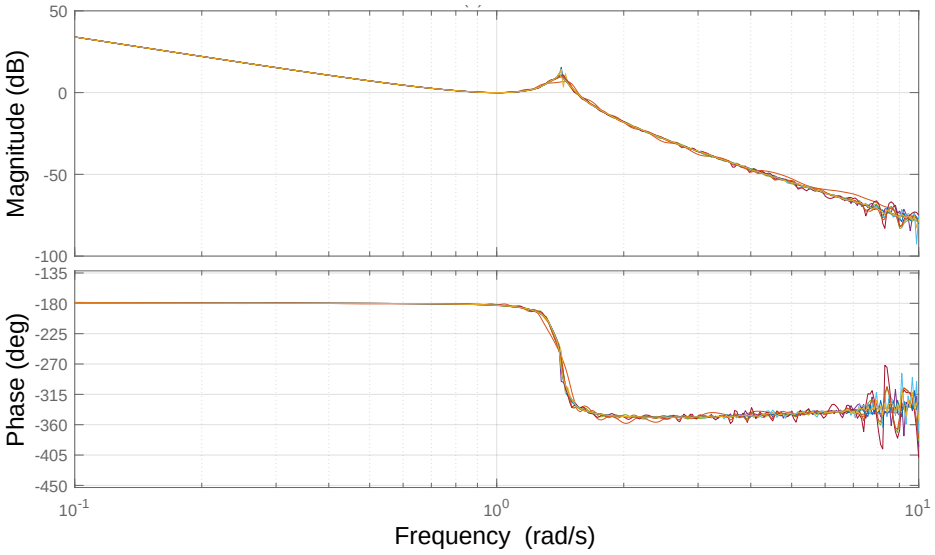

Figure 3-4: A typical example of multiple FRF measurements

A natural way to proceed in this case is to find the frequency at which the FRF models are no longer identical. For this purpose we define the parameter

$$b_i = \frac{G_i(j\omega) - \bar{G}(j\omega)}{\bar{G}(j\omega)} \quad \forall\omega, \quad i = 1, \cdots, M \tag{3-14}$$

which takes different values in every frequency, for each model. The main idea of this approach is that for the range of frequencies for which the parameter b_i remains below a certain value, which is to be defined by the designer, the multiple models can be accurately represented by the mean $\bar{G}(j\omega)$. For sake of ease of comprehension the frequency at which the FRF models start to differ is called critical frequency and it is denoted as ω_{cr}. The procedure of calculating the critical frequency can be better described by the following algorithm.

$$\begin{aligned}
&found = 0 \text{ and } k = 1\\
&\textbf{while}(found == 0)\\
&\quad max = 0\\
&\quad \textbf{for } i = 1, \cdots, M\\
&\qquad b_i = \frac{G_i(j\omega_k) - \bar{G}(j\omega_k)}{\bar{G}(j\omega_k)}\\
&\qquad \text{if } (\text{abs}(a_i) > max)\\
&\qquad\quad max = \text{abs}(b_i)\\
&\quad \textbf{end for}\\
&\quad \text{if}(max > limit)\\
&\qquad found = 1\\
&\qquad \omega_{cr} = \omega_k\\
&\quad k = k + 1\\
&\textbf{end while}
\end{aligned} \tag{3-15}$$

As it was mentioned above, the value of the variable *limit* is upon to the designer to be decided, yet in any case it should be selected with a low value since it describes the degree of similarity that is needed. For example, if we consider that some models are similar for a specific range of frequency only if the absolute value of b_i is below $-40dB$, then *limit* should be selected to be equal to 10^{-2}.

After having determined the critical frequency ω_{cr}, the mean model $\bar{G}(j\omega)$ and the multiple models $G_i(j\omega)$, for $i = 1, \cdots, M$, are used in different ranges of frequency in order to realize the linear inequalities. Specifically, in the interval $[\omega_0, \omega_{cr}]$ the mean model $\bar{G}(j\omega)$ is used, where ω_0 denotes the initial frequency. On the other hand, in the remaining range $[\omega_{cr}, \omega_f]$ the linear constraints are imposed on the multiple models, where ω_f denotes the final frequency that is taken into consideration for the optimization algorithm.

It is stressed that the final number of linear inequalities is not fixed, since it depends on the critical frequency ω_{cr}. Namely, suppose that this frequency corresponds to the N_{cr}^{th} point, out of the N frequency points that are considered in total. Then, the total number of linear inequalities will be $N_{cr} \cdot n_d + (N - N_{cr}) \cdot n_d \cdot M$. In other words, this approach eliminates $N_{cr} \cdot n_d \cdot (M - 1)$ linear inequalities.

3-3 Introducing multiplicative uncertainty

In chapter 2, the theoretical background for synthesis of a fixed-structure controller satisfying nominal performance based on frequency-domain data of the plant was deployed. Next, in chapter 3 and specifically in section 3-1, the nominal performance was extended to robust performance by considering the simultaneous stabilization of multiple models of the same plant. In this section we propose an alternative method for satisfying robust performance. Namely, the uncertainty, which is inherent in every system and so far has been dealt by just considering multiple models, can be described by an additive or a multiplicative term. Additive and multiplicative uncertainty are equivalent, since they differ only in terms of representation, and for that we are going to concentrate on the multiplicative part.

Consider a set Π of M models $G_i(j\omega)$, for $i = 1, \cdots, M$. Our purpose is to describe this set of models by a single transfer function

$$G_p(s) = G(s)(1 + w_I(s)\Delta_I(s)); \quad |\Delta_I(j\omega)| \leq 1, \forall\omega, \tag{3-16}$$

where $G(s)$ denotes the nominal model, $\Delta_I(s)$ is any stable transfer function which at each frequency is not larger than one in magnitude, and $w_I(s)$ is a weight that describes the complex uncertainty and is to be defined.

Following the theory that is developed in [11], we can consider as nominal model the mean of all M models, which can be described as

$$\bar{G}(j\omega) = \frac{\sum_{i=1}^{M} G_i(j\omega)}{M}. \tag{3-17}$$

Then, consider the function

$$q_I(\omega) = \max_{G_i \in \Pi} \left| \frac{G_i(j\omega) - \bar{G}(j\omega)}{\bar{G}(j\omega)} \right|. \tag{3-18}$$

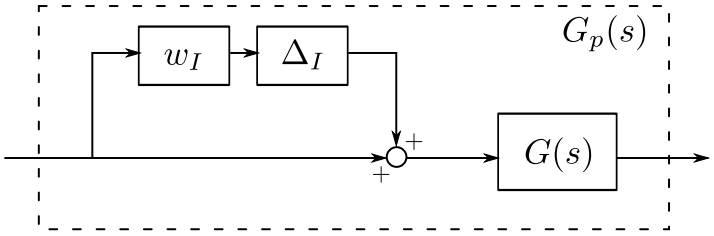

Figure 3-5: Block diagram of $G_p(s)$ representing multiplicative uncertainty

Finally, the weight $w_I(s)$ should be selected such that

$$|w_I(j\omega)| \geq l_I(\omega), \quad \forall\omega \tag{3-19}$$

Given this representation for uncertainty, the configuration of the generalized plant might end up having the form that is illustrated in figure 3-6. The multiplicative uncertainty can be absorbed into the generalized plant in a straight forward manner. Yet, there are some open issues with respect to the realization of the perturbation block Δ_I.

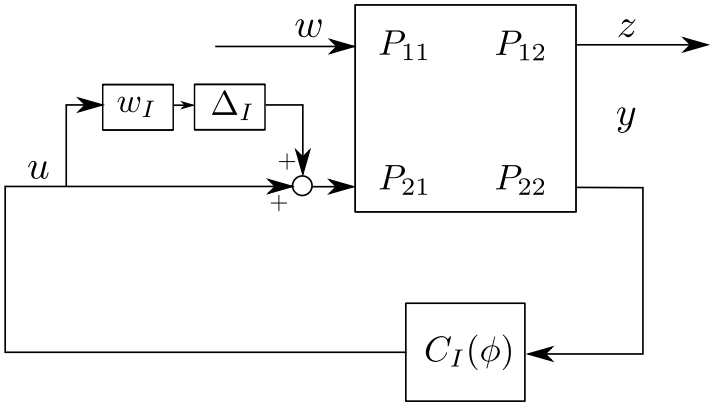

Figure 3-6: Configuration of the generalized plant when multiplicative uncertainty is considered

3-3-1 Realization of Δ_I

Similarly to the case of the performance perturbation Δ_p that was developed in 2-2-3, the perturbation block Δ_I should be manipulated properly so it can be used in the computational algorithm. It holds that, $|\Delta_I(j\omega)| \leq 1, \forall\omega$. Realizing Δ_I in this set would result to an infinite number of realizations, and thus in an infinite number of linear inequalities. This problem can be circumvented by realizing Δ_I within the set that corresponds to the worst case scenario. That is, a significant reduction of the resulting number of linear inequalities can be acquired by realizing Δ_I for which $|\Delta_I(j\omega)| = 1$. As a result, for the realization of this perturbation block we sample n_I points randomly drawn from the unit circle.

Of course, this simplification of the perturbation term is necessary in order to avoid an extreme number of realizations and linear inequalities. Yet, although the amount of models M that are considered for the construction of the multiplicative weight w_I does not affect the final number of inequalities, the number of realizations of Δ_I does affect it. Namely, the number

of linear inequalities that the optimization algorithm is subject to, results to be $n_I \cdot n_d \cdot N$, where n_I denotes the number of realizations of Δ_I, n_d denotes the number of realizations of Δ_p and N denotes the number of frequency points that are considered. When the multiple models that are considered exceed a certain number, introducing a multiplicative uncertainty might be a computationally attractive method. In any case, the performance and efficiency of this approach are to be investigated in a simulation setup.

3-4 An iterative algorithm to optimize H_∞ performance

Up to this point we have followed the optimization scheme suggested in [12], which is explained in this project in 2-2-5 and in 3-1-5. According to that scheme the optimization algorithm is constructed as

$$\begin{aligned} &\min \sum_{k=1}^{m} \phi_k^2 \\ \text{s.t. } &l_n^i(\phi, j\omega) < 0, \quad \forall \omega \in [\omega_n, \omega_{n+1}] \quad i = 1, \cdots, M, \quad n = 1, \cdots, c \\ &l_{\Delta n}^i(\phi, j\omega) < 0, \quad \forall \omega \in [\omega_n, \omega_{n+1}] \quad i = 1, \cdots, M, \quad n = 1, \cdots, c \end{aligned}$$

where c denotes the total number linear constraints and M the total number of models that are considered.

However, it was found through simulations, that were done during working on chapter 4, that the minimization of the sum of the squares of the controller parameters is not optimal with respect to the minimization of $||T_{wz}(\phi, s)||_\infty$, which is the ultimate objective. For example, in many simulations a maximization of $\sum_{k=1}^{m} \phi_k^2$ would lead to a better performance. Yet, in the general case none of the two schemes approaches the optimal performance. Finding a proper argument so as to minimize the infinity norm of the closed loop transfer function remains an open problem and it is going to be investigated in the following paragraphs.

An idea that seems functional in order to deal with this problem is to linearly approximate the norm $||T_{wz}(\phi, s)||$ for a specific frequency. Naturally, we should address the frequency at which the maximum value of $||T_{wz}(\phi, s)||$ appears, so as to find an approximation of its infinity norm. Finding this frequency is not only feasible but also straight forward to calculate as long as frequency-domain data of the plant exist. For sake of simplicity let us denote this frequency point, for a specific combination of stabilizing controller parameters ϕ^*, as ω_m. It is assumed that for a small neighborhood around the stabilizing solution ϕ^*, the infinity norm will still appear at that particular frequency point ω_m, or at a point really close to that. Thus, the infinity norm for this small neighborhood will behave similarly to how the magnitude of the closed loop system will behave, at that particular point. This can be expressed as

$$||T_{wz}(\phi, \omega j)||_\infty \approx ||T_{wz}(\phi, \omega_m j)||, \quad \text{for } \phi \in [\phi^* - \epsilon, \phi^* + \epsilon] \tag{3-20}$$

where ϵ is a sufficiently small constant of appropriate dimensions. Additionally, the behavior of $T_{wz}(\phi, \omega_m j)$ can be expressed analytically with respect to the controller parameters ϕ at this neighborhood, and it is

$$T_{wz}(\phi,\omega_m j) = P_{11}(\omega_m j) + P_{12}(\omega_m j)C_I(\phi,\omega_m j)(I - P_{22}(\omega_m j)C_I(\phi,\omega_m j))^{-1}P_{21}(\omega_m j)$$

The norm of this expression will be nonlinear with respect to the controller parameters ϕ. Let us denote the norm as a function of the parameters and let it be

$$f(\phi,\omega_m j) = ||T_{wz}(\phi,\omega_m j)||. \tag{3-21}$$

The key idea is to linearize this expression around a stabilizing solution ϕ^*. Such a solution exists by default, since it is necessary in order to acquire closed-loop frequency domain data. The linear approximation of $f(\phi,\omega_m j)$ at the point $\phi^* = [\phi_1^*, \cdots, \phi_m^*]$ for $T_{wz}(\phi,\omega_m j)$ can be expressed as

$$\tilde{f}(\phi,\omega_m j) \approx f(\phi^*,\omega_m j) + \left.\frac{\partial f(\phi,\omega_m j)}{\partial \phi_1}\right|_{\phi^*}(\phi_1 - \phi_1^*) + \cdots + \left.\frac{\partial f(\phi,\omega_m j)}{\partial \phi_m}\right|_{\phi^*}(\phi_m - \phi_m^*). \tag{3-22}$$

This expression, let it be denoted as $\tilde{f}(\phi)$, is apparently linear with respect to the controller parameters and thus it can be used as an argument in the optimization scheme, without violating the condition of convexity. The optimization scheme can thus be constructed as follows

$$\begin{aligned} &\min \tilde{f}(\phi) \\ \text{s.t. } &l_n^i(\phi,j\omega) < 0, \quad \forall\omega \in [\omega_n,\omega_{n+1}] \quad i = 1,\cdots,M, \quad n = 1,\cdots,c \\ &l_{\Delta n}^i(\phi,j\omega) < 0, \quad \forall\omega \in [\omega_n,\omega_{n+1}] \quad i = 1,\cdots,M, \quad n = 1,\cdots,c, \end{aligned}$$

which remains a convex optimization problem. Additionally, the optimization is directed towards minimizing an approximation of $||T_{wz}(\phi,s)||_\infty$, and not of a random or intuitive expression. For the sake of clarity and ease of comprehension let us denote the initially stabilizing solution ϕ^* as $\phi^{(0)}$ and the corresponding frequency point ω_m, at which the initial maximum of the closed loop appears, as $\omega_m^{(0)}$. Finally, the first linear approximation of the infinity norm at $\phi^{(0)}$, can be denoted as $\tilde{f}^{(0)}(\phi)$.

After the algorithm converges to some controller parameter values $\phi^{(1)}$, we can again compute the maximizing frequency point $\omega_m^{(1)}$ for the new controller parameters and the function $f^{(1)}(\phi,\omega_m^{(1)}j)$ can be approximated again around the optimized parameters. Next, the linear approximation $\tilde{f}^{(1)}(\phi)$, of the nonlinear approximation $f^{(1)}(\phi,\omega_m^{(1)}j)$ of the infinity norm, can be re-calculated around $\phi^{(1)}$. Then, a new optimization can be performed according to the following optimization scheme

$$\begin{aligned} &\min\max\left(\tilde{f}^{(k)}(\phi)\right) \quad k = 0,1 \\ \text{s.t. } &l_n^i(\phi,j\omega) < 0, \quad \forall\omega \in [\omega_n,\omega_{n+1}] \quad i = 1,\cdots,M, \quad n = 1,\cdots,c \\ &l_{\Delta n}^i(\phi,j\omega) < 0, \quad \forall\omega \in [\omega_n,\omega_{n+1}] \quad i = 1,\cdots,M, \quad n = 1,\cdots,c. \end{aligned}$$

Introducing the minimization of the maximum value of the two, or more, linear approximations corresponds to approximating the behavior of the actual infinity norm, for which we do

not have any analytical expression, by a combination of linear functions. A new stabilizing solution will result from this optimization, which will probably will be optimal with respect to the previous ones. To conclude, we propose an iterative optimization scheme that is based on approximating the behavior of the actual infinity norm of the closed loop by some linear functions that seeks to find a local minimum. Naturally, if the H_∞ norm has a highly non-convex behavior with respect to the controller parameters, then the algorithm will not succeed to find a local minimum. This will happen because minimizing $\max\left(\tilde{f}^{(k)}(\phi)\right)$ might exclude some solutions. In any case, the algorithm explores the behavior of the H_∞ norm and returns the optimal parameters that it finds. This iterative optimization scheme can be summarized by the following algorithm.

Algorithm for the revisited optimization scheme

1. **Input:** Initially stabilizing solution $\phi^{(0)}$, FRF model $G(\omega j)$.
2. Construct linear constraints $l_{\Delta n}(\phi, j\omega)$, $n = 1, \cdots, c$.
3. Find $\omega_m^{(0)}$ for $G(\omega j)$ and calculate $\tilde{f}^{(0)}(\phi)$ for $\phi^{(0)}$.
4. $J^{(0)} \leftarrow ||T_{wz}||_\infty$, when $G(\omega j)$ and $\phi^{(0)}$ are considered
5. $J_{min} \leftarrow J^{(0)}, \quad \phi_{min} \leftarrow \phi^{(0)}$
6. Solve $\min \tilde{f}^{(0)}(\phi), s.t. \quad l_{\Delta n}(\phi, j\omega) \quad n = 1, \cdots, c$ and $i \leftarrow 1$.
7. Find $\phi^{(1)}$ from optimization.
8. $J^{(1)} \leftarrow ||T_{wz}||_\infty$, when $G(\omega j)$ and $\phi^{(1)}$ are considered
9. **If** $J^{(1)} < J_{min}$ **then** $J_{min} \leftarrow J^{(1)}, \quad \phi_{min} \leftarrow \phi^{(1)}$
10. **while** $i < i_{max}$ **do**
11. Find $\omega_m^{(i)}$ for $G(\omega j)$ and calculate $\tilde{f}^{(i)}(\phi)$ for $\phi^{(i)}$.
12. Solve $\min \max \tilde{f}^{(k)}(\phi), s.t. \quad l_{\Delta n}(\phi, j\omega) \quad n = 1, \cdots, c \quad k = 1, \cdots, i.$
13. Find $\phi^{(i+1)}$ from optimization and $i \leftarrow i + 1$.
14. $J^{(i)} \leftarrow ||T_{wz}||_\infty$, when $G(\omega j)$ and $\phi^{(i)}$ are considered
15. **If** $J^{(i)} < J_{min}$ **then** $J_{min} \leftarrow J^{(i)}, \quad \phi_{min} \leftarrow \phi^{(i)}$
16. **end while**
17. **return** ϕ_{min} as optimal controller parameters for the given constraints.
18. **return** J_{min} as optimal infinity norm for the given constraints.

(3-23)

The parameter i_{max} denotes the number of iterations that are going to be performed, and it is a user-defined parameter. After a sufficient number of iterations, the function $\max \tilde{f}^{(k)}(\phi)$ for $k = 1, \cdots, i$, seeks to describe the behavior of the actual infinity norm of the closed-loop transfer function in the convex hull created by the controller parameter solutions $\phi^{(i)}$, each one of which can be also considered a vertex of that hull. Naturally, the algorithm is vulnerable to local minima and local maxima and to deal with that, considering multiple initial controller parameters $\phi^{(0)}$ increases the potential of finding the global minimum. Additionally, this iterative algorithm can be extended for the case of multi-model optimization in a straight forward manner, by considering multiple FRF models when constructing the linear constraints.

The ability of this algorithm to capture the behavior of the actual infinity norm with respect to the controller parameters is better illustrated in chapter 4 and specifically in section 4-3. There, one can see the actual relation between $||T_{wz}(\phi, s)||_\infty$, $f(\phi, \omega_m j)$ and $\tilde{f}(\phi)$ for a given FRF model and specific controller parameters. Moreover, the several stages of the algorithm are described graphically and the corresponding performance is discussed in detail.

3-5 An algorithm for optimal design of linear constraints

Selecting proper linear constraints is rather an important issue. As it will be shown later, in section 4-4-4, the choice of linear constraints is related to the set of controller parameters that will be available for optimal performance. In [12], the selection of the constraints is left to the designer and in fact it is not extremely difficult for a control engineer to come up with some linear functions that will allow frequency-domain optimization of fixed-structure controllers in the way that has been described so far.

However, being intuitive in the constraints' selection introduces some kind of conservatism in the controller design as it will be highlighted in 4-4-4. For this, it is considered important to design an algorithm that will allow an optimized way for designing the linear constraints. In order to do that, an initially stabilizing solution $\phi^{(*)}$ is necessary, and as mentioned previously such a solution does exist by default, since it is needed for the acquisition of frequency-domain data.

3-5-1 Single linear constraint of least conservatism

As mentioned in 3-1-2, the condition for stability relies on the Nyquist plot of the function

$$Q(\phi, j\omega) = 1 - C_I(\phi)P_{22}.$$

Specifically, one should ensure that its Nyquist plot does not encircle the origin. The key idea behind the proposed algorithm for optimal design of linear constraints lies on constructing the constraints that would introduce minimum conservatism on the Nyquist plot of the function $Q(\phi^{(*)}, j\omega)$. This idea can be better understood by considering figure 3-7.

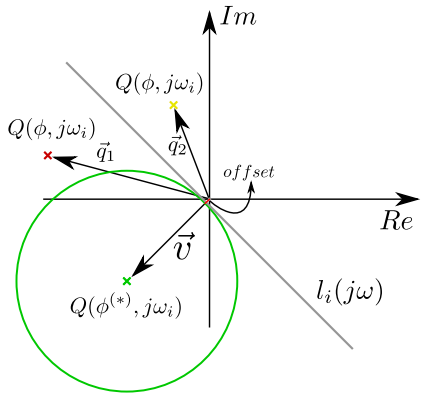

Figure 3-7: Representation of constructing optimal constraints on the Nyquist plot

For each frequency point ω_i, $i = 1, \cdots, N$, where N denotes the total number of frequency points considered, let the Nyquist plot of $Q(\phi^{(*)}, j\omega_i)$ be represented by the point $\{a, b\}$, where $a = \mathrm{Re}\left(Q\left(\phi^*, j\omega_i\right)\right)$ and $b = \mathrm{Im}\left(Q\left(\phi^{(*)}, j\omega_i\right)\right)$. In the context of this algorithm, we consider the least conservative linear constraint, that should be imposed at that frequency point, to be the one that is vertical to the line connecting the point $\{a, b\}$ and the origin. Additionally, such a linear constraint should necessarily have an offset from the origin, so as to allow any potential representation of $Q_\Delta(\phi, j\omega)$ to retain a certain distance from the origin. In figure 3-7 one can see in gray color, what would be the optimal linear constraint for some initial controller parameters $\phi^{(*)}$ and the frequency point ω_i, which is denoted as $l_i(j\omega)$.

Consider the Nyquist plot of the function $Q(\phi, j\omega_i)$, for the i^{th} frequency point and random variables ϕ, which can be denoted as $\vec{q}$. If the corresponding vector of $Q(\phi^{(*)}, j\omega_i)$ is denoted by $\vec{v}$, then the linear constraint that will be imposed can be expressed as

$$\vec{v} \cdot \vec{q} \geq 0.$$

For instance, in figure 3-7 the point $Q(\phi, j\omega_i)$ represented in red, will indeed satisfy the constraint $\vec{v} \cdot \vec{q}_1 \geq 0$, whereas the point $Q(\phi, j\omega_i)$ represented in yellow will not, since it holds that $\vec{v} \cdot \vec{q} < 0$. Finally, this approach can be extended to a multi-model approach in a straight forward manner.

A similar technique in order to construct linear constraints was proposed in [4], yet a desired open loop transfer function was necessary. In our technique, no additional external information is required, apart from an initially stabilizing solution, which actually is available by default.

3-5-2 Complex linear constraints

In the previous subsection we proposed an algorithm that constructs N linear constraints, that is, one per frequency point, based on the initially stabilizing controller parameter ϕ^*. However, designing the linear constraints based on an initial value of the controller parameters might still induce some conservatism. As it will be illustrated more clearly in section 4-4, linear constraints of the form that was presented in the previous paragraph is possible to make the optimization algorithm more biased to converge to controller parameters' combinations that are relatively "close" to the initially stabilizing solution.

For this reason, it is considered important to explore an improved version of the algorithm that constructs the linear constraints. The main principle remains the same, that is, to construct the linear constraint per frequency point that induces the least amount of conservatism. Yet, in this improved version of the algorithm, we propose a complex constraint, as opposed to the algorithm of the previous section, which proposed a single constraint per frequency point. With the term complex, it is meant that a combination of two linear constraints, $l^{(1)}(j\omega)$ and $l^{(2)}(j\omega)$, will be imposed per frequency point. In this way, one can ensure that the origin is not encircled, however by constraining the minimum amount of area of the Nyquist diagram. To illustrate better this idea, the figure 3-8 offers an enlightening description of the key idea of this algorithm.

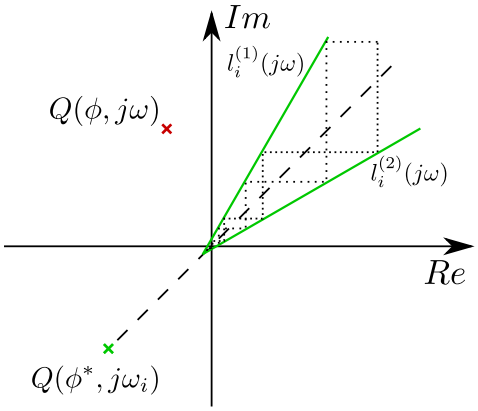

Figure 3-8: Representation of constructing complex optimal constraints on the Nyquist plot

As it can be noticed, a combination of two linear constraints is imposed in each frequency point and $Q(\phi, j\omega)$ in red color, should satisfy at least one of them. The combination of the two linear constraints prevents the value of $Q(\phi, j\omega)$ from entering the dashed area between $l^{(1)}(j\omega)$ and $l^{(2)}(j\omega)$. As a result, the area of the diagram that would imply instability is minimized and thus the introduced conservatism is minimized as well.

However, although this approach seems promising, it comes with a rather significant barrier. The set of figure 3-8 which satisfies the desired constraints is a non convex set. Consequently, imposing the complex constraint, that either of the two linear constraints should be satisfied, results to non convex optimization. Circumventing this barrier is not trivial and in the context of this project it still remains an open problem.

3-6 An algorithm for optimal construction of linear constraints and optimal controller parameters' design

In sections 3-4 and 3-5-1 we have proposed two innovative algorithms. Specifically, in 3-4 we have proposed an iterative algorithm, which attempts to find the controller parameters' combination that minimizes the infinity norm of a particular FRF model, and thus approaches the optimal controller parameters. Additionally, in 3-5-1 we have proposed an algorithm that constructs N linear constraints, one per frequency point that is considered, which induce the least possible amount of conservatism on the Nyquist plot of $Q(\phi^{(*)}, j\omega)$, where $\phi^{(*)}$ is an initially stabilizing solution.

As mentioned previously, an initially stabilizing solution $\phi^{(*)}$ exists by default, since it is necessary for the acquisition of FRF models. However, as it will be more clear in section 4-4-4, even the updated linear constraints, designed based on an initially stabilizing solution, do induce some conservatism which excludes a set of stabilizing solutions from the optimization algorithm. The algorithm that is proposed in this section is based on the idea that some improved linear constraints will potentially offer to the optimization algorithm more flexibility on finding optimal solutions for the minimization of the infinity norm. In other words, we propose an iterative algorithm that combines the two algorithms developed in 3-4 and 3-5-1. The most important features and principles this technique are presented in the following algorithm.

Algorithm for finding optimal linear constraints and controller parameters

1. **Input:** Initially stabilizing solution $\phi^*_{(0)}$, FRF model $G(\omega j)$.
2. Construct linear constraints $l_{\Delta n}(\phi, j\omega)$, $n = 1, \cdots, N$ based on $\phi^*_{(0)}$.
3. $J^{(0,0)} \leftarrow ||T_{wz}||_\infty$, when $G(\omega j)$ and $\phi^*_{(0)}$ are considered
4. $J_{min} \leftarrow J^{(0,0)}, \quad \phi_{min} \leftarrow \phi^*_{(0)}$
5. Find $\omega_m^{(0,0)}$ for $G(\omega j)$ and calculate $\tilde{f}^{(0,0)}(\phi)$ for $\phi^*_{(0)}$.
6. Solve $\min \tilde{f}^{(0,0)}(\phi), s.t. \quad l_{\Delta n}(\phi, j\omega) \quad n = 1, \cdots, N$ and $i \leftarrow 1$.
7. Find $\phi^{(1,0)}$ from optimization.
8. $J^{(1,0)} \leftarrow ||T_{wz}||_\infty$, when $G(\omega j)$ and $\phi^{(1,0)}$ are considered
9. **If** $J^{(1,0)} < J_{min}$ **then** $J_{min} \leftarrow J^{(1,0)}, \quad \phi_{min} \leftarrow \phi^{(1,0)}$
10. **while** $i < i_{max}$ **do**
11. Find $\omega_m^{(i,0)}$ for $G(\omega j)$ and calculate $\tilde{f}^{(i,0)}(\phi)$ for $\phi^{(i,0)}$.
12. Solve $\min \max \tilde{f}^{(k,0)}(\phi), s.t. \quad l_{\Delta n}(\phi, j\omega) \quad n = 1, \cdots, N \quad k = 1, \cdots, i.$
13. Find $\phi^{(i+1,0)}$ from optimization and $i \leftarrow i + 1$.
14. $J^{(i,0)} \leftarrow ||T_{wz}||_\infty$, when $G(\omega j)$ and $\phi^{(i,0)}$ are considered
15. **If** $J^{(i,0)} < J_{min}$ **then** $J_{min} \leftarrow J^{(i,0)}, \quad \phi_{min} \leftarrow \phi^{(i,0)}$
16. **end while**
17. $\phi^*_{(1)} \leftarrow \phi^{(i-1)}$, $i \leftarrow 0$, and $p \leftarrow 1$
18. **while** $p < p_{max}$ **do**
19. $\phi^{(i,p)} \leftarrow \phi^*_{(p)}$
20. Construct linear constraints $l_{\Delta n}(\phi, j\omega)$, $n = 1, \cdots, N$ based on $\phi^*_{(p)}$.
21. $J^{(i,p)} \leftarrow ||T_{wz}||_\infty$, when $G(\omega j)$ and $\phi^*_{(p)}$ are considered
22. **If** $J^{(i,p)} < J_{min}$ **then** $J_{min} \leftarrow J^{(i,p)}, \quad \phi_{min} \leftarrow \phi^*_{(p)}$
23. Find $\omega_m^{(i,p)}$ for $G(\omega j)$ and calculate $\tilde{f}^{(i,p)}(\phi)$ for $\phi^{(i,p)}$.
24. Solve $\min \tilde{f}^{(i,p)}(\phi), s.t. \quad l_{\Delta n}(\phi, j\omega) \quad n = 1, \cdots, N$
25. Find $\phi^{(i+1,p)}$ from optimization and $i \leftarrow i + 1$
26. $J^{(i,p)} \leftarrow ||T_{wz}||_\infty$, when $G(\omega j)$ and $\phi^{(i,p)}$ are considered
27. **If** $J^{(i,p)} < J_{min}$ **then** $J_{min} \leftarrow J^{(i,p)}, \quad \phi_{min} \leftarrow \phi^{(i,p)}$
28. **while** $i < i_{max}$ **do**
29. Find $\omega_m^{(i,p)}$ for $G(\omega j)$ and calculate $\tilde{f}^{(i,p)}(\phi)$ for $\phi^{(i,p)}$.
30. Solve $\min \max \tilde{f}^{(k,p)}(\phi), s.t. \quad l_{\Delta n}(\phi, j\omega) \quad n = 1, \cdots, N \quad k = 1, \cdots, i.$
31. Find $\phi^{(i+1,p)}$ from optimization and $i \leftarrow i + 1$.
32. $J^{(i,p)} \leftarrow ||T_{wz}||_\infty$, when $G(\omega j)$ and $\phi^{(i,p)}$ are considered

33. **If** $J^{(i,p)} < J_{min}$ **then** $J_{min} \leftarrow J^{(i,p)}, \quad \phi_{min} \leftarrow \phi^{(i,p)}$
34. **end while**
35. **return** J_{min} as optimal infinity norm for the specific constraints.
36. ϕ_{min} :optimal controller parameters for the specific constraints.
37. $i \leftarrow 0$ and $p \leftarrow p + 1$
38. **end while**
39. **return** ϕ_{min} as optimal controller parameters for the optimal constraints.
40. **return** J_{min} as optimal infinity norm for the optimal constraints.

It is stressed that the proposed algorithm can be extended to the multi-model approach in a straight forward manner. Simply, when considering the construction of linear constraints based on a single FRF model, one should consider linear constraints for as many models as desired. That is, the step

$$\text{Construct linear constraints } l_{\Delta n}(\phi, j\omega),\ n = 1, \cdots, N \text{ based on } \phi_{(0)}^{(*)},$$

should be extended to the steps described below.

1. **Input:** M FRF models, denoted as $G_{(i)}(j\omega)$, $i = 1, \cdots, M$.
2. **for** $i = 1 : M$
3. Construct linear constraints $l^i_{\Delta n}(\phi, j\omega)$, $n = 1, \cdots, N$ based on $\phi^*_{(0)}$ and $G_{(i)}(j\omega)$.
4. **Constraints** $\leftarrow$ **Constraints** $+ l^i_{\Delta n}(\phi, j\omega), \quad$ for $\ n = 1, \cdots, N$.
5. **end**

In the following chapter we employ a stable plant in order to evaluate the performance and efficiency of the proposed algorithms. Moreover, we present a detailed comparison with the corresponding performance of the default algorithm.

Chapter 4

Simulations and Results

Up to this point we have developed the main algorithm that facilitates frequency domain optimization of fixed-structure controllers. Additionally, an extension that enables the manipulation of multiple models has been presented, which is a significant contribution of this project. Moreover, the potential of reducing the size of the optimization problem has been explored, by eliminating a number of linear inequalities, as it was discussed in section 3-2. Additionally, in section 3-3 the introduction of multiplicative uncertainty was discussed as an alternative to the multi-model approach. Finally, in sections 3-4 and 3-6 the main contribution of this project is presented, which is an original iterative algorithm that seeks to optimize the H_∞ performance of the closed-loop system and in addition it constructs optimal linear constraints. In this chapter, we employ a simple plant and a corresponding Simulink model in order to apply the methods that have been presented so far.

4-1 System and dynamics

In this section we present the system that is going to be used for the implementation of the proposed techniques. Additionally, we describe the procedure of acquiring the frequency-domain data and present the configuration of the generalized plant that is going to be considered during the experiments.

4-1-1 Dynamics of the plant

The system that is used for the implementation of the proposed algorithm is a double-mass, spring, damper system, which is presented in figure 4-1. In the figure, x_1 and x_2 denote the position of the mass m_1 and m_2, respectively. Additionally, k denotes the constant of the spring and d denotes the constant of the damper. Finally, F stands for the force, which is the input of the system. For the dynamics of the system it holds

$$\begin{cases} m_1\ddot{x}_1(t) + d\left(\dot{x}_1(t) - \dot{x}_2(t)\right) + k\left(x_1(t) - x_2(t)\right) = f(t) \\ m_2\ddot{x}_2(t) + d\left(\dot{x}_2(t) - \dot{x}_1(t)\right) + k\left(x_2(t) - x_1(t)\right) = 0 \end{cases} \tag{4-1}$$

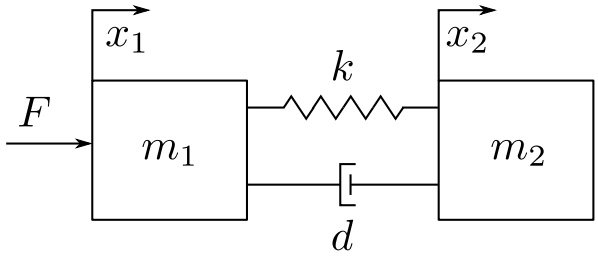

Figure 4-1: Diagram of a double-mass-spring-damper system

After a Fourier transformation, equation 4-1 becomes

$$\begin{cases} m_1 s^2 X_1(s) + d\,(sX_1(s) - sX_2(s)) + k\,(X_1(s) - X_2(s)) = F(s) \\ m_2 s^2 X_2(s) + d\,(sX_2(s) - sX_1(s)) + k\,(X_2(s) - X_1(s)) = 0 \end{cases} \tag{4-2}$$

From the second equation of 4-2, it can be seen that

$$X_1(s) = \frac{m_2 s^2 + ds + k}{ds + k} X_2(s). \tag{4-3}$$

After substituting in the first equation of 4-2, the transfer function between the input F and the position X_2 can be expressed as

$$G(s) = \frac{X_2(s)}{F(s)} = \frac{ds + k}{m_1 m_2 s^4 + (m_1 + m_2) d s^3 + (m_1 + m_2) k s^2}. \tag{4-4}$$

Apparently, $G(s)$ has no right-half plane (RHP) poles, which implies that the corresponding generalized plant will be stable. The values of the parameters of the system that are used are $m_1 = m_2 = k = 1$ and $d = 0.05$. The bode plot of the transfer function $G(s)$ is illustrated in figure 4-2.

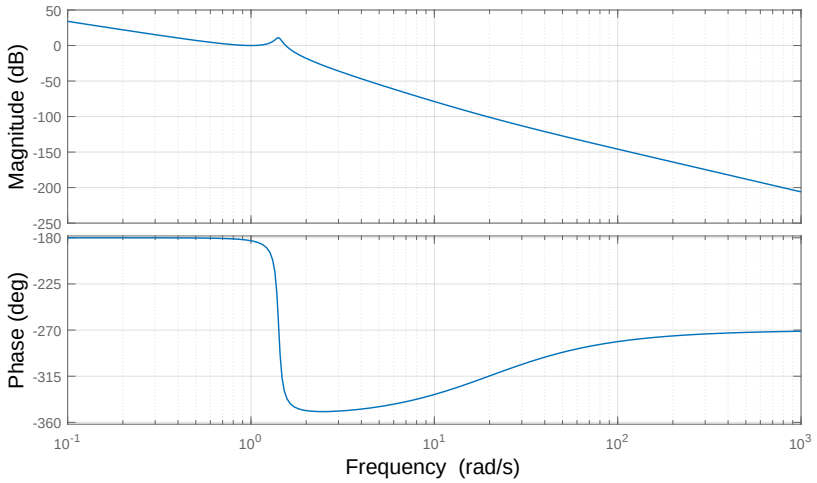

Figure 4-2: Bode plot of transfer function between input F and position X_2

4-1-2 System configuration

The implementation of the algorithm requires setting up the generalized plant. In other words, we need to configure the closed loop system and clarify the purpose of the controller design. We are interested in imposing a bound on the sensitivity function and for that we employ a second order performance weight of the form

$$W_p(s) = \alpha \frac{s^2/M_p^2 + 2\beta_p \omega_B s + \omega_B^2}{s^2 + 2\beta_p A_p \omega_B s + (A_p \omega_B)^2}, \tag{4-5}$$

where $\alpha = 0.7$, $\beta_p = 0.3, M_p = 2, A_p = 1 \cdot 10^{-3}$ and $\omega_B = 0.1$. Moreover, the nature of the plant requires a PD controller so as to be stabilized, and thus the controller is selected to be $C_I(\phi, s) = \frac{k_p + k_d s}{0.01s+1}$, where the parameter vector ϕ contains the proportional and derivative gains k_p and k_d. The complete form of the generalized plant can be seen in figure 4-3.

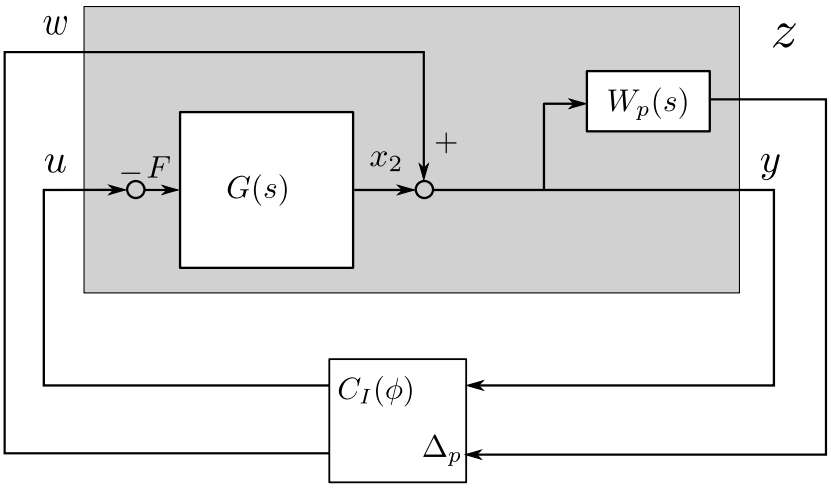

Figure 4-3: Configuration of the generalized plant

Given this form, the generalized plant is expressed as

$$\begin{bmatrix} z \\ y \end{bmatrix} = \begin{bmatrix} W_p(s) & -W_p(s)G_2(s) \\ I & -G_2(s) \end{bmatrix} \begin{bmatrix} w \\ u \end{bmatrix}. \tag{4-6}$$

4-1-3 Frequency-domain data

The implementation of the algorithm is based on frequency-domain data of the plant in the form of Frequency Response Function (FRF) measurements. The transfer function $G(s)$ is open loop unstable which implies that an application of FRF measurements is not feasible in the open loop. Instead, the experiment for the acquisition of data should be performed in a closed loop configuration. Naturally, an initially stabilizing controller is necessary for such an experiment. In the context of a simulation based experiment, such a controller can be found easily by considering the bode plot of the plant. In the general case of a practical application, given that the plant is initially totally unknown, the designer can refer to a theoretical model of the plant in order to find some initially stabilizing values for the controller parameters.

In our system, the controller parameters that satisfied closed loop stability for the FRF experiments are $k_p = 0.2$ and $k_d = 0.15$. The block diagram of the closed loop configuration that was used in Simulink in order to acquire frequency-domain data is illustrated in figure 4-4.

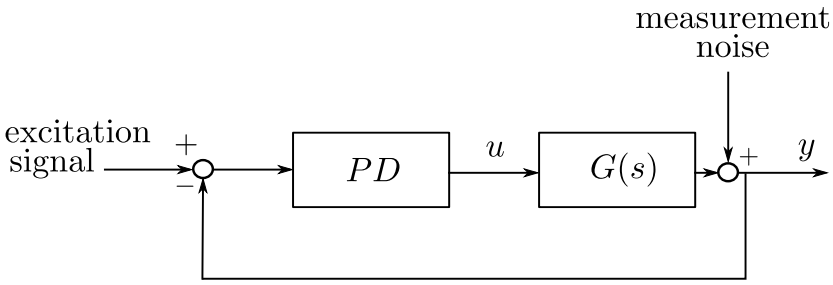

Figure 4-4: Configuration of the closed loop in Simulink for data acquisition

As it can be seen, there is a signal containing white noise that functions as measurement noise. During the experiments for the acquisition of data, the amplitude of this signal ranged between 10^{-5} and 10^{-4}. As an input excitation a sinestream signal was used, containing 400 frequencies logarithmically located in the interval $[0.1, 10] rad/sec$, with amplitude ranging between 10^{-3} and 10^{-2}. After acquiring data concerning the closed loop, the data of the plant were extracted. Specifically, 10 experiments were performed and the corresponding bode plots of the acquired data are illustrated in figure 4-5.

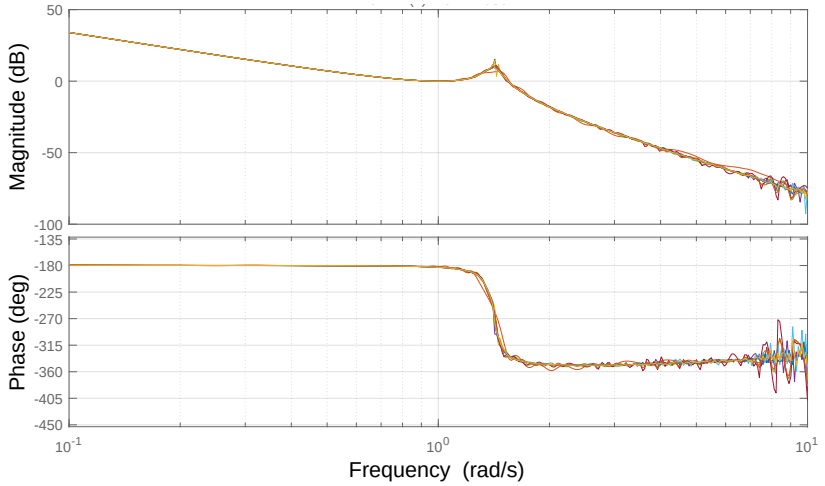

Figure 4-5: Bode plot of 10 FRF measurements

4-1-4 Multiplicative uncertainty

In the case that a multiplicative uncertainty is used in order to robustify the controller design, a different configuration of the generalized plant should be taken into consideration. This form is illustrated in figure 4-6, where as it can be seen the branch containing the uncertainty block has been absorbed into the generalized plant.

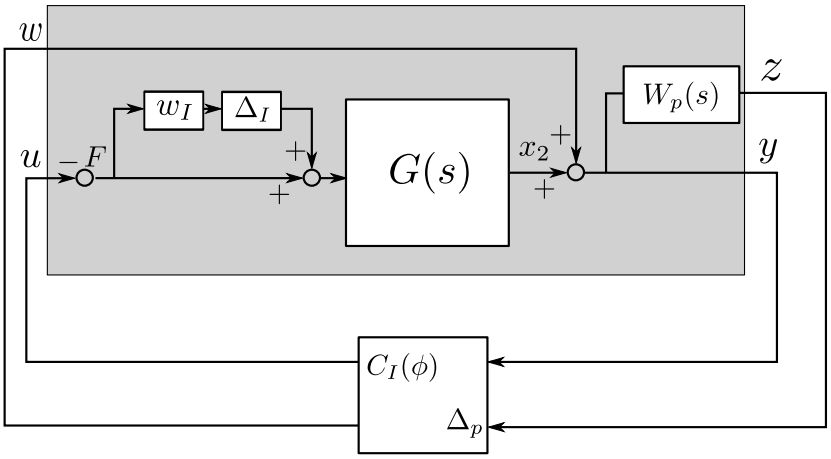

Figure 4-6: Configuration of the generalized plant with multiplicative uncertainty

Of course, the complex weight w_I should be determined. As described in section 3-3, the complex weight is subject to the FRF models that are acquired. Let's consider the mean of all 10 models, denoted as $\bar{G}(j\omega)$, to be the nominal model. It will be

$$\bar{G}(j\omega) = \frac{\sum_{i=1}^{10} G_i(j\omega)}{10}. \tag{4-7}$$

and its bode plot can be seen in figure 4-7.

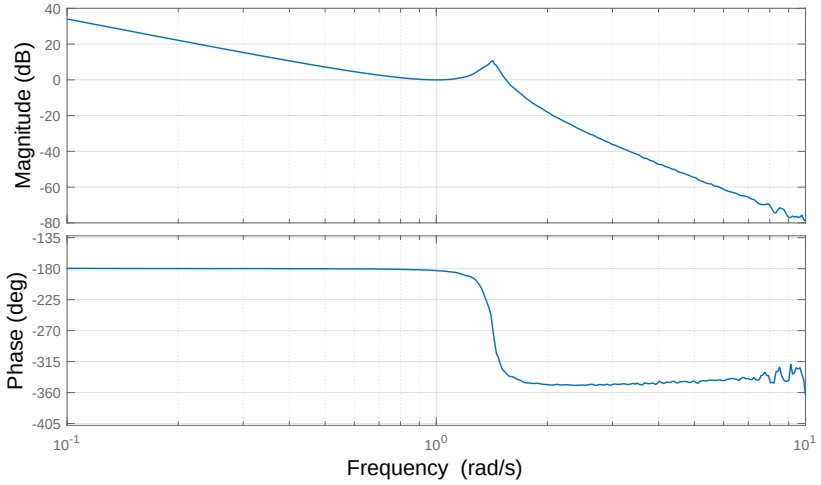

Figure 4-7: Bode plot of the mean of all models

Then, we are interested in the function $q_I(\omega)$, which is expressed as

$$q_I(\omega) = \max_{G_i} \left| \frac{G_i(j\omega) - \bar{G}(j\omega)}{\bar{G}(j\omega)} \right|, \quad i = 1, \cdots, 10. \tag{4-8}$$

Finally, $w_I(s)$ should be selected such that it satisfies the relation $|w_I(j\omega)| \geq q_I(\omega)$. Thus, we propose a fourth order weight transfer function that is expressed as

$$w_I(s) = \frac{0.03\,(10s^2 + 2s + 1.8)}{s^2 + 0.5s + 2.2} \frac{s^2 + 10s + 70}{s^2 + 2s + 70}, \tag{4-9}$$

where as it can be seen, the second fraction describes a notch filter that enhances the magnitude of $w_I(s)$ at the frequency $8.33 rad/sec$. The magnitude plot of $w_I(s)$ in bold purple color, together with the relative errors related to the function $q_I(\omega)$ are illustrated in figure 4-8. As it can be seen the condition $|w_I(j\omega)| \geq q_I(\omega)$ holds for the entire range of frequencies.

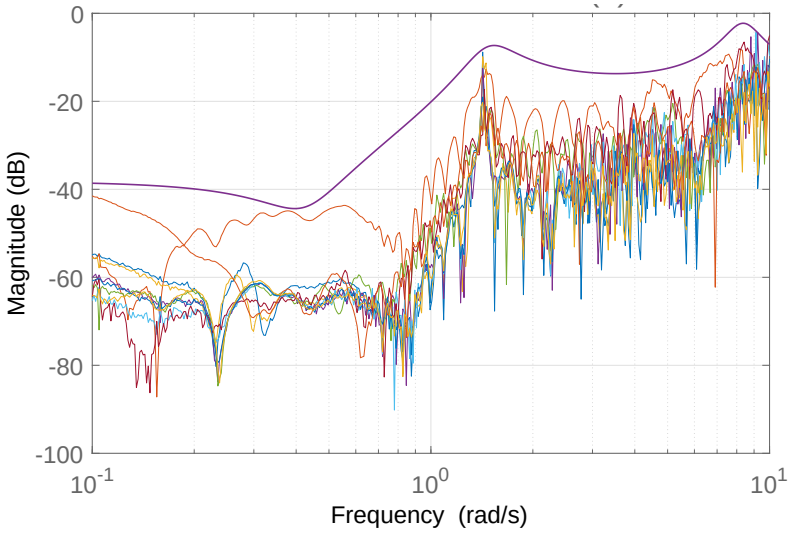

Figure 4-8: Magnitude plot of the weight transfer function $w_I(s)$ and the relative errors related to the function $q_I(\omega)$

4-2 Default, single-model optimization with manually selected constraints

In this section we employ the default algorithm, deployed in chapter 2 and proposed by [12], in order to synthesize a fixed-structure controller that satisfies stability and performance conditions for the double-mass, spring, damper system. All the simulations in this project, were performed in matlab and by making use of the YALMIP toolbox [5]. During the optimization procedures that follow in this section of the project, the implementation of the algorithm is subject to a single FRF model. Additionally, the performance of the resulting controllers will be evaluated with respect to FRF models, as well as with respect to the actual model $G(s)$ expressed as a transfer function.

It is first important to define the linear constraints that are active in the different frequency ranges in the interval $[0.1, 10] rad/sec$. As it was mentioned in the previous section, for stability we employ three linear constraints which are expressed as

$$\begin{aligned} l_1: &\quad \mathrm{Im}\left(Q(j\omega)\right) + 0.2\,\mathrm{Re}\left(Q(j\omega)\right) - 0.001 < 0 \quad \text{for} \quad \omega < 0.16 \\ l_2: &\quad \mathrm{Im}\left(Q(j\omega)\right) - 0.05\,\mathrm{Re}\left(Q(j\omega)\right) + 0.001 < 0 \quad \text{for} \quad 0.16 \leqslant \omega \leqslant 0.20 \\ l_3: &\quad -\mathrm{Im}\left(Q(j\omega)\right) - 5\,\mathrm{Re}\left(Q(j\omega)\right) + 0.001 < 0 \quad \text{for} \quad \omega > 0.20. \end{aligned} \tag{4-10}$$

Additionally, the linear constraints that are imposed to ensure performance are expressed as

$$\begin{aligned} l_{\Delta 1}: &\quad \mathrm{Im}\left(Q_\Delta(j\omega)\right) + 0.2\,\mathrm{Re}\left(Q_\Delta(j\omega)\right) - 0.001 < 0 \quad \text{for} \quad \omega < 0.16 \\ l_{\Delta 2}: &\quad \mathrm{Im}\left(Q_\Delta(j\omega)\right) - 0.05\,\mathrm{Re}\left(Q_\Delta(j\omega)\right) + 0.001 < 0 \quad \text{for } 0.16 \leqslant \omega \leqslant 0.20 \\ l_{\Delta 3}: &\quad -\mathrm{Im}\left(Q_\Delta(j\omega)\right) - 5\,\mathrm{Re}\left(Q_\Delta(j\omega)\right) + 0.001 < 0 \quad \text{for} \quad \omega > 0.20. \end{aligned} \tag{4-11}$$

Apparently, the resulting linear inequalities that concern stability are more conservative than the ones concerning performance. For that, if the objective is to synthesize a controller that satisfies the performance criterion, it suffices to consider only the linear inequelities that are related with performance. In this case, according to [12] the optimization algorithm can be summarized in the following optimization scheme

$$\begin{aligned} &\min k_p^2 + k_d^2 \\ \text{s.t. } &l_{\Delta 1}, \quad \forall \omega \in [0.1, 0.16] rad/sec \\ &l_{\Delta 2}, \quad \forall \omega \in [0.16, 0.20] rad/sec \\ &l_{\Delta 3}, \quad \forall \omega \in [0.20, 10] rad/sec. \end{aligned} \tag{4-12}$$

4-2-1 Evaluating on the actual plant

In the context of this subsection, we performed the optimization algorithm individually, for all 10 FRF models that were acquired for this purpose, considering the default optimization scheme, and evaluated the resulting controllers on the actual plant, as if it was available for testing.

For the case that the optimization scheme proposed in [12] is used, the controller parameters together with the corresponding value of the infinity norm of the closed-loop transfer function T_{wz} can be seen in the following table 4-1.

s.t.	1	2	3	4	5	6	7	8	9	10
k_p	0.0521	0.0516	0.0515	0.0515	0.0516	0.0513	0.0515	0.0515	0.0517	0.0522
k_d	0.0881	0.0885	0.0889	0.0887	0.0886	0.0885	0.0885	0.0886	0.0859	0.0879
$\|\|T_{wz}\|\|_\infty$	1.0649	1.0691	1.0577	1.0599	1.0609	1.0631	1.0621	1.0607	1.0963	1.0681

Table 4-1: Table containing the resulting controller parameters and the corresponding evaluation on the actual system

Of course, in practice the actual plant will not be available for evaluating any controller parameters. For this reason we performed evaluations of the corresponding controller parameters on other FRF models. These evaluations are presented in the following subsection.

4-2-2 Evaluating on the FRF models

Although it seems natural to evaluate the resulting controller of each optimization on the actual plant $G(s)$ expressed as a transfer function, it violates the assumption that $G(s)$ is practically unknown. As a result, even though $G(s)$ offers an objective evaluation of the

result, it is decided to evaluate the result of each optimization with respect to different FRF models as well. The results of the evaluation for the default optimization scheme can be seen in table 4-2. The integer numbers on the first row indicate the FRF model that was considered by the optimization algorithm. Respectively, the integer numbers on the first column of the table indicate the FRF model that was used in order to evaluate the corresponding controller parameter.

	1	2	3	4	5	6	7	8	9	10
1	0.9987	0.9967	0.9931	0.9953	0.9955	0.9992	0.9976	0.9966	1.0263	1.0003
2	0.9944	0.9922	0.9880	0.9903	0.9911	0.9936	0.9925	0.9964	1.0216	0.9961
3	0.9979	0.9959	0.9917	0.9940	0.9947	0.9976	0.9962	0.9942	1.0254	0.9995
4	0.9959	0.9939	0.9898	0.9920	0.9928	0.9947	0.9942	0.9975	1.0233	0.9975
5	0.9956	0.9935	0.9894	0.9916	0.9924	0.9954	0.9938	0.9924	1.0229	0.9972
6	0.9943	0.9923	0.9884	0.9906	0.9912	0.9944	0.9928	0.9924	1.0217	0.9959
7	0.9942	0.9921	0.9880	0.9902	0.9910	0.9933	0.9925	0.9910	1.0215	0.9958
8	0.9953	0.9933	0.9897	0.9919	0.9921	0.9958	0.9941	0.9975	1.0227	0.9969
9	0.9666	0.9645	0.9606	0.9627	0.9635	0.9660	0.9648	0.9674	0.9922	0.9682
10	0.9956	0.9935	0.9894	0.9916	0.9924	0.9951	0.9938	0.9927	1.0229	0.9972

Table 4-2: Evaluation table for the minimization scheme. Each column corresponds to a different design, and the rows describe which FRF model the controller is evaluated on.

It is understandable that a 10×10 table is not very easy to analyze. For that it is considered useful to add some additional table which will contain the mean of all evaluations for each controller design. Thus, in the following table one can see the controller parameters resulting from an optimization subject to a specific FRF model, together with the average value of $||T_{wz}||_\infty$ from evaluations on other FRF models. For the default optimization scheme this table is illustrated in 4-3.

Design s.t.	1	2	3	4	5	6	7	8	9	10
k_p	0.0521	0.0516	0.0515	0.0515	0.0516	0.0513	0.0515	0.0515	0.0517	0.0522
k_d	0.0881	0.0885	0.0889	0.0887	0.0886	0.0885	0.0885	0.0886	0.0859	0.0879
$\|\|\tilde{T}_{wz}\|\|_\infty$	0.9928	0.9907	0.9868	0.9890	0.9896	0.9925	0.9912	0.9918	1.020	0.9944

Table 4-3: Evaluation table containing the means of evaluations of controller parameters on other FRF models

From a first look on tables 4-2 and 4-3 one can observe that they constitute a trusty approximation of the table 4-1, containing the evaluations of the controller parameters on the actual plant. However, there is an eye-catching difference, which is that all the infinity norm values on table 4-1 are slightly higher than 1, and thus failing to satisfy $||T_{wz}||_\infty \leq 1$, whereas the corresponding values on table 4-3 are in general slightly lower than 1. This difference is attributed to the fact that this default optimization algorithm converges to a conservative

solution that simply satisfies the specific linear constraints that it is subject to. However, apparently, it is not implied that this conservative solution will satisfy the performance criterion for the actual plant neither for other FRF models.

A prominent example that highlights this behavior is the controller parameters' combination that results from optimization subject to the 9^{th} FRF model. The evaluation of this controller on other FRF models is presented on the 10^{th} column of table 4-2, that is, the column below number 9. In this column one can see the evaluation of the controller with parameters $k_p = 0.0517$ and $k_d = 0.0859$, on the 10 models. As it can be seen, the only value of this column that is lower than 1 is the one corresponding to evaluation on the 9^{th} FRF model itself. In other words, the combination $k_p = 0.0517$ and $k_d = 0.0859$ satisfies the constraints built for the 9^{th} model. However it does not satisfy the constraints for any other model. In general, all the values on the diagonal of table 4-2, will have by default an infinity norm value lower than 1, given that the corresponding optimization has converged. Nevertheless, this optimization scheme ensures in no way that the resulting controller parameters will be performing satisfactorily. For this reason, it is interesting to examine the corresponding perforance of the refined optimization scheme that was proposed in section 3-4. This examination is presented in the following section.

A graphical representation of the Nyquist plot of the function Q and the corresponding Q_Δ, including the linear constraints that we employed, is presented in figure 4-9.

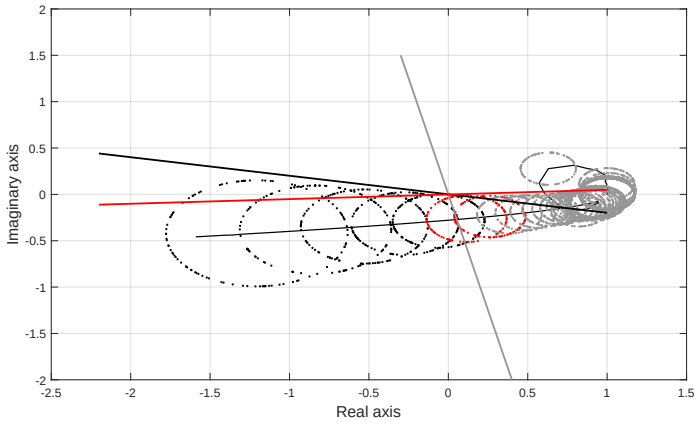

Figure 4-9: Nyquist plot of Q and Q_Δ for the 5^{th} FRF model, with $k_p = 0.0516$ and $k_d = 0.0886$

4-3 Iterative, single-model optimization s.t. manually selected constraints

In this section we employ the refined, iterative algorithm, that was proposed in 3-4, in order to synthesize a fixed-structure controller that satisfies stability and performance conditions for the double-mass, spring, damper system. Similarly to the previous section, during optimization procedures that follow, the implementation of the algorithm is subject to a single FRF model. Additionally, the performance of the resulting controllers will be evaluated with respect to FRF models, as well as with respect to the actual model $G(s)$ expressed as a transfer function.

4-3-1 Explanation of the basic idea of the algorithm

Let us recall the iterative algorithm, proposed in 3-4.

Algorithm for the revisited optimization scheme

1. **Input:** Initially stabilizing solution $\phi^{(0)}$, FRF model $G(\omega j)$.
2. Construct linear constraints $l_{\Delta n}(\phi, j\omega)$, $n = 1, \cdots, c$.
3. Find $\omega_m^{(0)}$ for $G(\omega j)$ and calculate $\tilde{f}^{(0)}(\phi)$ for $\phi^{(0)}$.
4. $J^{(0)} \leftarrow ||T_{wz}||_\infty$, when $G(\omega j)$ and $\phi^{(0)}$ are considered
5. $J_{min} \leftarrow J^{(0)}, \quad \phi_{min} \leftarrow \phi^{(0)}$
6. Solve $\min \tilde{f}^{(0)}(\phi), s.t. \quad l_{\Delta n}(\phi, j\omega) \quad n = 1, \cdots, c$ and $i \leftarrow 1$.
7. Find $\phi^{(1)}$ from optimization.
8. $J^{(1)} \leftarrow ||T_{wz}||_\infty$, when $G(\omega j)$ and $\phi^{(1)}$ are considered
9. **If** $J^{(1)} < J_{min}$ **then** $J_{min} \leftarrow J^{(1)}, \quad \phi_{min} \leftarrow \phi^{(1)}$
10. **while** $i < i_{max}$ **do**
11. Find $\omega_m^{(i)}$ for $G(\omega j)$ and calculate $\tilde{f}^{(i)}(\phi)$ for $\phi^{(i)}$.
12. Solve $\min \max \tilde{f}^{(k)}(\phi), s.t. \quad l_{\Delta n}(\phi, j\omega) \quad n = 1, \cdots, c \quad k = 1, \cdots, i.$
13. Find $\phi^{(i+1)}$ from optimization and $i \leftarrow i + 1$.
14. $J^{(i)} \leftarrow ||T_{wz}||_\infty$, when $G(\omega j)$ and $\phi^{(i)}$ are considered
15. **If** $J^{(i)} < J_{min}$ **then** $J_{min} \leftarrow J^{(i)}, \quad \phi_{min} \leftarrow \phi^{(i)}$
16. **end while**
17. **return** ϕ_{min} as optimal controller parameters for the given constraints.
18. **return** J_{min} as optimal infinity norm for the given constraints.

The linear constraints l_Δ that are active in the different frequency ranges in the interval $[0.1, 10] rad/sec$ remain the same as previously and are expressed as

$$\begin{array}{lll} l_{\Delta 1}: & \mathrm{Im}\left(Q_\Delta(j\omega)\right) + 0.2\,\mathrm{Re}\left(Q_\Delta(j\omega)\right) - 0.001 < 0 & \text{for} \quad \omega < 0.16 \\ l_{\Delta 2}: & \mathrm{Im}\left(Q_\Delta(j\omega)\right) - 0.05\,\mathrm{Re}\left(Q_\Delta(j\omega)\right) + 0.001 < 0 & \text{for } 0.16 \leqslant \omega \leqslant 0.20 \\ l_{\Delta 3}: & -\mathrm{Im}\left(Q_\Delta(j\omega)\right) - 5\,\mathrm{Re}\left(Q_\Delta(j\omega)\right) + 0.001 < 0 & \text{for} \quad \omega > 0.20, \end{array} \tag{4-13}$$

whereas the corresponding linear constraints referring to stability are omitted, since they are more conservative than the ones that are related with performance. Given an initially stabilizing solution $\phi^{(0)}$, that is a stabilizing combination of k_p and k_d, and a particular FRF model, denoted as $G(\omega j)$, one should first calculate the frequency $\omega_m^{(0)}$ at which the maximum magnitude of the closed loop, with controller parameters $\phi^{(0)}$, appears. That is, the frequency at which the infinity norm, denoted as $J^{(0)}$, appears for this particular controller. In general, an analytical expression of the infinity norm of the closed loop with respect to the controller parameters does not exist. However, under the assumption that, for a small

neighborhood around $\phi^{(0)}$ the infinity norm appears in the same frequency point $\omega_m^{(0)}$, one can calculate an analytical expression of the behavior of the magnitude of the closed loop at this particular frequency. This behavior is described by the nonlinear function $f^{(0)}(\phi, \omega_m^{(0)} j)$. Next, a linear approximation of this nonlinear behavior can be calculated by linearizing the function $f^{(0)}(\phi, \omega_m^{(0)} j)$ around $\phi^{(0)}$. This linearization can be expressed as

$$\tilde{f}^{(0)}(\phi, \omega_m^{(0)} j) \approx f^{(0)}(\phi^{(0)}, \omega_m^{(0)} j) + \left.\frac{\partial f^{(0)}(\phi, \omega_m^{(0)} j)}{\partial \phi_1}\right|_{\phi^{(0)}} (\phi_1 - \phi_1^{(0)}) + \cdots + \left.\frac{\partial f^{(0)}(\phi, \omega_m^{(0)} j)}{\partial \phi_m^{(0)}}\right|_{\phi^{(0)}} (\phi_m - \phi_m^{(0)}).$$

For sake of ease of comprehension, we present an example by employing $\phi^{(0)} = [0.05 \quad 0.09]$, or in other words $k_p = 0.05$ and $k_d = 0.09$, and the 1^{st} FRF model to demonstrate the approximation of the behavior of the infinity norm by a nonlinear function $f^{(0)}(\phi, \omega_m^{(0)} j)$ and next by a linear function $\tilde{f}^{(0)}(\phi, \omega_m^{(0)} j)$. This example is illustrated in figure 4-10.

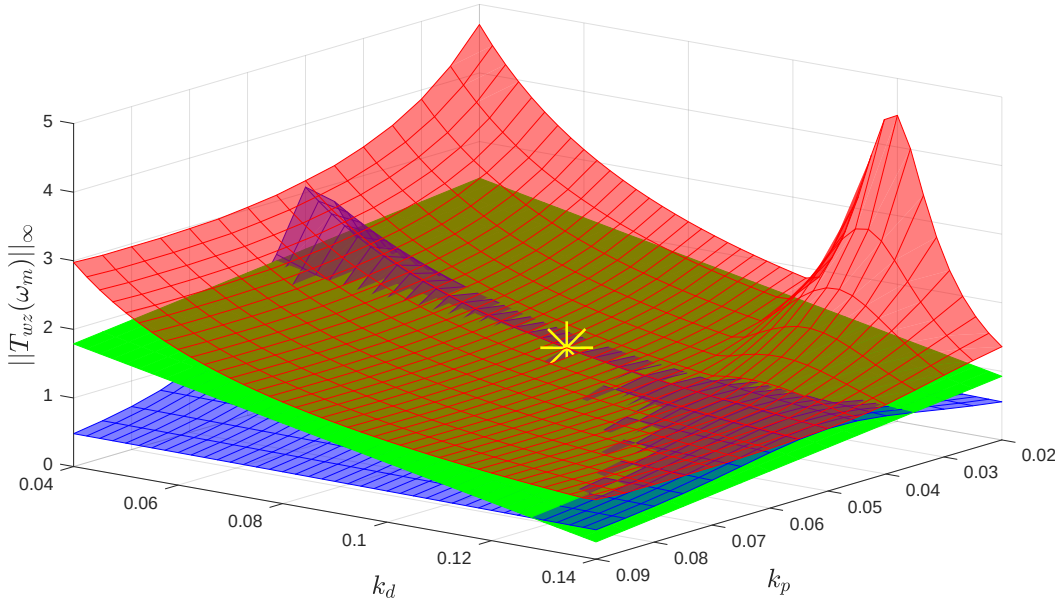

Figure 4-10: Figure of the infinity norm and its approximations for $k_p = 0.05$ and $k_d = 0.09$

In this figure, the behavior of the actual infinity norm is described by the red curve. The behavior of $f^{(0)}(\phi, \omega_m^{(0)} j)$ is represented by the curve in blue color and the behavior of $\tilde{f}^{(0)}(\phi, \omega_m^{(0)} j)$ is described by the green plane. Additionally, the initially stabilizing point around which we approximate the behavior of the actual infinity norm is illustrated by the yellow star. As it can be seen, both the nonlinear and linear approximations describe sufficiently accurately the pattern of the infinity norm for a small neighborhood around $\phi^{(0)} = [0.05 \quad 0.09]$. On top of that, it appears that the linear approximation $\tilde{f}^{(0)}(\phi, \omega_m^{(0)} j)$ which is illustrated in green, describes accurately the behavior of the infinity norm for a larger neighborhood than its nonlinear counterpart. This behavior can be roughly explained by the fact that the nonlinear approximation is based on the assumption that the infinity norm appears at the particular frequency point $\omega_m^{(0)}$. Although this is a strong assumption for a small neighborhood around $\phi^{(0)}$, it appears to fall apart for any broader neighborhood. On the other hand, the linear approximation $\tilde{f}^{(0)}(\phi, \omega_m^{(0)} j)$ seems to express the pattern of

the actual infinity norm in a much more reliable manner.

Nevertheless, although the linear function $\tilde{f}^{(0)}(\phi, \omega_m^{(0)} j)$ describes the behavior of the infinity norm sufficiently accurately for a remarkable neighborhood around $\phi^{(0)}$, it seems to deviate significantly for ϕ away from this neighborhood. For this reason, the proposed algorithm suggests an iterative minimization procedure that aims to describe the behavior of the infinity norm within the convex hull created by the attained controller parameters' combinations, as the intersection of a number of planes. Specifically, the behavior of the infinity norm is approximated by the term $J = \max \tilde{f}^{(k)}(\phi, \omega_m^{(k)} j)$, for $k = 1, \cdots, i$. Minimizing this approximation, subject to the corresponding linear constraints, that ensure stability and performance, is projected to result to some optimal values for the controller parameters. After a number of iterations, the minimum value of J that has been found is returned as the result of the optimization. The iterative part of the optimization is described between the lines 10 and 16. It is highlighted that the proposed algorithm remains convex, since both the optimization argument and the linear constraints are convex.

Let us describe in detail the stages of the optimization when applied to the 5^{th} FRF model, with initial controller parameters $k_p = 0.3$ and $k_d = 0.04$. The infinity norm of the closed-loop, when evaluated on the 1^{th} model is quite large, and specifically it is $J^{(0)} = 3.4164$ and it appears at the frequency point $\omega_m^{(0)} = 0.4041 rad/sec$. The linear approximation $\tilde{f}^{(0)}([k_p, k_d]^{(0)}, \omega_m^{(0)} j)$ results from the linearization of $f([k_p, k_d], \omega_m^{(0)} j)$, which is the nonlinear relation between the magnitude of the closed-loop transfer function at the frequency point $\omega_m^{(0)}$. Considering that the closed-loop transfer function for that frequency can be expressed as

$$T_{wz}(\omega_m^{(0)} j) = \frac{W_p(\omega_m^{(0)} j)}{1 + G_2(\omega_m^{(0)} j) C_I([k_p, k_d], \omega_m^{(0)} j)},$$

where $C_I([k_p, k_d], \omega_m^{(0)} j)$ denotes the PD controller and $G_2(\omega_m^{(0)} j)$ denotes the 5^{th} FRF model of the plant, the nonlinear function approximating $||T_{wz}||_\infty$ can expressed at the frequency point ω_m as:

$$f(k, \omega_m^{(0)} j) = \frac{|W_p(\omega_m^{(0)})|}{\sqrt{(1 + k_p a_1 + k_d a_2)^2 + (k_p a_3 + k_d a_4)^2)}}, \tag{4-14}$$

where

$$\begin{aligned} a_1 &= \mathrm{Re}\left(G_2(\omega_m^{(0)} j)\right) \\ a_2 &= -\mathrm{Im}\left(G_2(\omega_m^{(0)} j)\right) \omega_m^{(0)} \\ a_3 &= \mathrm{Im}\left(G_2(\omega_m^{(0)} j)\right) \\ a_4 &= \mathrm{Re}\left(G_2(\omega_m^{(0)} j)\right) \omega_m^{(0)} \end{aligned}$$

A linearization of this function around the point $k^{(0)} = [0.3, 0.04]$, will give

$$\begin{aligned} \tilde{f}([k_p, k_d], \omega_m^{(0)} j) &= f(k^{(0)}, \omega_m^{(0)} j) + \left.\frac{\partial f(k, \omega_m^{(0)} j)}{\partial k_p}\right|_{k^{(0)}} (k_p - k_p^{(0)}) + \left.\frac{\partial f(k, \omega_m^{(0)} j)}{\partial k_d}\right|_{k^{(0)}} (k_d - k_d^{(0)}) \\ &= 6.7114 - 1.1957 k_p - 79.8912 k_d. \end{aligned}$$

Apparently, $\tilde{f}([k_p, k_d], \omega_m^{(0)} j)$ describes the relation between $||T_{wz}([k_p, k_d], \omega j)||_\infty$ and the controller parameters $[k_p, k_d]$, around $[k_p, k_d]^{(0)}$, as a simple plane. For this specific combination of parameters, this plane together with the actual nonlinear relation between $||T_{wz}([k_p, k_d], \omega j)||_\infty$ and $[k_p, k_d]$ is illustrated in figure 4-11.

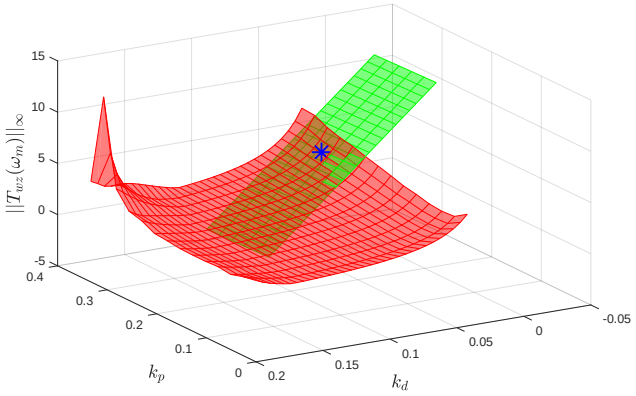

Figure 4-11: Illustration of the actual infinity norm, and its linearization around $[0.3, 0.04]$

It is stressed that there is no analytical expression that describes the nonlinear relation between $||T_{wz}([k_p, k_d], \omega j)||_\infty$ and $[k_p, k_d]$ that is illustrated in red color in figure 4-11. In the context of this project we perform a grid search to calculate it for several combinations of k_p and k_d.

The first iteration of the algorithm proposed in 3-4, results to controller parameters $k_p = 0.0545$ and $k_d = 0.1770$ and a corresponding infinity norm $J^{(1)} = 0.9625$, when evaluation is done on the 5^{th} FRF model, i.e. on itsself. The updated controller parameter, together with $J^{(1)}$, is represented by the yellow star in figure 4-12, only from a different perspective than the previous one. Additionally, in figure 4-12 one can also see the blue plane by which the infinity norm is approximated for the updated controller parameters.

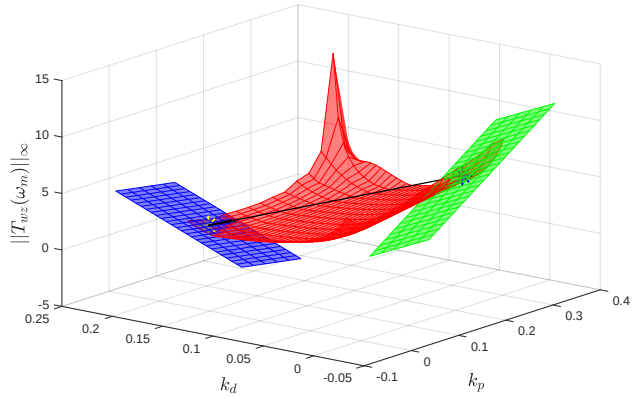

Figure 4-12: Illustration of the actual infinity norm, and its linearization around $[0.0545, 0.1770]$

After 6 iterations, the proposed algorithm will converge to a local minimum and specifically to the controller parameters $k_p = 0.0556$ and $k_d = 0.1495$ with an infinity norm $J^{(6)} = 0.5798$.

The details of the iterative procedure are described in table 4-4. Additionally, in figure 4-13 one can see the planes resulting from all linearizations that were performed, and the corresponding controller parameter values.

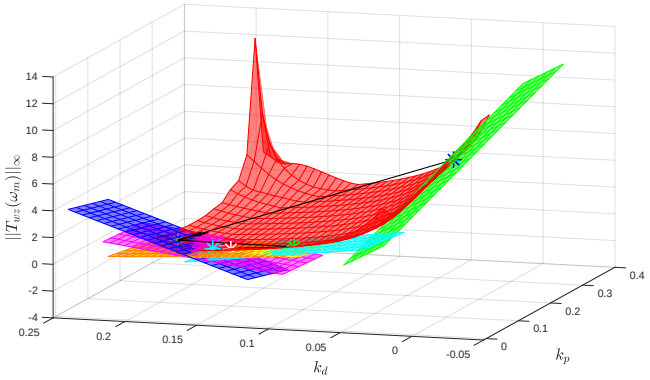

Figure 4-13: Illustration of the actual infinity norm, and its linearization around $[0.0556, 0.1495]$

Iteration	k_p	k_d	$J^{(*)}$	Point Color	Plane Color
0	0.3	0.04	3.4164	Blue	Green
1	0.0545	0.1770	0.9625	Yellow	Blue
2	0.0577	0.0966	0.8857	Green	Cyan
3	0.0555	0.1529	0.6015	Cyan	Magenta
4	0.0560	0.1405	0.6156	White	Yellow
5	0.0556	0.1494	0.5804	Black	Orange
6	0.0556	0.1495	0.5798	None	None

Table 4-4: Details of the iterative algorithm for 6 iterations

4-3-2 Evaluation the refined algorithm on the actual plant

In order to be able to compare this proposed technique with the default optimization algorith that was proposed in [12], we employ the same conditions with the ones of the previous section and run respective simulations. As an initially stabilizing solution the combination $k_p = 0.2$ and $k_d = 0.15$ is employed, which was the combination that was used during the data acquisition. The algorithm is applied to all 10 FRF models, subject to the linear constraints that have been described previously, and the resulting controller parameters are first evaluated on the actual plant, and next on other FRF models as well. In all the following simulations the value $i_{max} = 10$ was sufficient for the algorithm to converge to a minimum solution. The resulting controller parameters together with the corresponding evaluation on the actual plant is presented in table 4-5.

s.t.	1	2	3	4	5	6	7	8	9	10
k_p	0.0574	0.0520	0.0560	0.0548	0.0540	0.0551	0.0542	0.0550	0.0541	0.0487
k_d	0.1026	0.2018	0.1007	0.1306	0.1498	0.1231	0.1465	0.1243	0.1516	0.1365
$\|\|T_{wz}\|\|_\infty$	0.8397	∞	0.8609	0.6662	0.7636	0.7060	0.7131	0.6998	0.7944	0.6589

Table 4-5: Table containing the resulting controller parameters and the corresponding evaluation on the actual system

The results presented in table 4-5 are rather interesting. As it can be seen, for most of the designed controllers, the corresponding infinity norm of the actual plant appears to have a very improved performance comparing to the corresponding table of the default optimization algorithm 4-1. However, the controller parameters, that result from optimization on the 2^{nd} FRF model, lead to $||T_{wz}||_\infty = \infty$, or in other words, they lead to an unstable closed loop system. After examining the reason behind this behavior, it was concluded that it stems from the fact that the 2^{nd} FRF model is corrupted. That is, it fails to capture sufficiently accurately the behavior of the plant.

At this point, it is important to note that, in order to assess stability and performance for an FRF model and a particular parameters' combination, the only reliable method is to consider whether the specific controller parameters satisfy the linear constraints imposed on the model. For this reason, the result of a grid search can be very enlightening with respect to the reliability of data, since it reveals the set of controller parameters which are acceptable for a particular model. Consequently, we employ the result of a grid search on the 2^{nd} FRF model in order to have an insight on its behavior and assess the degree of its corruption.

In figure 4-14a one can see the set of controller parameters that imply stability and performance for the 2^{nd} FRF model. The area that is represented in deep blue color corresponds to controller parameters' combinations that lead to instability, whereas the green area represents the combinations for which the stability constraints are satisfied. Finally, the yellow are represents the combinations for which performance is additionally attained. On the other hand, in figure 4-14b, one can see the result of the corresponding grid search when the stability of the actual plant is considered in addition to the satisfaction of the linear constraints, that prevent the encirclement of the origin. As it can be seen, there is a slight, yet significant difference between the two figures. Namely, in figure 4-14a, the green and yellow area extends to parameters combinations for which the corresponding area in 4-14b is deep blue, that is, the actual closed loop system is unstable. All in all, by figure 4-14 it can be concluded that the satisfaction of the linear constraints does not ensure stability of the actual plant when the linear constraints are imposed on corrupted data.

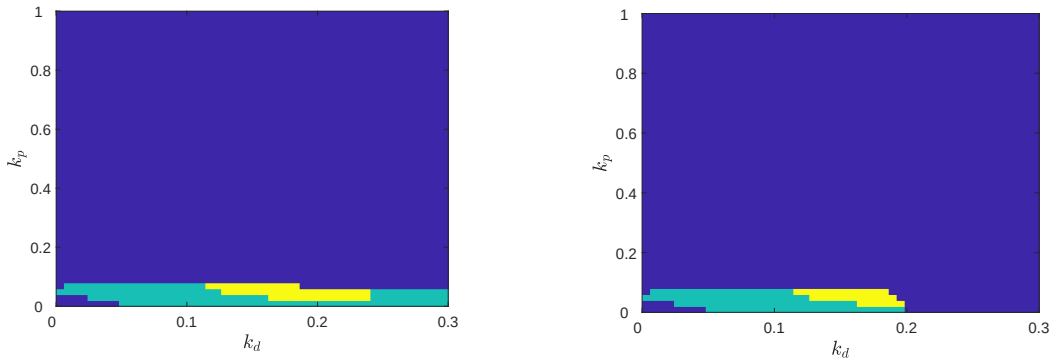

(a) Checking only linear constraints

(b) Checking poles of the actual closed loop as well

Figure 4-14: Grid search comparison

To illustrate even better this behavior, it is interesting to present the bode plots of the closed loop, when the 2^{nd} FRF model and the actual plant are considered. The bode plots can be seen in figure 4-15. As expected, when the 2^{nd} FRF model is considered, it seems that there is no violation of the performance condition, whereas when from the bode plot of the actual plant it is obvious that the performance specification is not satisfied. The behavior of other FRF models for such controller parameters will be presented in the following subsection, where the evaluation of the proposed algorithm on FRF models is presented.

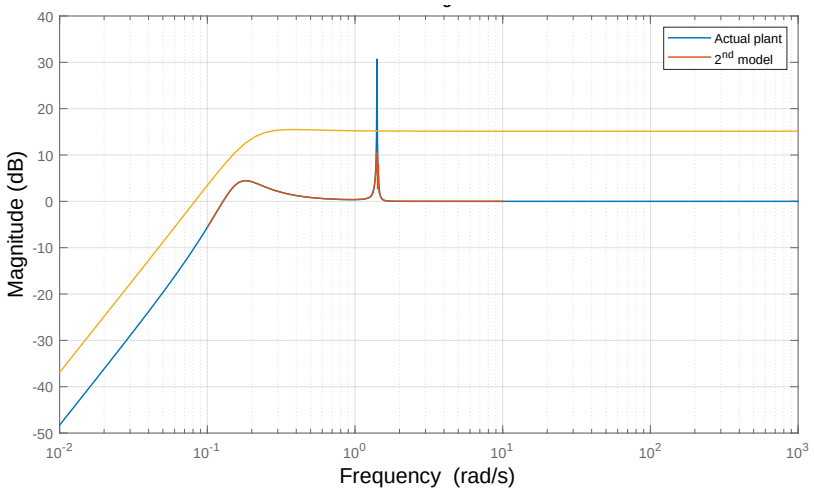

Figure 4-15: Bode diagrams with $k_p = 0.0520$ and $k_d = 0.2018$ for the actual plant and the 2^{nd} FRF model.

4-3-3 Evaluation of the refined algorithm on FRF models

Similarly to the previous section, the evaluation of the resulting controller parameters on other FRF models is of high interest, since the actual plant is never available in practice. The evaluation of the controllers, presented in table 4-5, with respect to other models is presented in the following table.

	1	2	3	4	5	6	7	8	9	10
1	0.8364	∞	0.8578	0.6666	0.5849	0.7058	0.5971	0.6993	0.5777	0.6627
2	0.8339	0.4504	0.8552	0.6654	0.5839	0.7047	0.5961	0.6982	0.5768	0.6590
3	0.9316	∞	0.8632	4.6542	1.0347	3.9290	1.2083	4.5392	0.9604	1.9229
4	0.8347	0.7071	0.8555	0.6652	0.6652	0.7042	0.6428	0.6977	0.6789	0.6613
5	0.8346	∞	0.8551	0.6651	0.5838	0.7040	0.5960	0.6976	0.5911	0.6615
6	0.8336	0.8706	0.8545	0.6643	0.8652	0.7036	0.8180	0.6971	0.8943	0.6607
7	0.8337	∞	0.8538	0.6646	0.6170	0.7034	0.5956	0.6970	0.6357	0.6603
8	0.8346	0.8458	0.8554	0.6652	0.8266	0.7042	0.7850	0.6978	0.8523	0.6613
9	0.8150	∞	0.8345	0.6526	0.5740	0.6901	0.5859	0.6839	0.5672	0.6483
10	0.8347	0.9492	0.8556	0.6650	0.9004	0.7042	0.8452	0.6978	0.9347	0.6670

Table 4-6: Evaluation table for the minimization scheme. Each column corresponds to a different design, and the rows describe which FRF model the controller is evaluated on.

The ∞ values that appear on table 4-6 imply that the controller parameters that resulted from optimization based on the FRF model of the corresponding column, result to encirclement of the origin when other FRF models are used for evaluation. However, since it is remarkably complicated to extract conclusions from a 10×10 table, we summarize the mean of the evaluations on a smaller table presented below.

s.t.	1	2	3	4	5	6	7	8	9	10
k_p	0.0574	0.0520	0.0560	0.0548	0.0540	0.0551	0.0542	0.0550	0.0541	0.0487
k_d	0.1026	0.2018	0.1007	0.1306	0.1498	0.1231	0.1465	0.1243	0.1516	0.1365
$\|\|T_{wz}\|\|_\infty$	0.8423	∞	0.8541	1.0628	0.7236	1.0253	0.7270	1.0806	0.7269	0.7865

Table 4-7: Table containing the resulting controller parameters and the corresponding evaluation on the actual system

By comparing the tables 4-7 and 4-3, one can not directly notice that the performance of the controllers designed based on the proposed algorithm of this work is improved. As a matter of fact, many results on table 4-7 appear to have $||T_{wz}||_\infty > 1$, although the evauation on the actual plant presented in table 4-5 indicates otherwise. This is attributed on the fact that the evaluation of all controllers on the 3^{rd} FRF model appears to have an unexpectedly increased value as it appears in table 4-6. This indicates that the 3^{rd} FRF model does not offer trust worthy evaluations and these evaluations can be neglected as some kind of outliers. By neglecting the evaluations on the 3^{rd} FRF model the values on tables 4-7 and 4-5 would be very close as it can be noticed from the values on table 4-6. All in all, the efficiency of the algorithm proposed in section 3-4 outperforms the efficiency of the default algorithm.

4-4 Grid search

Given that the optimization problem is relatively simple, since only two controller parameters need to be optimized, we can first apply a grid search to explore the range of the parameters k_p and k_d for which the closed loop system is stable and robust. It is stressed that robustness implies that $||T_{wz}||_\infty \leq 1$.

4-4-1 Grid search on the actual plant

When the actual transfer function $G(s)$ is used, the interval that corresponds to stability and performance is illustrated in figure 4-16. As it can be seen, the grid search was performed in the interval $[0, 1]$ for the parameter k_p and $[0, 0.3]$ for the parameter k_d.

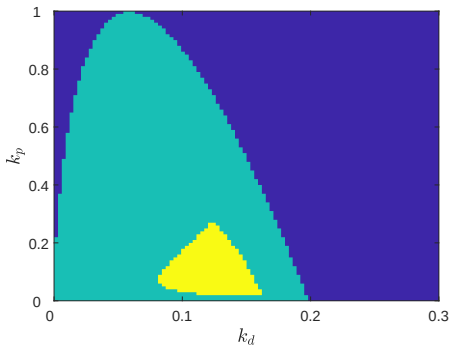

Figure 4-16: Results of the grid search for the parameters k_p and k_d.

The blue area represents the controller parameters' combinations for which the closed-loop system is unstable. The light green area corresponds to parameter combinations that result to a stable closed-loop system. Finally, the yellow area represents the combinations for which $||T_{wz}||_\infty \leq 1$.

4-4-2 Grid search for stability on the FRF measurements

In this paragragh we perform a grid search on the same intervals for the controller parameters k_p and k_d as in the previous paragraph. Specifically, we explore the area on which each model satisfies the stability condition, which is checked by using the generalized Nyquist criterion. As it was deployed in subsection 2-2-5, a sufficient condition, for stability for the convex feasibility problem, is that the Nyquist plot of the function

$$Q(\phi, j\omega) = 1 - C_I(\phi)P_{22} \tag{4-15}$$

does not encircle the origin. The linear constraints that are employed for this purpose are

$$\begin{aligned} l_1: &\quad \mathrm{Im}\left(Q(j\omega)\right) + 0.2\,\mathrm{Re}\left(Q(j\omega)\right) - 0.001 < 0 \quad \text{for} \quad \omega < 0.16 \\ l_2: &\quad \mathrm{Im}\left(Q(j\omega)\right) - 0.05\,\mathrm{Re}\left(Q(j\omega)\right) + 0.001 < 0 \quad \text{for } 0.16 \leqslant \omega \leqslant 0.20 \\ l_3: &\quad -\mathrm{Im}\left(Q(j\omega)\right) - 5\,\mathrm{Re}\left(Q(j\omega)\right) + 0.001 < 0 \quad \text{for} \quad \omega > 0.20. \end{aligned} \tag{4-16}$$

The result of the grid search is illustrated in figure 4-17.

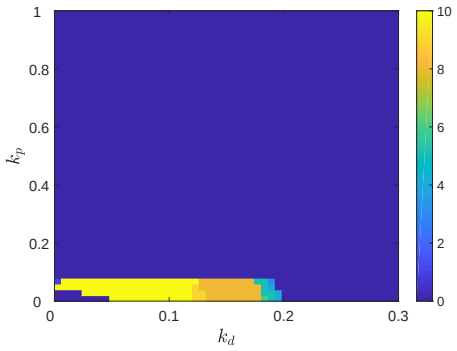

Figure 4-17: Results of the grid search for the parameters k_p and k_d with respect to stability.

The blue area represents the controller parameters' combinations for which no model is stable. The color bar on the right of the figure indicates how many models are stable for each parameter combination.

4-4-3 Grid search for performance on the FRF measurements

In this paragraph we explore the parameter combinations for which the closed-loop system satisfies the performance condition $||T_{wz}||_\infty \leq 1$. The result of the grid search is illustrated in figure 4-18

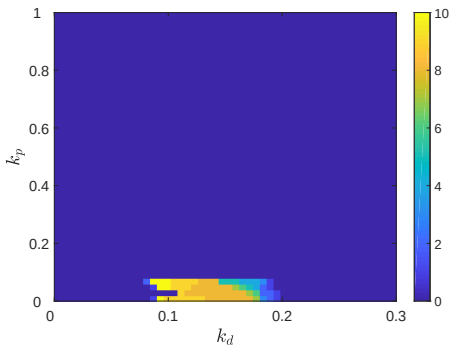

Figure 4-18: Results of the grid search for the parameters k_p and k_d with respect to performance.

The blue area represents the controller parameters' combinations for which no model satisfies the performance condition. The color bar on the right of the figure indicates how many models satisfy the performance condition for each parameter combination. An interesting feature of figure 4-18 is that for $k_p \approx 0.01$ and $k_d \approx 0.09$ all FRF models satisfy the performance specification. However, this parameter combination does not satisfy performance for the actual plant. This interesting behavior is attributed to the fact that, although the linear constraints that are imposed are not violated for any frequency point in $[0.1, 10] rad/sec$, the performance condition is violated in a frequency point which does not belong to that interval, and specifically at a freuqency lower that $0.1 rad/sec$. In other words, the frequency range that we used in order to identify the behavior of our plant partially fails to do so. It is noted

that considering the frequency range to be $[0.01, 10] rad/sec$, would prevent this defect from happening.

4-4-4 Linear constraints and conservatism

One can notice that the map of the grid search that corresponds to stability and performance of the actual plant differs significantly from the respective map for stability and performance of the considered FRF models. Namely, in figure 4-16 the intervals of the controller parameters, k_p and k_d for which the closed loop system satisfies stability and performance, are much larger than the respective ones in figures 4-17 and 4-18 that describe the behavior of the closed loop when FRF models are used instead of the actual model.

The reason behind this difference lies on the way that stability is assessed in the two different cases. Specifically, when the actual system is assessed for stability, it suffices if all the poles of the closed loop system lie on the LHP. On the other hand, when the FRF models are assessed it is not feasible to check on this condition, since FRFs are not expressed analytically and thus it is not possible to check where the poles of the closed loop lie on. Instead, in order to check on stability one will have to ensure that the Nyquist plot of the function

$$Q(\phi, j\omega) = 1 - C_I(\phi)P_{22}$$

does not encircle the origin. Appartently, this condition is checked by making use of the linear constraints 4-16. If an FRF model for a certain controller parameters' combination satisfies these constraints then stability is inferred. However, checking for stability by checking the satisfaction of these linear constraints is rather conservative, since there are certainly controller parameters' combinations for which there is no encirclement of the origin, yet these particular linear constraints are violated. These parameter combinations are approximately illustrated in figure 4-16, and specifically by the part of the green and yellow area of the figure for which the corresponding spots on figure 4-17 are in deep blue. To illustrate this fact, it is useful to present figure 4-19, which describes the intervals of k_p and k_d for which the actual plant satisfies stability, and respectively performance, however by evaluating the satisfaction of the linear constraints 4-16.

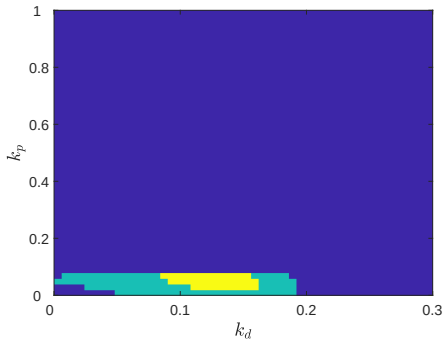

Figure 4-19: Results of the grid search for the parameters k_p and k_d, checking stability of the actual plant by evaluating the satisfaction of the linear constraints.

As it can be noticed, figure 4-19 is much closer to figures 4-17 and 4-18. The conservativeness that is implied by the use of the linear constraints is inevitable, yet relatively managable. This

means that the area in which the figures 4-16 and 4-17 differ significantly, can be reduced. Namely, this can be done by dividing the entire range of frequency in more than just 3 pieces, which was so far the case, and construct corresponding linear constraints that will induce less conservatism. In other words, it is crucial to construct linear constraints that prevent the Nyquist plot of $Q(\phi, j\omega)$ from encircling the origin, but do not constrain the expansion of the Nyquist plot of $Q(\phi, j\omega)$ to, after all, "legitimate" areas, that is, to allow all the possible patterns that do not imply instability.

An algorithm that attempts an automatic constraints' design was proposed in section 3-5. This algorithm can be evaluated in the context of this chapter and this evaluation is presented in the following paragraph.

4-4-5 Algorithm for optimal design of the linear constraints.

In this subsection we evaluate the algorithm, proposed in 3-5 ,and next the one proposed in 3-6, which constructs one linear constraint per frequency point, based on the Nyquist plot of the function $Q(\phi^*, j\omega)$, that is, when the initial controller parameters ϕ^* are considered.

In order to perform this evaluation we employ the 2^{nd} FRF model and construct the corresponding linear constraints for $k_p = 0.2$ and $k_d = 0.15$, for which the infinity norm for the 2^{nd} FRF model results to be 0.6727. It is stressed that although the 2^{nd} FRF model has been identified as corrupted data, it is very suitable so as to demonstrate the behavior of the algorithm for updated versions of the linear constraints. Next we evaluate stability and performance by applying a grid search within the interval $[0, 1]$ for k_p and $[0, 0.3]$ for k_d, by examining the satisfaction of the N constructed linear constraints. The result of the grid search is presented in figure 4-20.

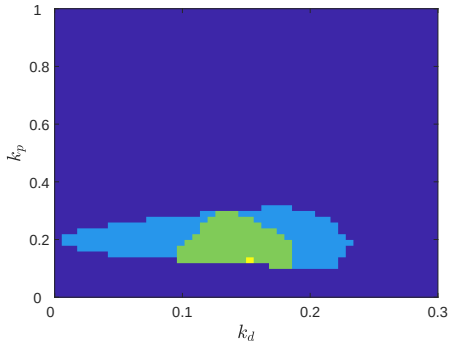

Figure 4-20: Results of the grid search for the parameters k_p and k_d, checking stability and performance imposing N linear constraints on the 2^{nd} FRF model

As it can be seen, by imposing N linear constraints, constructed based on the initially stabilizing solution ϕ^*, still induces some conservatism. In other words, it appears that some controller parameters' combinations that indeed result to stability, are not "visible" to the optimization algorithm if the specific constraints are imposed. However, in this case one can see a different kind of conservatism, since the updated constraints motivate the algorithm to explore solutions in the neighborhood around the initially stabilizing solution, which at this case was $k_p = 0.2$ and $k_d = 0.15$. In other words, we can say that the algorithm becomes more biased towards specific solutions.

Having considered this behavior of the algorithm, a new question arises and specifically, what would happen if we could optimize the controller parameters, then re-construct the linear constraints and re-apply the optimization. In other words, what if we applied an iterative procedure that includes both the stage of constructing linear constraints and the stage of optimizing our controller parameters. This iterative procedure is what the algorithm proposed in 3-6 suggests. In fact, it combines the algorithm proposed in 3-4 and the one proposed in 3-5

By performing the optimization algorithm suggested in 3-4, subject to the updated linear constraints, would result to some controller parameters $k_p = 0.1266$ and $k_d = 0.1559$. This parameters' combination indeed leads to an improved performance for the 2^{nd} FRF model and specifically its infinity norm results to be 0.5827. It is noticed that the light yellow area of the figure corresponds to infinity norm less than 1, whereas the bold yellow area corresponds to infinity norm lower than 0.6. We choose to highlight this detail because it turns out that this controller parameters' combination corresponds to the bold yellow area of figure 4-20, which confirms the effectiveness of the optimization algorithm proposed in 3-4. It is then implied that constructing new linear constraints will be based on an improved initial solution ϕ^*.

After constructing the updated linear constraints, the grid search was once again performed and the results are presented in figure 4-21.

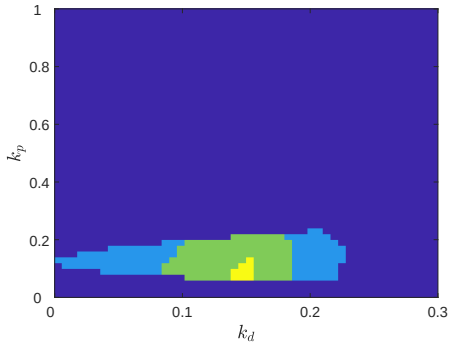

Figure 4-21: Results of the grid search for the parameters k_p and k_d, checking stability and performance imposing N updated, linear constraints on the 2^{nd} FRF model

As it can be seen, this figure is very similar to figure 4-20, yet there is a slight but rather interesting difference. The interval of the parameters k_p and k_d which are visible to the optimization algorithm is extended. In fact, it is extended towards an interval of the parameters k_p and k_d for which the corresponding value of the infinity norm is improved. Again the bold yellow area represents parameters' combinations for which the infinity norm of the 2^{nd} FRF model is even lower that 0.6. Consequently, the optimization algorithm that is subject to these updated linear constraints will be "free" to explore the resulting performance of a more promising parameters' interval.

If we perform a third iterative optimization using the algorithm proposed in 3-4, the resulting controller parameters will be $k_p = 0.1001$ and $k_d = 0.1486$, and it is once again noted that this parameters' combination is located at the heart of the bold yellow are of figure 4-21, and result to infinity norm of the 2^{nd} FRF being 0.5654. The resulting grid search, that

reveals the parameters' combinations that will be "visible" from the optimization algorithm, is presented in figure 4-22.

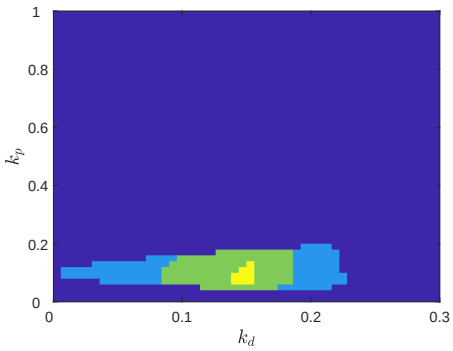

Figure 4-22: Results of the grid search for the parameters k_p and k_d, checking stability and performance imposing N updated, linear constraints on the 2^{nd} FRF model

Finally, in this figure, one can notice that the entire interval of the controller parameters that correspond to infinity norm being lower that 0.6 is visible when the optimization algorithm is subject to the updated linear constraints. Apparently, this implies that a local minimum of the infinity norm is located in this interval. After performing the optimization algorithm proposed in 3-4 once again, the controller parameters will result to be $k_p = 0.08571$ and $k_d = 0.1519$, and the corresponding infinity norm will be 0.5350. Iterating again will not give any improved results neither for the optimal constraints nor for the optimal controller parameters, which means that the algorithm, proposed in 3-6, has converged. At this point it is important to mention that the global minimum, where searched with a grid search, is indeed around 0.5350, meaning that our algorithm managed to find the global optimum. Although this might not be the case for more complicated systems and controllers' structure, an update on the initial values of the controller parameters and more importantly an refinement on the optimization scheme, as suggested for future work in 6-2, is likely to solve this problem. In the next section we are going to evaluate the performance of this advanced algorithm on all 10 FRF models and explore its behavior.

4-5 Iterative algorithm with optimal linear constraints

On the previous section it has been highlighted that employing used-defined linear constraints induces an amount of conservatism that does not allow the proposed optimization algorithm to converge to a minimum of the controller paramters' set. For this reason, in section 3-6 we have integrated the algorithm proposed in 3-4 with the algorithm proposed in 3-6, in order to build an updated algorithm that considers an iterative optimization of the linear constraints that are imposed, together with an iterative optimization of the controller parameters. The steps of the algorithm proposed in 3-4 have extensively described in section 4-3-1 and, thus we are not going to repeat its steps. In the following subsection we will present the way that optimal constraints can be constructed for an initially stabilizing solution $\phi^{(*)}$.

4-5-1 Explanation of the basic idea of the updated algorithm

As mentioned in 3-1-2, the condition for stability of closed loop system relies on the Nyquist plot of the function

$$Q(\phi, j\omega) = 1 - C_I(\phi)P_{22},$$

and specifically, one should ensure that the Nyquist diagram does not encircle the origin. The main idea of the proposed algorithm, that constructs linear constraints, is schematically illustrated by figure 4-23.

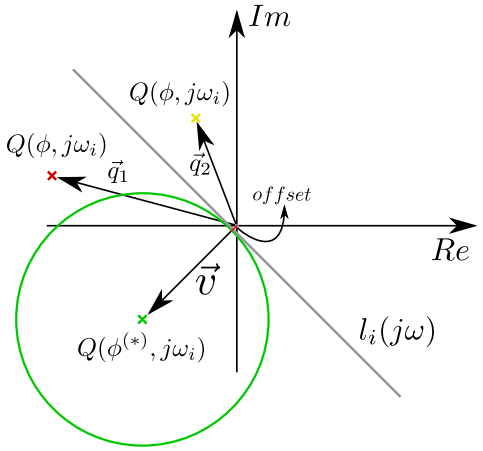

Figure 4-23: Representation of constructing optimal constraints on the Nyquist plot

From a geometrical perspective, the satisfaction of the linear constraint $l_i(j\omega)$ relies on the satisfaction of the following inequality that express the relative position of vetors with respect to a line $\vec{v} \cdot \vec{q} \geq 0$, where $\vec{v}$ descrives the vector that is vertical to the line $l_i(j\omega)$, and pointing towards the point $Q(\phi^{(*)}, j\omega_i)$, and $\vec{q}$ denotes the position of a random $Q(\phi, j\omega_i)$ on the complex plane. For example, by considering figure 4-23, $\vec{v} \cdot \vec{q}_1 \geq 0$ is indeed satisfied, whereas $\vec{v} \cdot \vec{q}_2 \geq 0$ is not. In order to robustify the procedure, a designer should consider some margin between the line $l_i(j\omega)$ and the origin. This margin is called $offset$. The entire procedure of defining optimal linear constraints is best illustrated by the following algorithm.

Algorithm for construction of optimal constraints

1. **Input:** Initially stabilizing solution $\phi^{(*)}$, FRF model $G(\omega j)$.
2. Calculate $Q(\phi^{(*)}, j\omega) = 1 - C_I(\phi^{(*)})P_{22}$.
3. **for** $i = 1 : N$
4. $\quad a_i \leftarrow \text{Real}\left(Q(\phi^{(*)}, j\omega_i)\right)$
5. $\quad b_i \leftarrow \text{Imag}\left(Q(\phi^{(*)}, j\omega_i)\right)$
6. **end**
7. Define optimization parameters: ϕ and the function: $Q(\phi, j\omega) = 1 - C_I(\phi)P_{22}$.
8. Define the offset: $offset \leftarrow \epsilon, \quad$ with $0 < \epsilon \ll 1$.
9. **Constraints:** $a_i \cdot \text{Real}\left(Q(\phi, j\omega_i)\right) + b_i \cdot \text{Imag}\left(Q(\phi, j\omega_i)\right) - |b_i| \cdot offset \geq 0$.

It is stressed that it is necessary to use the absolute value for the parameter b when it is multiplied with the $offset$, so as to preserve the line $l_i(j\omega)$ on the proper side with respect to the origin. It is noted that in all the following simulations the value $p_{max} = 3$ was sufficient for the iterative algorithm to converge to some optimal solution. In the following paragraph we present the performance of this proposed algorithm when it is integrated with the iterative algorithm proposed in 3-4.

4-5-2 Evaluation on the actual plant

In this section we employ the algorithm that was analytically explained in section 3-6, to synthesize frequency-domain fixed-structure controllers, which we plan to evaluate using the actual plant. The resulting controllers for the FRF measurements that are considered are presented in table 4-8.

s.t.	1	2	3	4	5	6	7	8	9	10
k_p	0.0586	0.0806	0.1107	0.1666	0.0870	0.0579	0.0834	0.0674	0.0793	0.0556
k_d	0.1398	0.1894	0.1272	0.1419	0.1505	0.1316	0.1495	0.1287	0.1523	0.1322
$\|\|T_{wz}\|\|_\infty$	0.6330	8.9838	0.6756	0.9048	0.8460	0.6526	0.8196	0.6502	0.8636	0.6554

Table 4-8: Table containing the resulting controller parameters and the corresponding evaluation on the actual system

By examining the evaluation of the updated algorithm on the actual plant, one can observe that for specific FRF models the resulting controller performs worse than in the corresponding table of section 4-3-2. This is attributed to the fact that the updated linear constraints reveal a new controller parameters' set to the optimization algorithm. In this new set, it appears that some FRF models suffer from corrupted data, since even though the linear constraints are satisfied for themselves, they are not satisfied for the actual plant.

This behavior is simular to the behavior that was illustrated in figure 4-15, which presented the bode plot of the closed-loop for the actual plant and the 2^{nd} FRF model, which appears to be corrupted. The problem of corrupted data can be generally dealt by considering more sampling frequency points around the resonance peak of a certain plant. The reason why some FRF models fail to capture the behavior around the resonance frequency of the plant is that this behavior is changing "fast".

4-5-3 Evaluation on FRF models

In this paragraph we aim to evaluate the performance of the controllers that were designed using the updated iterative algorithm that was proposed in section 3-6. Similarly to previous sections, in table 4-9 we present the evaluation of each controller on all 10 FRF models.

	1	2	3	4	5	6	7	8	9	10
1	0.6123	∞	0.6721	0.7132	0.6826	0.6521	0.6529	0.6480	0.6511	0.6561
2	0.6116	0.4273	0.6893	0.6701	0.5416	0.6511	0.5416	0.6403	0.5300	0.6554
3	1.9140	∞	0.6715	0.7191	0.7953	5.3399	0.8639	4.7758	0.8381	4.0721
4	0.6197	1.2981	0.6733	0.6901	1.0122	0.6510	0.9471	0.6468	0.9536	0.6547
5	0.6114	0.9460	0.6741	0.6897	0.5491	0.6510	0.5518	0.6470	0.5458	0.6546
6	0.7584	1.8858	0.6726	0.6901	1.3161	0.6503	1.2377	0.6549	1.3197	0.6542
7	0.6111	1.0381	0.6727	0.6880	0.5577	0.6502	0.5508	0.6461	0.5703	0.6541
8	0.7335	1.8189	0.6733	0.6900	1.2697	0.6510	1.1900	0.6467	1.2527	0.6547
9	0.6010	0.9460	0.6673	0.6871	0.5432	0.6391	0.5456	0.6367	0.5347	0.6426
10	0.7724	2.1953	0.6741	0.6904	1.2795	0.6566	1.2187	0.6553	1.3224	0.6547

Table 4-9: Evaluation table for the minimization scheme. Each column corresponds to a different design, and the rows describe which FRF model the controller is evaluated on.

Given that a 10×10 table is relatively not easy to analyze, we present the mean of the evaluations in table 4-10.

s.t.	1	2	3	4	5	6	7	8	9	10
k_p	0.0586	0.0806	0.1107	0.1666	0.0870	0.0579	0.0834	0.0674	0.0793	0.0556
k_d	0.1398	0.1894	0.1272	0.1419	0.1505	0.1316	0.1495	0.1287	0.1523	0.1322
$\|\|T_{wz}\|\|_\infty$	0.7845	∞	0.6740	0.6928	0.8547	1.1192	0.8300	1.0598	0.8518	0.9953

Table 4-10: Table containing the resulting controller parameters and the mean of evaluation on the 10 FRF models

Similarly to the corresponding table of section 4-3, it appears that the values of the mean infinity norm presented in table 4-10 are increased due to the evaluation on the 3^{rd} FRF model. As it can be seen in the third row of table 4-9, the evaluation of some controller parameters' combinations is not proper. Naturally, these values can be considered outliers and thus one could neglect them when calculating the mean values of table 4-10. In this case, the mean of the evaluations on the 9 FRF models, omitting the 3^{rd}, would give a very representative description of the evaluations on the actual plant presented in table 4-8.

An illustration of the initially designed linear constraints based on $k_p = 0.0516$ and $k_d = 0.0886$, for the 5^{th} FRF model, is presented in figure 4-24. As one can see, for each frequency point a different linear constraint is constructed.

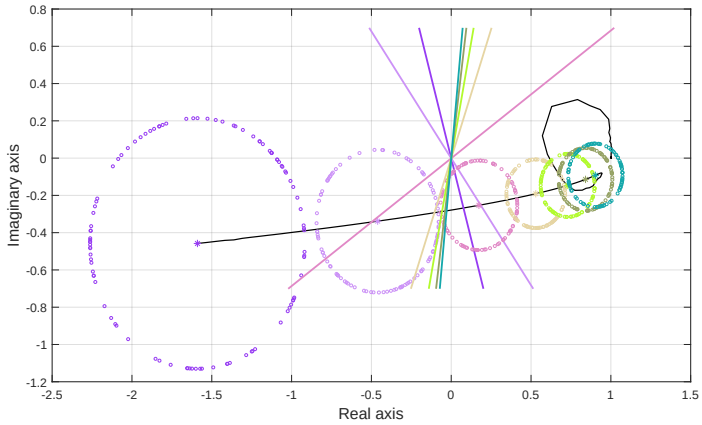

Figure 4-24: Nyquist plot of Q and Q_Δ for the 5^{th} FRF model, and optimal constraints, with $k_p = 0.0516$ and $k_d = 0.0886$

4-6 Multi-model optimization

As it was stressed in the previous sections, corrupted data is one of the most significant barriers of the proposed algorithms. Regardless the way that linear contraints are defined, that is manually or by an optimized algorithm, corrupted data, especially around the area of the reasonance peak, hurt the reliability of both the default and the proposed iterative algorithm. Consequently, it is considered of crucial importance to find a way to deal with data corruption, or else with the insufficiency of data to describe accurately the behavior of the system. As suggested previously, a straight forward manner to deal with this problem is to consider taking more samples of the actual plant around the reasonance peak, when performing the FRF measurements. This way, the behavior of the actual plant can be better captured and corruption of data should reduce.

An alternative manner to deal with corrupted data is to employ a multi-model approach on the problem that was dealt so far. The problem of data corruption concerns mainly our proposed algorithms and does not affect the default minimization scheme. This is reasonable, since the default minimization scheme is a relatively conservative algorithm as it does not aim to minimize the infinity norm. Instead it just proposes the minimization of the controller parameters which, as it was illustrated in section 4-2, results to solutions that do not succeed to satisfy the performance specification for the actual plant.

On the other hand, the proposed algorithms, deployed in section 3-4 and 3-6, are characterized by a more greedy minimization behavior, and search for the controller parameters that minimize the approximation of the infinity norm. This greediness, motivates the algorithm to look for the solution that seems to lead to minimization. However, when an FRF model has not captured accurately the behavior of the actual plant, the approximation of the norm fails to describe the actual infinity norm, resulting to solutions with low quality performance, or even to instability. In this section, we introduce a multi-model approach for the proposed algorithms, in order to deal with corruption of data.

4-6-1 Iterative algorithm with optimal, multi-model, linear constraints

The algorithm that was proposed in 3-6, is easily compatible with constraining multiple models, instead of just one. Simply at the step,

$$\text{Construct linear constraints } l_{\Delta n}(\phi, j\omega),\ n = 1, \cdots, N \text{ based on } \phi^*_{(0)},$$

one should consider applying this construction to as many FRF models as desired. That is,

1. **Input:** M FRF models, denoted as $G_{(i)}(j\omega)$, $i = 1, \cdots, M$.
2. **for** $i = 1 : M$
3. Construct linear constraints $l^{(i)}_{\Delta n}(\phi, j\omega)$, $n = 1, \cdots, N$ based on $\phi^*_{(0)}$ and $G_{(i)}(j\omega)$.
4. **Constraints** $\leftarrow$ **Constraints** $+ l^{(i)}_{\Delta n}(\phi, j\omega)$, for $n = 1, \cdots, N$.
5. **end**

Naturally, the approximation of the infinity norm has to be done with respect to a specific FRF model. Yet, it is interesting to examine how corrupted FRF models will perform, when the linear constraints are imposed to multiple models. In the following paragraphs, we employ this updated algorithm by considering a multi-model optimization.

Evaluation on the actual plant

During the simulations that were performed in this section, we employ 3 FRF models in each experiment. Specifically, when we are using the 1^{st} FRF model to approximate the actual H_∞ norm, we impose constraints on the 10^{th}, the 1^{st} and the 2^{nd} model. Respectively, when the 2^{nd} FRF model is used for approximation, we impose constraints on the the 1^{st} , the 2^{nd} and 3^{rd} model, and so on. The result of the corresponding simulations are presented in table 4-11, where the evaluation of the respective controllers is done with respect to the actual plant.

s.t.	1	2	3	4	5	6	7	8	9	10
k_p	0.1087	0.1086	0.1157	0.1667	0.0659	0.0638	0.0700	0.0511	0.0689	0.0671
k_d	0.1256	0.1254	0.1354	0.1423	0.1488	0.1290	0.14686	0.1370	0.1466	0.1275
$\|\|T_{wz}\|\|_\infty$	0.6815	0.6823	0.6726	0.9131	0.7700	0.6534	0.7450	0.6467	0.7404	0.6567

Table 4-11: Table containing the resulting controller parameters and the corresponding evaluation on the actual system

The most significant observation that one can make by observing the information on table 4-11 is that when we perform a multi-model, iterative optimization, minimizing the infinity norm approximation based on the data of the 2^{nd} FRF model, though imposing linear constraints on the 1^{st}, the 2^{nd} and the 3^{nd}, results to a controller that, not only produces a stable closed loop system, but also satisfies the performance specification with $||T_{wz}||_\infty = 0.6823$. This is a terrific result, given that the 2^{nd} FRF model was identified as a corrupted one in the previous sections. Yet, when multiple models are considered in the optimization algorithm, even a

corrupted model results to robust performance. In fact, when performing a multi-model approach on our optimization algorithm, a single non-corrupted FRF model, among as many corrupted ones, suffices to result to a solution that satisfies the performance specification, since a non-corrupted model, by default, can not lead to violation of performance constraints.

The value of this conclusion is of exceptional importance in practical applications. Namely, since corrupted data is hard to be identified in practice, it is crucial to have a data-driven controller design algorithm which is robust against such corruption. As it has been demonstrated, considering a multi-model approach within the context of our iterative frequency-domain algorithm succeeds this robustification.

Evaluation on the FRF models

In this paragraph we evaluate the performance of the resulting controller parameters on all 10 FRF models. The results of the evaluations are directly presented in a form of a mean of all 10 evaluations, and not with a 10×10 table, for sake of simplicity. The results are presented in table 4-12.

s.t.	1	2	3	4	5	6	7	8	9	10
k_p	0.1087	0.1086	0.1157	0.1667	0.0659	0.0638	0.0700	0.0511	0.0689	0.0671
k_d	0.1256	0.1254	0.1354	0.1423	0.1488	0.1290	0.14686	0.1370	0.1466	0.1275
$\|\|T_{wz}\|\|_\infty$	0.6635	0.6983	0.6972	0.9006	0.8053	0.6952	0.7645	0.6851	0.7525	0.6724

Table 4-12: Table containing the resulting controller parameters and the mean of evaluation on 10 FRF models

It appears that table 4-12 offers a trust worthy description of table 4-11, which contains the values of the actual closed-loop performance. The results presented in this section confirm that considering a multi-model approach robustifies the controller design procedure against corrupted data. Additionally, in combination with optimizing the linear constraints the iterative algorithm yields very satisfying results. Yet, an open problem remains the performance of the proposed algorithm on unstable systems. This case is going to be examined in chapter 5, where the proposed technique is extended in order to cover the case of plants with RHP poles.

4-6-2 Optimization through multiplicative uncertainty

In this subsection we apply a multi-model approach that is based on multiplicative uncertainty as it was described in section 3-3. We consider the mean of the FRF models $\bar{G}(j\omega)$ as described in 4-1-4, and the weight function $w_I(j\omega)$ is

$$w_I(s) = \frac{0.03\left(10s^2 + 2s + 1.8\right)}{s^2 + 0.5s + 2.2} \frac{s^2 + 10s + 70}{s^2 + 2s + 70}.$$

The number of realizations of the multiplicative uncertainty Δ_I remains to be defined. A highly accurate description of the uncertainty, for which it holds that $|\Delta_I(j\omega)| \leq 1$, would

require a high number of realizations n_I. However, considering for example $n_I = 100$, $N = 400$ frequency points, and the number of realizations of Δ_p to be $n_d = 100$, would result to $100 \cdot 100 \cdot 400 = 4000000$ linear inequalities. This is an extremely high number and in practice the corresponding optimization would not converge. For this reason we are going to consider a number of combinations for n_I and n_d.

3 realizations of Δ_I: For $n_I = 3$ and $n_d = 100$, the total number of linear inequalities is equal to the number that corresponds to having 3 FRF models. The results of this optimization and the evaluation of the resulting controller on the actual plant are presented in table 4-13.

s.t.	$\bar{G}(j\omega)$
k_p	0.0493
k_d	0.1189
$\|\|T_{wz}\|\|_\infty$	0.7514
$J_{\bar{G}}$	0.7562

Table 4-13: Table containing the resulting controller parameters and the evaluation on the actual plant

As it can be seen in table 4-13, the evaluation on the actual plant gives $||T_{wz}||_\infty = 0.7514$, whereas the evaluation on the mean of all FRF models gives $J_{\bar{G}} = 0.7562$, which are both acceptable. The evaluation of the resulting controller on the FRF models is presented in table 4-14.

Eval	1	2	3	4	5	6	7	8	9	10
$\|\|T_{wz}\|\|_\infty$	0.7638	0.7516	1.9833	0.7535	0.7539	0.7527	0.7527	0.7532	0.7365	0.7533

Table 4-14: Table containing the resulting controller parameters and the mean of evaluation on 10 FRF models

As it can be seen in table 4-14, the evaluation of the resulting controller on the 3^{rd} FRF model gives $||T_{wz}||_\infty = 1.9833$, which means that the performance condition is violated. This behavior is clearly attributed to the fact that the number of realizations of Δ_I is $n_I = 3$, which apparently is not sufficient. In the following paragraph simulate for $n_I = 15$ and thus we expect a satisfying performance even for the 3^{rd} FRF model.

15 realizations of Δ_I: For $n_I = 15$ and $n_d = 100$, the total number of linear inequalities is equal to the number that corresponds to having 15 FRF models. The results of this optimization and the evaluation of the resulting controller on the actual plant are presented in table 4-15.

s.t.	$\bar{G}(j\omega)$
k_p	0.0493
k_d	0.1189
$\|\|T_{wz}\|\|_\infty$	0.7514
$J_{\bar{G}}$	0.7514

Table 4-15: Table containing the resulting controller parameters and the evaluation on the actual plant

The evaluation of the resulting controller on the FRF models is presented in table 4-16.

Eval	1	2	3	4	5	6	7	8	9	10
$\|\|T_{wz}\|\|_\infty$	0.6635	0.6983	0.6972	0.9006	0.8053	0.6952	0.7645	0.6851	0.7525	0.6724

Table 4-16: Table containing the resulting controller parameters and the mean of evaluation on 10 FRF models

As expected, realizing Δ_I with more samples on the unitary disc robustifies the controller design against corrupted data. However, in the general case the size of the problem grows extremely when Δ_I is realized by a relatively large number of samples. This implies that the implementation of the optimization algorithm with multiplicative uncertainty might prove to be inpractical, since for n_I and n_d larger than 50 the problem grows immensely and convergence is not guaranteed. However, the idea of multiplicative uncertainty might be useful for the generation of additional linear inequalities when the number of available FRF models is not sufficient.

Chapter 5

Extension to Unstable Systems

In chapter 4 we have employed a plant with no right-half plane (RHP)-poles or RHP-zeros, in order to apply our proposed technique. The resulting controller design was proven to be very promising, since during simulations it was shown that the performance can be significantly optimized, while the existance of corrupted data can be succesfully dealt with, by considering a multi-model approach, where a single non-corrupted Frequency Response Function (FRF) was sufficient for the satisfaction of the performance specification. However, one can reasonably question the effectiveness of the proposed algorithm in the general case, for systems with RHP poles and zeros. For this reason, in this chapter we extend the existing theory, so that it includes such systems. Next, we employ a certain plant with RHP-poles to apply the proposed algorithm and evaluate its effectiveness in such plants.

5-1 Stability and performance

The theory deployed in chapter 3, can be extended for unstable systems in a straight forward manner. In this section we briefly review the differences that arise and construct the theoretical background for the experiments that will be performed in the following sections.

5-1-1 Condition for stability and performance based on the Nyquist diagram

Let us assume that we deal with an unstable plant $G(s)$, which has p RHP poles and z RHP zeros, yet we do have an initially stabilizing controller from which we can acquire closed-loop frequency-domain data in the form of FRF measurements. Consequently, consider that the multiple FRF models of the generalized plant $P(s)$ are denoted as $P^i(j\omega)$, for $i = 1, \cdots, M$. The generalized configuration of the plant can be expressed as

$$\begin{bmatrix} z_i \\ y_i \end{bmatrix} = \begin{bmatrix} P^i_{11}(j\omega) & P^i_{12}(j\omega) \\ P^i_{21}(j\omega) & P^i_{22}(j\omega) \end{bmatrix} \begin{bmatrix} w_i \\ u_i \end{bmatrix} \quad i = 1, \cdots, M.$$

We consider a fixed structure controller of the form $C_I(\phi, s)$, where ϕ denotes the controller parameters, and thus the control law can be expressed as

$$u_i = C_I(\phi, s)y_i, \quad i = 1, \cdots, M. \tag{5-1}$$

Given that, the closed-loop systems for $i = 1, \cdots, M$ are obtained by

$$T^i_{wz}(s) = F_l(P^i, C_I) = P^i_{11} + P^i_{12}C_I(I - P^i_{22}C_I)^{-1}P^i_{21}, \tag{5-2}$$

where F_l denotes the lower linear fractional transformation (LFT). The objective is to find controller parameters ϕ that satisfy $||T^i_{wz}(s)||_\infty < 1$, for $i = 1, \cdots, M$.

Definition for stability Let P_{ol} denote the number of open-loop unstable poles in $C_I(\phi, s)P^i_{22}(s)$ and P_{cl} denote the number of closed-loop unstable poles in $C_I(\phi, s)P^i_{22}(s)$. Then, the closed-loop systems T^i_{wz}, for $i = 1, \cdots, M$ in figure 3-1 are stable if for the generalized plants $P^i(j\omega)$, the Nyquist plots of

$$Q^i(\phi, j\omega) = \det\left(1 - C_I(\phi, j\omega)P^i_{22}(j\omega)\right) \tag{5-3}$$

make $\mathcal{N} = P_{cl} - P_{ol}$ clockwise encirclements of the origin and do not pass through the origin. This is the generalized Nyquist theorem considering positive feedback systems with open loop transfer functions $C_I(\phi, j\omega)P^i_{22}(j\omega)$. It is stressed that the number of closed-loop unstable poles P_{cl} is equal to the number of RHP-zeros of $G(s)$ and P_{ol} equals the number of RHP-poles of $G(s)$.

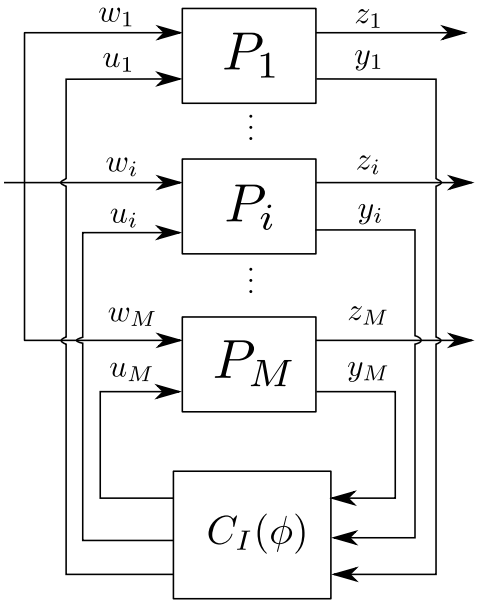

Figure 5-1: Generalized plant configuration considering multiple models

Definition for performance Let P_{ol} denote the number of open-loop unstable poles in $C_I(\phi, s)P^i_{22}(s)$ and P_{cl} denote the number of closed-loop unstable poles in $C_I(\phi, s)P^i_{22}(s)$. Then, the closed-loop systems T^i_{wz} satisfy H_∞ performance with $||T^i_{wz}||_\infty < 1$, if for the generalized plants $P^i(j\omega)$, the Nyquist plots of

$$Q^i_\Delta(\phi, j\omega) = \det\left(I - \begin{bmatrix}\Delta_p(j\omega) & 0\\ 0 & C_I(\phi, j\omega)\end{bmatrix} P^i(j\omega)\right), \quad \forall\omega, \forall\Delta_P(j\omega), \tag{5-4}$$

make $\mathcal{N} = P_{cl} - P_{ol}$ clockwise encirclements of the origin and do not pass through the origin, for any stable rational transfer function $\Delta_P \in \mathcal{RH}_\infty^{n_w \times n_z}$ and $||\Delta_P(s)||_\infty \leq 1$.

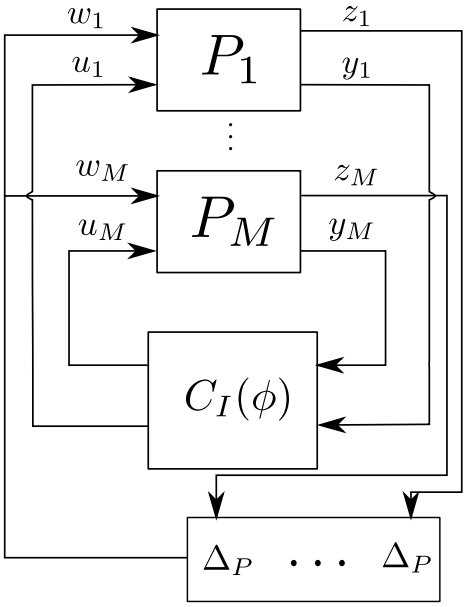

Figure 5-2: Generalized plant configuration considering multiple models and performance perturbation

In addition to the updated definitions for closed-loop stability and performance, the existance of RHP-zeros and RHP-poles implies a number of limitations which are described in detail in the following subsections, in the manner that they are deployed in [11].

5-1-2 Limitations imposed by RHP-zeros

As described in [11], RHP-zeros appear as a result of competing effects of slow and fast dynamics. A useful example is the plant

$$G(s) = \frac{1}{s+2} - \frac{2}{s+15} = \frac{-s+11}{(s+2)(s+15)},$$

which has a RHP-zero at $z = 11$. Complex RHP-zeros might also appear and, given that they always appear in conjugate pairs, they are expressed as $z = x \pm jy$, where $x \geq 0$.

The existence of a RHP-zero implies the inverse response phenomenon and some high gain instability as depicted in [11]. In addition to that, such zeros impose some limitations on the bandwidth, which are discussed in the following paragraphs.

5-1-2-1 Bandwidth limitation I

For a real RHP-zero z the bandwidth limitation is that

$$\omega_B \approx \omega_C < \frac{z}{2}, \tag{5-5}$$

where ω_B denotes the bandwidth of the closed-loop system and ω_C denotes the crossover frequency for the complementary sensitivity transfer function. For a complex pair of RHP-zeros $z = x \pm jy$ the limitations that are implied can be expressed as

$$\omega_B \approx \omega_c < \begin{cases} |z|/4 & \mathrm{Re}(z) \gg \mathrm{Im}(z) \quad (y/x \ll 1) \\ |z|/2.8 & \mathrm{Re}(z) = \mathrm{Im}(z) \quad (y/x = 1) \\ |z| & \mathrm{Re}(z) \ll \mathrm{Im}(z) \quad (y/x = 1) \end{cases} \tag{5-6}$$

To conclude, RHP-zeros that are located close to the origin have bad influence on the control of the system. Additionally, RHP-zeros being closer to the real axis is worse than being close to the imaginary axis, as depicted in 5-6.

5-1-2-2 Bandwidth limitation II

The interpolation constraint for RHP-zeros implies that for z being one, it will be $S(z) = 1$ and $T(z) = 0$, where $S(s)$ denotes the sensitivity transfer function and $T(s)$ denotes the complementary sensitivity. Suppose we are interested in bounding the infinity norm of the sensitivity transfer function, that is $||W_pS||_\infty < 1$, where $W_p(s)$ is a weight function. However, it will be $||W_pS||_\infty \geq |W_p(z)S(z)| = |W_p(z)|$, so as we must at least require that

$$|W_p(z)| < 1. \tag{5-7}$$

We can use the requirement described in 5-7 so as to explore the limitations that are implied by RHP-zeros. There are two cases that should be explored. Namely, the definition of a weight function $W_p(s)$ that requires good performance at low frequencies and, on the other hand, a weight function $W_p(s)$ that requires good performance at high frequencies.

Performance at low frequencies Consider a performance weight of the form

$$W_p(s) = \frac{s/M + \omega_B^*}{s + \omega_B^* A} \tag{5-8}$$

This weight specifies a minimum bandwidth ω_B^* for the sensitivity function $S(s)$. In fact, ω_B^* is the frequency at which the linear extension of W_p crosses 1. Additionally, the weight function specifies a maximum peak of S less than M, a steady-state offset less than $A < 1$, and at frequencies lower than the bandwidth the sensitivity is required to improve by at least $20dB/decade$, as depicted in [11]. If the plant has a RHP-zero at $s = z$, then we must require

$$|W_p(z)| = \left| \frac{z/M + \omega_B^*}{z + \omega_B^* A} \right| < 1 \tag{5-9}$$

Real zero In the case that z is real, then all variables are real and positive and 5-9 is equivalent to

$$\omega_B^* < z\frac{1-1/M}{1-A}. \tag{5-10}$$

For instance, with $A = 0$ (no steady-state offset) and $M = 2$ ($||S||_\infty < 2$), we must at least require $\omega_B^* < 0.5z$, which is consistent to the requirement $\omega_B < 0.5z$ in 5-5.

Imaginary zero For a RHP-zero on the imaginary axis, that is $z = j|z|$, an analogous derivation results for $A = 0$:

$$\omega_B^* < |z|\sqrt{1-\frac{1}{M^2}} \tag{5-11}$$

For instance, with $M = 2$ we require $\omega_B^* < 0.86|z|$, which results to be very close to the requirement $\omega_B < |z|$, that is given in 5-6.

Performance at high frequencies In this paragraph we explore the limitations that are imposed in the case that we want tight control at high frequencies, by using a performance function of the form

$$W_p(s) = \frac{1}{M} + \frac{s}{\omega_B^*} \tag{5-12}$$

This requires tight control ($|S(j\omega)| < 1$) at frequencies higher than ω_B^*, while the only requirement at low frequencies is that the peak of S is less than M. It is stressed that the requirement imposed by this particular performance weight, described in 5-12, is admittedly unrealistic, since it requires $S \to 0$ at higher frequencies, yet it reveals the bandwidth limitations that are imposed. Nevertheless, in order to satisfy $||W_pS||_\infty < 1$ we must at least require that the performance weight satisfies $|W_p(z)| < 1$, and for a real RHP-zero we conclude for the weight in 5-12

$$\omega_B^* > z\frac{1}{1-1/M}. \tag{5-13}$$

For instance, with $M = 2$ the requirement is $\omega_B^* > 2z$, and thus we can only achieve tight control at frequencies over the frequency of the RHP-zero.

5-1-3 Limitations imposed by unstable RHP-poles

In this subsection, we explore the limitations that are imposed by the existance of RHP-poles. For instance, the plant $G(s) = \frac{1}{s-2}$ has a RHP-pole with $p = 2$.

For plants with RHP-poles, feedback is necessary for stabilization. Namely, the existance of an unstable pole p requires for internal stability $T(p) = 1$, where $T(s)$ denotes the complementary sensitivity transfer function, and as a result two limitations are imposed.

RHP-pole Limitation 1 (input usage).

Basically, we have to manipulate the system's input u, and the transfer function $C_I S$ from plant outputs to plant outputs must always satisfy [2], [3],

$$\|C_I S\|_\infty \geq \left|G_s(p)^{-1}\right|, \tag{5-14}$$

where G_s is the "stable version" of G, with its RHP-poles mirrored in the left-half plane (LHP),

$$G(s) = G_s(s) \cdot \prod_i \frac{s + \bar{p}_i}{s - p_i}. \tag{5-15}$$

For instance, for the plant $G(s) = \frac{1}{s-4}$ we have $G_s = \frac{1}{s+4}$ and the lower bound of the peak of $C_I S$ is $|G_s(p)^{-1}| = 4 + 4 = 8$.

This limitation is imposed by the need to avoid saturation of the input signal in practical applications. Specifically, it is $u = -C_I S\,(G_d d + n)$, where d denotes the disturbance signal and n denotes the measurement noise signal. Additionally, $G_d(s)$ denotes the transfer function of the disturbance, as illustrated in figure 5-3. In this general case, in order to avoid input saturation, that would lead to instability issues, it should hold

$$\|C_I S G_d\|_\infty \geq \left|G_s(p)^{-1} G_{d,ms}(p)\right|, \tag{5-16}$$

where $G_{d,ms}$ denotes the "stable version" of G_d, as depicted in [11]. The proof of the first limitation imposed by RHP-poles is omitted, since it is derived in full detail in [11].

RHP-pole Limitation 2 (bandwidth).

In the presence of a RHP-pole p we need to ensure that the system reacts sufficiently fast, and specifically we must require that the bandwidth of the closed-loop system is larger than $2p$, approximately. This limitation results from the bound $\|W_i T\|_\infty \geq |W_i(p)|$. As a result, while the presence of a RHP-zero imposes an upper bound on the bandwidth, the presence of a RHP-pole implies a lower bound on the feasible bandwidth. Similarly to the case of the first limitation, imposed by an unstable pole, the proof of the second limitation is omitted as well, and a detail derivation is provided in [11].

5-1-4 Combination of RHP-zeros and RHP-poles

Stabilization. Theoretically, any linear plant can be stabilized irrespectively of the position of its RHP-zeros and RHP-poles, as long as the plant does not contain any hidden unstable modes. Nonetheless, this might require an unstable controller, and in practice it is often required that a stable controller is used. If there exist a stable controller that stabilizes the closed-loop system, then the plant is said to be *strongly stabilizable*. It has been proved by Youla et al. [13], that a strictly proper Single-Input Single-Output (SISO) plant is strongly stabilizable by a proper controller if and only if every RHP-zero in $G(s)$ lies to the left of an even number (including zero) of real RHP-poles in $G(s)$, as described in [11]. It is

stressed that the presence of any complex RHP-zeros or complex RHP-poles does not affect this requirement.

For example, consider the strictly proper plant $G(s) = \frac{s-z}{(s-p)(\tau s+1)}$. According to the requirement described in the previous paragraph, $G(s)$ can be stabilized by a stable proper controller if and only if $z > p$. However, in order to acquire acceptable performace, the limitations imposed by RHP-zeros and RHP-poles should be better examined. Previously, it was derived for a real RHP-zero the approximate bound $\omega_B < z/2$ (with $M_S = 2$), and for a real RHP-pole the approximate bound $\omega_c > 2p$ (with $M_T = 2$). This implies that for a system with a single real RHP-zero and a single real RHP-pole, one must require $z > 4p$ so as to get acceptable performance and robustness.

Sensitivity peaks. For a plant with a single real RHP-zero and a single real RHP-pole, we always have

$$\|S\|_\infty \geq c, \|T\|_\infty \geq c, \quad c = \frac{|z+p|}{|z-p|}. \tag{5-17}$$

5-1-5 Controllability analysis with feedback control

In this subsection, we discuss the consequences of limitations, that are imposed by the presence of RHP-zeros and RHP-poles, on the controller design procedure. Additionally, we summarize on the necessary conditions that should hold in order to satisfy performance on unstable systems. The block diagram presented in figure 5-3 illustrates the configuration of the closed-loop, of a SISO system, including the disturbance signal d. In the following paragraphs, we consider that all signals are scaled.

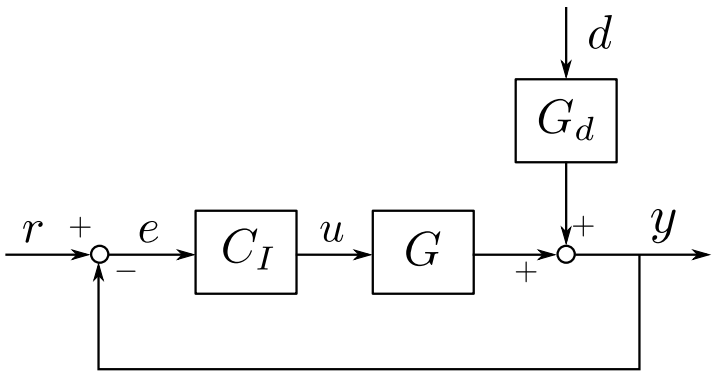

Figure 5-3: Block diagram of the scaled general closed-loop system.

The limitations that were described in the previous paragraphs can be summarized as follows.

Speed of response to track reference changes We may require that $|S(j\omega)| \leq 1/R$ up to the frequency ω_r at which reference tracking is required, where R denotes the maximum value that the reference signal is allowed to take.

Input constraints arising from disturbances. For acceptable control ($|e| < 1$), it should hold that $|G(j\omega)| > |G_d(j\omega)| - 1$ for frequencies that $|G_d(j\omega)| > 1$. For perfect control ($e = 0$), one must require that $|G(j\omega)| > |G_d(j\omega)|$.

Input constraints arising from setpoints. The designer must require that $G(j\omega) > R - 1$, up to the frequency ω_r, that reference tracking is required.

Tight control at low frequencies with a RHP-zero z in $G(s)$. For a real RHP-zero we require $\omega_c < z/2$ and for an imaginary RHP-zero we approximately require $\omega_c < |z|$.

Real open-loop unstable pole in $G(s)$ at $s = p$. In this case, we need high feedback gains to stabilize the system and we require $\omega_c > 2p$. Moreover, for unstable plants we need $|G_s(p)| > |G_{d,ms}(p)|$, in order to avoid input saturation in the presence of disturbances.

All these limitations, have to be considered by a designer in order to synthesize a proper control analysis problem. In the general case that the closed-loop system is represented by a generalized plant, these limitations are absorbed into the design of suitable weight functions W_p and W_i. Moreover, in this general case, the controller design is done by considering a disturbance signal that is constructed by the designer.

Finally, nominal performance is ensured by imposing linear constraints that, when satisfied, guarantee that the resulting controller satisfies the performance specifications. Respectively, for robust performance a multi-model approach can be implemented, ensuring that the performance specifications are satisfied for all the models that are under consideration.

5-2 Simulations and results for unstable systems

In this section we present an additional experiments' session in order to evaluate our proposed technique on unstable plants. Moreover, the entire procedure of acquiring FRF measurements of the considered plant is described in detail.

5-2-1 Dynamics of the plant

For the purposes of this chapter we employ an unstable system, and specifically the magnetically levitated train.

This type of train "flies" on an air gap above its rail system. The gap control is exceptionally critical for the operation of the train, and the transfer function describing this gap can be expressed as

$$G(s) = \frac{8(s+1)(s+3)}{s(s-1)(s+4)(s+8)}. \tag{5-18}$$

Apparently, this system has a RHP-pole, which is located at $p = 1$. This implies that the theory deployed in chapter 3 does not apply in this case, since the satisfaction of stability and performance requires a single, anti-clockwise encirclement of the origin, instead of no

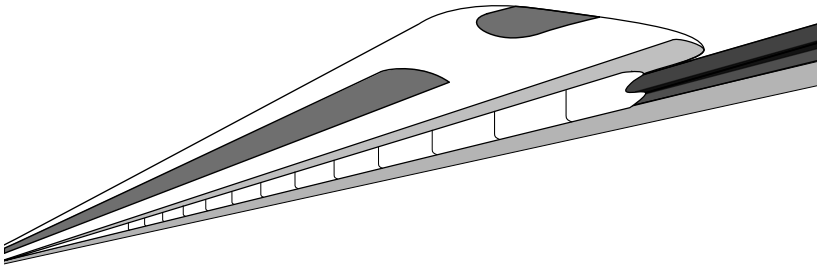

Figure 5-4: A sketch of a magnetically levitated train.

encirclement. However, the case of unstable systems was theoretically covered in section 5-1. As a result, in this section we are going to employ our proposed algorithm and evaluate its performance on this unstable system. In figure 5-4, one can see a schematic representation of the magnetically levitated train. The bode plot of the transfer function $G(s)$ describing the gap of the magnetically levitated train is presented in figure 5-5.

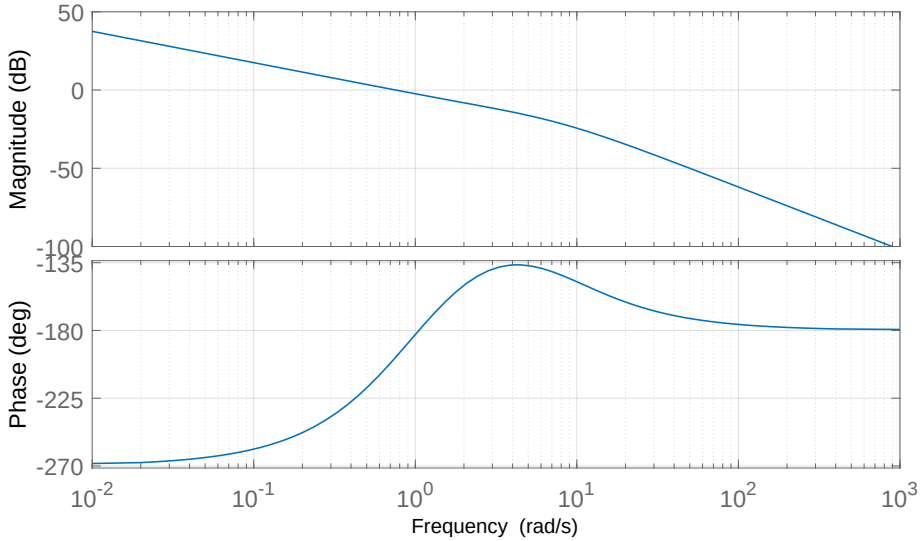

Figure 5-5: Bode plot the transfer function $G(s)$

5-2-2 System configuration

The implementation of the proposed algorithm on the unstable system requires setting up the generalized plant. That is, we have to set the objective of the controller design by deciding on the form of the perfromance weights W and on the signals of the closed-loop that we are interested in bounding. In figure 5-6 one can see the configuration of the generalized plant, where W_p is the performance weight that corresponds to the sensitivity and W_i is the respective performance weight for the complementary sensitivity.

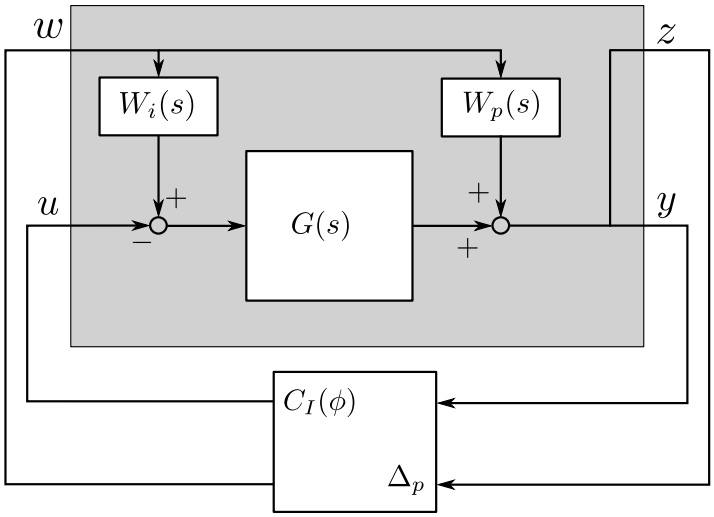

Figure 5-6: Configuration of the closed-loop for mixed-sensitivity controller design

Apparently, we are interested in performing a mixed-sensitivity controller design, for which the performance specification can be described as $||T_{wz}||_\infty \leq 1$, or specifically

$$\left\| \begin{array}{c} W_p S \\ W_i T \end{array} \right\|_\infty = \max_\omega \sqrt{|W_p S|^2 + |W_i T|^2} < 1. \tag{5-19}$$

The nature of such a plant requires a PID controller in order to be stabilized, and thus the structure of the controller is decided to be $C_I(s) = \frac{k_p}{T_f s+1} + \frac{k_i}{s} + \frac{k_d s}{T_f s+1}$, where k_p, k_i and k_d are the proportional, integral and derivarive gains, respectively. Given that, the generalized plant can be expressed as

$$\begin{bmatrix} z \\ y \end{bmatrix} = \begin{bmatrix} W_p(s) + G(s)W_i(s) & -G(s) \\ W_p(s) + G(s)W_i(s) & -G(s) \end{bmatrix} \begin{bmatrix} w \\ u \end{bmatrix}. \tag{5-20}$$

Defining properly the performance weights W_p and W_i is related to the control objective of the designer. In our case we have selected

$$W_p(s) = \alpha_p \frac{s^2/M_p^2 + 2\beta_p \omega_B s + \omega_B^2}{s^2 + 2\beta_p A_p \omega_B s + (A_p \omega_B)^2},$$

where $\alpha_p = 5$, $\beta_p = 0.6, M_p = 3, A_p = 10^{-2}$ and $\omega_B = 1.5$. Given the performance objective, the sensitivity transfer function of the closed-loop system should lie below the bode plot $\frac{1}{|W_p(s)|}$.
Additionally, for the performance weight W_i we have

$$W_i(s) = \alpha_i \frac{s^2/M_i^2 + 2\beta_i \omega_B s + \omega_B^2}{s^2 + 2\beta_i A_i \omega_B s + (A_i \omega_B)^2},$$

where $\alpha_i = 0.5 \cdot 10^6$, $\beta_i = 0.5, M_i = 3, A_i = 1 \cdot 10^3$ and $\omega_B = 50$. Given the performance objective, the complementary sensitivity transfer function of the closed-loop system should lie below the bode plot $\frac{1}{|W_i(s)|}$. The bode plots of the inverse of W_p and W_i are illustrated in figure 5-7. The red bode plot corresponds to W_i, whereas the blue plot corresponds to W_p.

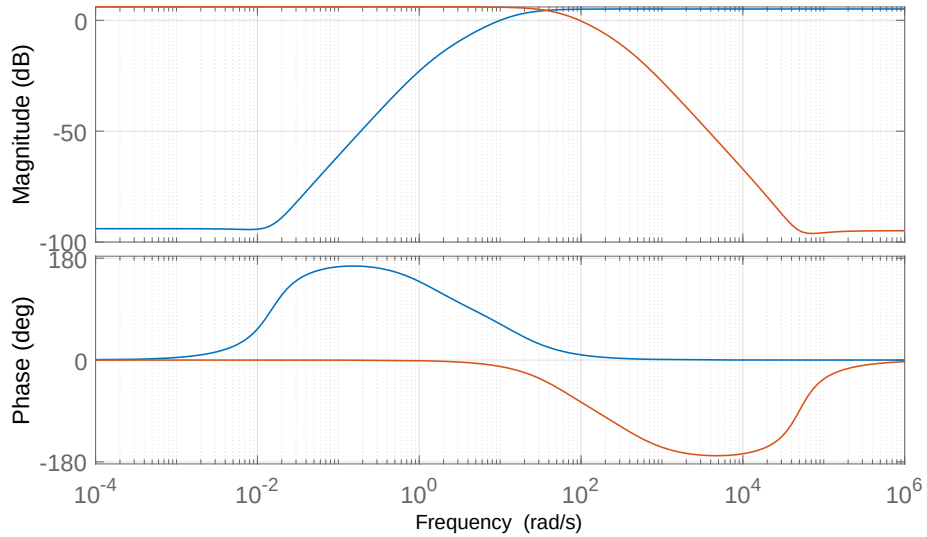

Figure 5-7: Bode plot of the inverse of $W_p(s)$ and $W_i(s)$

5-2-3 Frequency-domain data

As it was stressed previously, the implementation of the algorithm is based on frequency-domain data of the plant in the form of FRF measurements. Given that $G(s)$ is an unstable plant, we need a closed-loop configuration in order to stabilize the system and acquire frequency-domain data. Naturally, an initially stabilizing controller is necessary for such an experiment. The block diagram of the closed loop configuration that can be used in Simulink in order to acquire frequency-domain data is illustrated in figure 5-8.

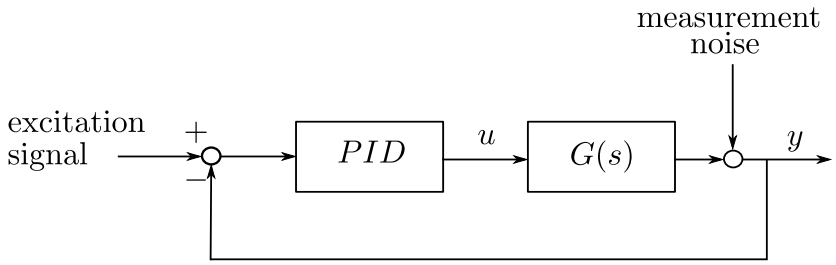

Figure 5-8: Configuration of the closed loop for data acquisition

For sake of simplicity, and given that system identification is not of the main interest of this project, we produced the FRF models by making use of the original transfer function $G(s)$ and by adding noise. In other words, we artificially created the FRF models that are going to be used in this section. This technique offers the priviledge to directly control the amount of noise that is added on a specific model, which implies that one can also consider the case of creating very noisy models or artificially constructed corrupted data. Additionally, for the needs of our algorithm we used an initially stabilizing solution with $k_p = 12.5$, $k_i = 12.5$ and $k_d = 2.5$, which results to $||T_{wz}||_\infty = 1.4057$ when evaluated on the actual plant. For the purposes of our experiments we created 5 FRF models, which are illustrated in figure 5-9. Each FRF model consists of 1000 frequency points, logarithmically located in the interval

$[0.01, 1000] rad/sec$.

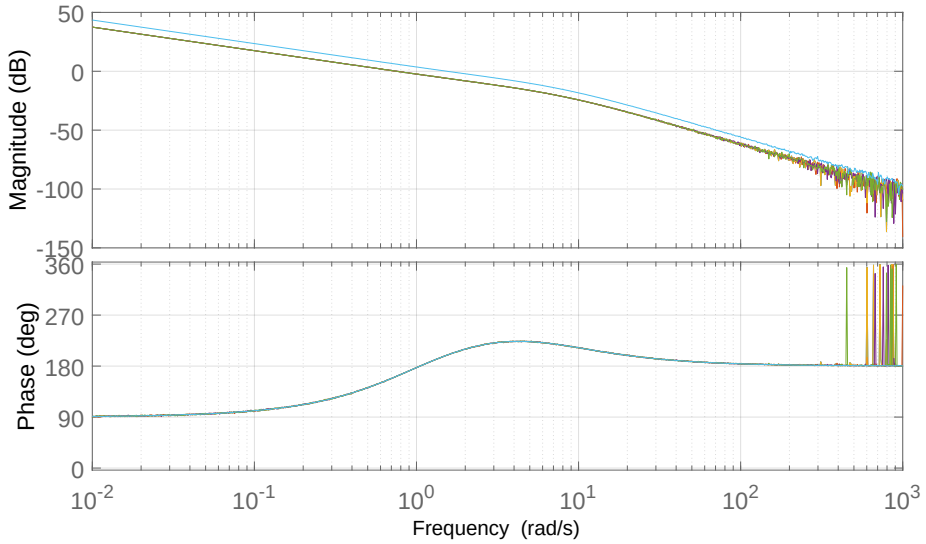

Figure 5-9: Bode plot of 5 FRF models

As it can be seen, the magnitude bode plot of the 5^{th} FRF model illustrated in cyan in figure 5-9 deviates significantly with respect to the remaining 4. This is done on purpose in the procedure of constructing our data as a mean to artificially construct corrupted data. In other words, we have created this corrupted model of the plant in order to be able to assess the performance of our algorithm in the presence of data disruption.

5-3 Iterative algorithm with optimal constraints

In this section, we employ the 5 FRF models that were acquired previously in order to implement our proposed algorithms to an unstable system. In particular, in the following paragraphs we employ the iterative algorithm based on optimal constraints that was deployed in section 3-6, for the single-model case. A multi-model approach will be considered in the next section of this chapter.

5-3-1 Evaluation on the actual plant

In this paragraph, we evaluate the resulting fixed-structure controllers on the actual plant as if it was available for such evaluations. These results are useful in order to compare them with the corresponding results of the evaluation on other FRF models, which is described in the next paragraph. The evaluations on the actual plant are presented in table 5-2.

s.t.	1	2	3	4	5
k_p	32.672	30.507	33.456	40.342	17.1200
k_i	61.343	35.420	56.046	31.959	34.1189
k_d	3.2418	2.9701	3.1713	2.7808	1.6259
$\|\|T_{wz}\|\|_\infty$	0.6949	0.6962	0.6979	0.7677	1.0669

Table 5-1: Table containing the resulting controller parameters and the corresponding evaluation on the actual system

As it can be seen, the controller parameters that correspond to optimization subject to the 5^{th} FRF model do not satisfy the performance condition when evaluated on the actual plant. This was expected, since the 5^{th} FRF model deviates from the actual plant on purpose, as described previously. On the other hand, the controller parameters for the first 4 models satisfy the performance condition.

5-3-2 Evaluation on FRF models

In this paragraph we evaluate the controllers that resulted from optimization, also presented in the previous paragraph, on other FRF models. Such an evaluation is very critical, since the actual plant is not available in practical applications. The results are presented in table 5-2.

	1	2	3	4	5
1	0.7044	0.7015	0.7061	0.7718	1.0733
2	0.7261	0.7050	0.7209	0.7719	1.0770
3	0.7017	0.6989	0.7044	0.7717	1.0704
4	0.7027	0.7008	0.7038	0.7726	1.0706
5	0.8657	0.8345	0.8598	0.8311	0.6987

Table 5-2: Table containing the evaluation of the controller parameters on all FRF models

As it can be seen, the controller parameters that result from optimization that is subject to the 5^{th} FRF model violate the performance condition when evaluated on the other FRF models. This behavior has been explained in the previous paragraph.

Additionally, It is useful to present the result Nyquist diagram of Q, that corresponds to stability. For $k_p = 32.672$, $k_i = 61.343$ and $k_d = 3.2418$ and using the data of the 1^{st} FRF model, the Nyquist diagram is illustrated in figure 5-10. Althought it is not visible, the encirclement of the origin is an anti-clockwise encirclement.

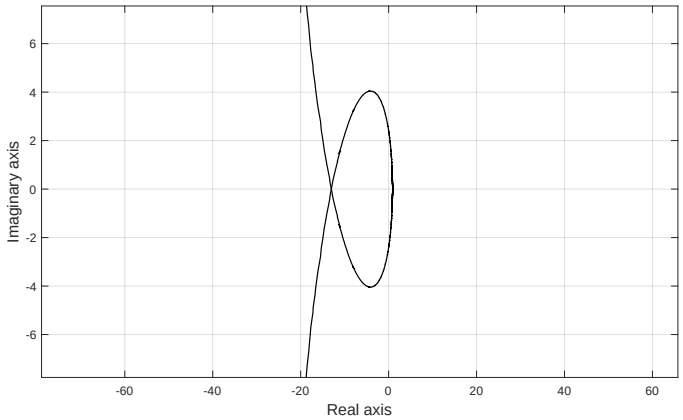

Figure 5-10: Nyquist diagram for the 1^{st} FRF model with $k_p = 32.672$, $k_i = 61.343$ and $k_d = 3.2418$

5-4 Iterative, multi-model, approach with optimal constraints

In this section, we employ the 5 FRF models and implement the algorithm deployed in section 3-6, only by considering a multi-model approach. As it was also illustrated in section 4-6, a multi-model approach can be used to robustify the controller design procedure against corrupted data. Similarly to the procedure followed in 4-6, we apply the multi-model approach by considering 3 FRF models at each optimization in order to evaluate the proposed technique.

5-4-1 Evaluation on the actual plant

During the simulations that were performed in this section, we employ 3 FRF models in each experiment. Specifically, when we are using the 1^{st} FRF model to approximate the actual H_∞ norm, we impose constraints on the 5^{th}, the 1^{st} and the 2^{nd} model. Respectively, when the 2^{nd} FRF model is used for approximation, we impose constraints on the the 1^{st} , the 2^{nd} and 3^{rd} model, and so on. The result of the corresponding simulations are presented in table 5-3, where the evaluation of the respective controllers is done with respect to the actual plant.

s.t.	1	2	3	4	5
k_p	31.252	33.506	35.536	43.231	22.2951
k_i	59.225	38.536	52.235	29.257	45.3595
k_d	3.231	3.256	3.3215	2.9563	1.8839
$\|\|T_{wz}\|\|_\infty$	0.7019	0.6905	0.6966	0.7581	0.9112

Table 5-3: Table containing the resulting controller parameters and the corresponding evaluation on the actual system

As it can be seen on the fifth column of table 5-3, a multi-model approach robustifies the controller design even in the case that corrupted data are used, since it is now $||T_{wz}||_\infty =$

0.9112, whereas in the previous subsection it was $||T_{wz}||_\infty = 1.0669$. Namely, when the 5^{th} FRF model is used for optimization, subject to constraints on the 4^{th}, 5^{th} and 1^{st} model, the resulting controller does indeed satisfy the performance condition when evaluated on the actual plant. A similar result is expected for evaluation on other FRF models as well.

5-4-2 Evaluation on FRF models

In this paragraph we evaluate the performance of the resulting controller parameters on all 5 FRF models. The results are presented in table 5-4.

	1	2	3	4	5
1	0.7083	0.7054	0.7107	0.7651	0.9124
2	0.7248	0.7210	0.7331	0.7651	0.9131
3	0.7077	0.7036	0.7093	0.7651	0.9137
4	0.7073	0.7045	0.7101	0.7643	0.9144
5	0.8622	0.8680	0.8784	0.8543	0.7230

Table 5-4: Table containing the evaluation of the controller parameters on the FRFmodels

As it can be seen in the 5^{th} column of table 5-4 and 5-3, in the multi-model approach the algorithm converges to controller parameters that satisfy performance even when corrupted data is used for optimization. By considering the results presented in this section we can derive that imposing linear constraints on multiple models robustifies the controller design even in the presence of corrupted data. This result was expected given the corresponding results in chapter 4, yet it is of high importance to confirm that this behavior applies also for unstable systems.

Chapter 6

Conclusions and Future Work

6-1 Conclusions

In this thesis project we have examined the problem of frequency-domain optimization of fixed-structure controllers. Specifically, the main idea of the technique is to ensure H_∞ performance by imposing linear constraints on the Nyquist diagram of the closed-loop system, making use of Frequency Response Function (FRF) models of the plant.

Throughout chapter 3 we have extended the initial approach so that it considers optimization subject to multiple FRF models, instead of just one, resulting to robust performance controller design. Additionally, we have proposed a method to reduce the size of the problem by reducing the number of the resulting linear inequalities. More importantly, we have proposed an iterative algorithm that succeeds to minimize the H_∞ norm of the closed-loop system by using an approximation of the norm, which is linear with respect to the controller parameters. The linear approximation of the H_∞ norm is based on the assumption that the maximum magnitude of a certain transfer function, for an initially stabilizing solution, will still appear in the same frequency for a small neighborhood around the initial solution. Moreover, given the fact that user-defined linear constraints induce some significant amount of conservatism on the resulting solution, we have proposed an algorithm that constructs linear constraints, which are optimal in the sense that they induce the least amount of conservatism for a given initially stabilizing solution. Being able to combine these two algorithms, we have proposed the final optimization scheme, which suggests a procedure that iteratively optimizes the controller parameters and the corresponding linear constraints.

In chapter 4 we employed the plant of a double mass-spring-damper system in order to apply our proposed algorithm and to compare it with the default technique. Simulations that were performed for 10 FRF models revealed that our proposed algorithm outperforms the default technique. The remarkably improved performance that was succeeded is mainly attributed to the fact that the default algorithm uses a conservative optimization scheme that aims to minimize the sum of the squares of the controller parameters. On the other hand, the objective of our proposed algorithm is to minimize a linear approximation of the H_∞ norm,

which indeed proves to be more effective in terms of closed-loop performance. On top of that, optimizing the linear constraints also improves the performance of the closed-loop. Moreover, although our proposed algorithm appears to be vulnerable to corrupted data, since such data might lead to unstable controllers, in 4-6 it has been demonstrated that considering a multi-model approach robustifies the controller design even when corrupted data are present.

However, although our proposed algorithm was proved to be very efficient for a stable plant, one could reasonably question its effectiveness for unstable plants with right-half plane (RHP)-poles. For this reason, in chapter 5 we extended the existing theory so as it covers the general case of both stable and unstable plants. Next, we employed the dynamics that describe the behavior of the gap of a magnetically levitated train, that is an unstable plant, to demonstrate the performance of our algorithm. The algorithm showed to be effective also in such systems, whereas it was also tested for the multi-model approach.

Yet, although we have succeeded a remarkable improvement upon the initial algorithm, presented in [12], there are still margins for further development and future work. These issues are discussed in the following section.

6-2 Future Work

The main contribution of this thesis project is the iterative algorithm which seeks to minimize the approximation of the H_∞ norm of the closed-loop system. However, this search is being done by approximating the behavior of the norm by a linear function around a given solution, and by minimizing the maximum of the resulting linear functions as described in detail in 3-4. In the case that the infinity norm shows a convex behavior with respect to the controller parameters, this technique will succeed to find the minimum inside a given parameters' interval. Yet, in the general non-convex case there is no guarantee that the algorithm will explore optimal solutions, which during the iterations might get excluded from the set of feasible solutions, due to the form of the optimization scheme. In other words, although in practice it will succeed to find a very satisfying solution, the proposed algorithm will not succeed to find a global-, or even a local-mimimum of the H_∞ norm of the closed-loop.

This weakness of the algorithm can be dealt by introducing a different kind of optimization. Such optimization algorithms could be Powell's perpendicular method [10] with multi-start local optimization, so as a global minimum can be found. Additionally, for small-sized problems the Nelder-Mead method [8] with multi-start local optimization could also be functional. It should be noted though, that a multi-start local optimization is not directly feasible, since in the context of the considered problem there is just one initially stabilizing solution. A solution to this barrier would be to make use of our proposed algorithm in order to generate multiple stabilizing solutions and then employ one of the two suggested algorithms to perform multi-start local optimization. It would be interesting to explore the computational complexity that would be implied by such an implementation

Moreover, in order to consider an additional improvement on the controller design procedure, one should examine the entire procedure of system identification and controller synthesis. The procedure that we have used up to this point can be described by the diagram in figure 6-1.

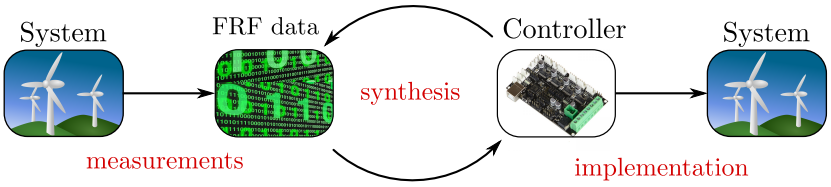

Figure 6-1: Schematic representation of the current control strategy

As it can be seen, the current approach assumes that we can acquire measurements, given an initially stabilizing controller, in order to construct FRF data. Next, using our proposed algorithm we iteratively optimize the controller parameters and finally we implement the resulting controller to the actual system. However, a procedure with a single measurement might lead to disruption of data, and thus to low performance of the resulting controller. In order to deal with this danger, we suggest to develop a data-driven control cycle. In this case, the controller design can be performed upon data which are iteratively improved by repetitive measurements. This control strategy is better illustrated by figure 6-2. Such a strategy would significantly robustify the controller synthesis procedure, and would improve the resulting performance.

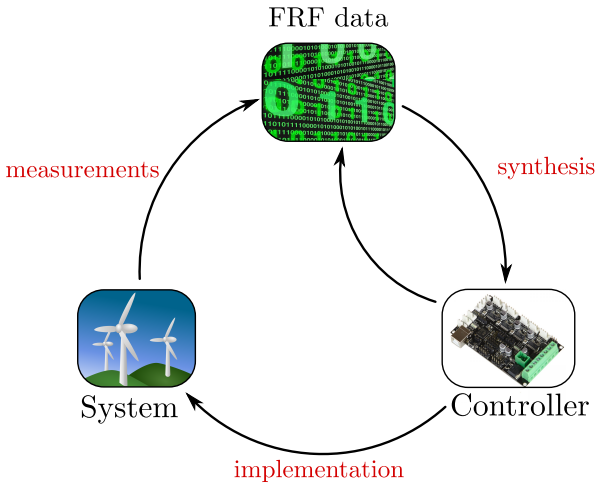

Figure 6-2: Schematic representation of the data-drive control cycle

All in all, although the proposed algorithm succeeds to outperform the default technique, there are still margins for improvement of the overall method. By refining the optimization scheme so that it can converge to local- and global-minima, and by consdering a data-driven control cycle, as described previously, the proposed method appears to have potential for further improvements. In the light of the results of this project, the iterative algorithm that is contributed offers a powerful toolbox which can be proved to be very useful in practical applications for both stable and unstable plants where FRF models are available.

Bibliography

[1] Sippe G Douma and Paul MJ Van den Hof. Relations between uncertainty structures in identification for robust control. *Automatica*, 41(3):439–457, 2005.

[2] K Havre and S Skogestad. Limitations imposed by rhp zeros/poles in multivariable systems. In *1997 European Control Conference (ECC)*, pages 3071–3076. IEEE, 1997.

[3] Kjetil Havre and Sigurd Skogestad. Achievable performance of multivariable systems with unstable zeros and poles. *International Journal of Control*, 74(11):1131–1139, 2001.

[4] Alireza Karimi and Gorka Galdos. Fixed-order h controller design for nonparametric models by convex optimization. *Automatica*, 46(8):1388–1394, 2010.

[5] Johan Lofberg. Yalmip: A toolbox for modeling and optimization in matlab. In *2004 IEEE international conference on robotics and automation (IEEE Cat. No. 04CH37508)*, pages 284–289. IEEE, 2004.

[6] Alistair GJ MacFarlane and Ian Postlethwaite. The generalized nyquist stability criterion and multivariable root loci. *International Journal of Control*, 25(1):81–127, 1977.

[7] Pertti M Mäkilä. Approximation of stable systems by laguerre filters. *Automatica*, 26(2):333–345, 1990.

[8] John A Nelder and Roger Mead. A simplex method for function minimization. *The computer journal*, 7(4):308–313, 1965.

[9] Rik Pintelon and Johan Schoukens. *System identification: a frequency domain approach*. John Wiley & Sons, 2012.

[10] Michael JD Powell. An efficient method for finding the minimum of a function of several variables without calculating derivatives. *The computer journal*, 7(2):155–162, 1964.

[11] Sigurd Skogestad and Ian Postlethwaite. *Multivariable feedback control: analysis and design*, volume 2. Wiley New York, 2007.

[12] E van Solingen, JW van Wingerden, and T Oomen. Frequency-domain optimization of fixed-structure controllers. *International Journal of Robust and Nonlinear Control*, 28(12):3784–3805, 2018.

[13] DC Youla, JJ Bongiorno Jr, and CN Lu. Single-loop feedback-stabilization of linear multivariable dynamical plants. *Automatica*, 10(2):159–173, 1974.

[14] Kemin Zhou, John Comstock Doyle, Keith Glover, et al. *Robust and optimal control*, volume 40. Prentice hall New Jersey, 1996.

Glossary

List of Acronyms

LQ	Linear Quadratic
FRF	Frequency Response Function
SISO	Single-Input Single-Output
MIMO	Multiple-Input Multiple-Output
MISO	Multiple-Input Single-Output
SIMO	Single-Input Multiple-Output
LFT	linear fractional transformation
RHP	right-half plane
LHP	left-half plane